Implementing Meta-GGA Functionals in PAW Formalism and Applications in Molecular and Nanoscale Thin-Film Systems

---

Konstantin Tamoev

June 04, 2024
Version: Final Version

University of Paderborn

Dissertation

Implementing Meta-GGA Functionals in PAW Formalism and Applications in Molecular and Nanoscale Thin-Film Systems

Konstantin Tamoev

1. Reviewer Thomas D. Kühne
HZDR

2. Reviewer Martin Brehm
University of Paderborn

June 04, 2024

Konstantin Tamoev

Implementing Meta-GGA Functionals in PAW Formalism and Applications in Molecular and Nanoscale Thin-Film Systems

Dissertation, June 04, 2024

Reviewers: Thomas D. Kühne and Martin Brehm

University of Paderborn

Abstract

The following thesis explores extensions of density functional theory (DFT). For that purpose one of the objectives of this work is on implementing the meta-GGA functional SCAN developed by Perdew et al. into the CP-PAW framework using the projector augmented wave (PAW) formalism. With this, we aim to enhance the accuracy and utility of DFT in predicting the properties of complex systems.

Furthermore, this thesis includes application studies on the Carbon Suboxide (C_3O_2) monomer and the growth of nanoscale Cu(In,Ge)Se (CIGS) thin-films. In the structural analysis of C_3O_2 we employ both the local hybrid functional PBE0r by Blöchl et al. and an approach that combines reduced density-matrix functional theory (RDMFT) with the adaptive cluster approximation (ACA) by Schade et al. These two methodologies provide insights into the electronic structure and bonding behaviour of C_3O_2, establishing the effectiveness of incorporating DFT and RDMFT for such analyses.

Finally, as an integral part of high-efficiency photovoltaic systems, the second application study focuses on the mechanisms of nanostructure growth of CIGS thin-films. Utilizing tight-bonding molecular dynamics (TBMD), we study the first stages of CIGS growth on the Molybdenum (Mo) back contact, aiming to provide helpful data for the efficiency and scalability enhancement of these systems.

Overall, this work contributes to the theoretical tools available for the study of intricate molecular and nanostructure materials, giving new insights and a look into potential practical applications in material science and photovoltaics.

Acknowledgement

I want to begin by thanking Thomas D. Kühne for the opportunity to pursue my PhD in his research group and his guidance, support and patience throughout. His expertise and insightful observations and comments have been instrumental in shaping this research. Special thanks also goes to my former supervisor, Manjusha Chugh, for her mentorship and support during the first years of my PhD. Her analytical skills and constructive criticism have greatly contributed to the early foundation of this work. I am also grateful to all my colleagues and members of the Arbeitskreis Kühne who have made this journey both productive and enjoyable: Britta Fremerey, Andres Henao Aristizabal, Hossam Elgabarty, Hossein Mirhosseini, Ramya Kormath Raghupathy, Frederik Zysk, Julian Heske, Karlo Nolkemper, Simon Richter, Svetlana Pylaeva. My squash games with Karlo and Hossam provided much-needed breaks and kept me physically and mentally fit.

This thesis would not have been possible without the support of my family and friends, who have always encouraged me on this journey.

Finally, I would like to thank the University of Paderborn and the HZDR for providing the resources and environment that enabled me to conduct this research.

Contents

1 Introduction

The research on molecular and nanostructure materials within the scope of density functional theory (DFT) has had significant advancements, necessitated by the need to understand and predict the properties of complex systems. The present work adds to this area of research through the implementation of Perdew et al.'s[SRP15a] meta-generalized gradient approximation (meta-GGA) functional SCAN within the CP-PAW code base using the projector augmented wave (PAW) formalism. Complementary to the theoretical foundation and computational implementation we present practical applications, investigating the nature of carbon suboxide C_3O_2 and the growth of nanostructure materials in $Cu(In_{1-x}Ga_x)Se_2$ (CIGS) thin films.

Ever since its first synthesis in 1874 by Brodie[Bro74] and except for its initial identification as a semiconducting material and its other properties in the early and mid 20th century[SB08; DW06; YCD90; SHY78; CPP86; Smi+63] Carbonsuboxide (C_3O_2) barely garnered any interest in the field of chemistry. However, the rising interest in solar-cells and solar-to-chemical energy conversion in the last two decades shed a spotlight on the suboxide, in particular due to its extended π-conjugated systems and its direct band-gap within the visible light spectrum[Ban+21]. The demonstration of photocatalytic water splitting over carbon nitride further accelerated the interest towards carbonaceous materials[Wan+09]. Unlike other polymeric semiconductors, such as carbon nitride, the suboxide, which in its polymeric form is a planar 2D structure of adjacent infinite C_3O_2 monomers, has the structural advantage of good processability. Additionally, due to the solubility of C_3O_2 it can be coated onto different substrates and can be used for a range of applications, e.g. OLEDs[Xu+21], organic field-effect transistors (OFET)[Car+21] and many others[Liu+20; MS20]. Antonietti et al.[Odz+22] developed a liquid phase dehydration method that, unlike previous methods, which only work at high temperatures (HT), synthesises the suboxide at lower temperatures (LT), down to even 0°C. These low-temperature methods, unlike HT methods, allow for greater control over the chemical structure of the molecule in particular for tuning of the band-gap for photocatalytic/-voltaic applications. To further the possibility of fine-tuning the chemical properties of the suboxide, an understanding of the assembly of the building blocks of the polymer is of key importance. Thus, this thesis offers a theoretical study of the C_3O_2 monomer, analyzing its structural and chemical properties within the framework of DFT - where we propose the use of Crystal Orbital Overlap Populations (COOP) and Density of

States (DOS) - to see whether it can open up the door to a whole new class of LT 2D carbonaceous materials.

In parallel, we study the mechanisms involved in the growth of nanostructure materials, notably in the context of CIGS thin films. The latter are essential components[Liu+22; Yos+17] in the development of high-efficiency photovoltaic systems. Understanding the growth process of these thin films at the nanoscale can substantially improve their performance and scalability. To achieve even higher efficiencies, the limiting factors, e.g. the charge carrier recombination at various junctions (interfaces), have to be addressed. One such interface is the CIGS/Mo back contact, which is the first interface forming during the three-stage growth process of the CIGS absorber.

In addition, sodium from soda-lime glass diffuses into the CIGS absorber layer through this interface that is also the location for the formation of secondary phases of unknown composition [AH17]. To understand the atomic and electronic properties of the interfaces in thin-film solar cells, early growth dynamics have to be investigated. A suitable method to study these crystal growth is a tight-binding molecular dynamics (TBMD) [GBS17] approach. TBMD methods have been used to study nucleation and growth of 2D materials like graphene, silicine, and transition metal dichalcogenides [ABD06; KK04]. These methods are more accurate than kinetic Monte Carlo (kMC) simulations since there is no need to provide rates of the elementary processes a priori. This approach comes in mid-way between *ab-initio* MD and kMC techniques in terms of computational cost and system sizes that can be studied. Within TBMD, finite temperature dynamics of the atoms are computed by Newton's equations of motion, while interatomic forces are calculated using the tight-binding (TB) approach. Using TBMD, the dynamics of a large system can be studied for hundreds of picoseconds, mimicking the experimental conditions as closely as possible.

In this work, we address the underlying kinetics of the growth of thin-films employing a TBMD method. We have performed static and dynamical computations to understand the early stages of growth of CIGS absorber layer on $MoSe_2$ substrate. The primary focus of this thesis is on the first stage of the 3-stage growth process of CIGS in which an In_2Se_3 layer is formed on the $MoSe_2$ substrate. The results of the present study provide new insights into the early stages of growth of CIGS thin-films which could be of interest to research groups active in the field of designing photovoltaic systems. The understanding of these early stages of growth mechanisms can be applied to other thin-film growth processes as well.

The main objectives of this thesis are to first implement and validate the SCAN functional within the PAW formalism in the CP-PAW code base and ,secondly, to

offer a structural analysis of C_3O_2 and the growth dynamics of CIGS thin films. By achieving the latter two we hope to augment the theoretical tools available for investigating complicated molecular and nanostructure materials and contribute with new insights into possible practical applications.

The structure of the thesis is as follows. First, we set the foundations by elaborating on the theories and techniques involved in DFT in Sec. 2. This is followed by an extensive overview of the PAW method in Sec. 3. In Sec. 5 we give an introduction to Reduced Density-Matrix Functional Theory (RDMFT) in accompaniment of a theoretical overview of the Adaptive Cluster Approximation (ACA) to allow for a high-level study of the C_3O_2 monomer. The theoretical backbone of this thesis will be followed by a study of C_3O_2 on the DFT and RDMFT+ACA level respectively in Sec. 4 and a study on the growth of nanostructure materials in Sec. 6. We finish with conclusory remarks in Sec. 7. Unless otherwise stated we will be using atomic units.

2

Density Functional Theory

In Density Functional Theory (DFT) we seek to replace the arduous N-electron wave function $|\Psi(x_1, ..., x_n)\rangle$ with its Schrödinger equation by a single three-dimensional density $\rho(r)$. Any property of a system can then be treated as a unique functional of that density, in particular the ground state density $\rho_{\mathrm{gs}}(r)$. The object of this chapter is to outline density functional theory as a technique for many-particle systems and we structure it as follows: we give the existence proofs by Hohenberg and Kohn for functionals of the ground state densities as mentioned above in Sec. 2.1. In Sec. 2.2 we elaborate on the Kohn-Sham (KS) method, that replaces the interacting system with a complementary non-interacting system, as well as on exchange-correlation functionals, that play the role of retaining all the many-particle effects of the original system in the non-interacting KS approach. Finally, Sec. 2.3 deals with the Levy constrained-search formulation, a way for finding the wave function associated with the ground state.

2.1 Hohenberg-Kohn Theorems

Though the historic foundation can be found with Thomas and Fermi, who then sought to prove that the kinetic and potential energy can be put into direct relation to the electron probability density ρ, or rather to $\rho(r)$, the electron density at point r for a system of N electrons[AF11], it wasn't until Hohenberg-Kohn, that the assumptions and approximatinos set by Thomas-Fermi were rigorously proven and DFT became an exact theory. These assumptions being that the electron density determines all properties of a system and that the total energy is uniquely determined by ρ using the Variation Principle. Note that in the original formulation the densities had to be v-representable. Only later did Levy [Lev79b] extend this to be valid for the weaker condition of N-representability. For the full proof refer to the original paper of Hohenberg-Kohn[HK64] or, for example, the works of Atkins and Friedman[AF11] or Parr and Yang[PW94].

Prior to the introduction of DFT, in particular the proofs given by HK, the two ingredients needed to solve the Hamiltonian for an electronic system of form[PW94]

$$\hat{H} = \sum_{i}^{N}(-\frac{1}{2}\nabla_i^2) + \sum_{i}^{N} v(r_i) + \sum_{i<j}^{N} \frac{1}{r_{ij}} \tag{2.1}$$

were the total number of electrons N and the external potential $v(r)$ as these fix the Hamiltonian given in Eqn. 2.1. The idea of the first HK theorem then was to prove that both N and $v(r)$ (within an additive constant) can be determined by ρ, thus proving that the wave function and in fact all properties of a system given by Eqn. 2.1 can be determined by the latter. The first theorem of HK states that the external potential of an interacting system with Hamiltonian of form (2.1) is uniquely determined by its ground state density. To prove this, consider two external potentials v_{ext} and v'_{ext}, differing from each other by more than a constant but leading to the same ground state density ρ_{gs}. Each external potential determines uniquely different Hamiltonians $\hat{H}$ and $\hat{H}'$ with their respective ground state wave functions $|\Psi_{\mathrm{gs}}\rangle$ and $|\Psi'_{\mathrm{gs}}\rangle$. Assuming a non-degenerate ground state [HK64] we have for the system of Hamiltonian $\hat{H}$

$$\begin{aligned} E_{\mathrm{gs}} = \langle\Psi_{\mathrm{gs}}|\hat{H}|\Psi_{\mathrm{gs}}\rangle < \langle\Psi'_{\mathrm{gs}}|\hat{H}|\Psi'_{\mathrm{gs}}\rangle &= \langle\Psi'_{\mathrm{gs}}|\hat{H}'|\Psi'_{\mathrm{gs}}\rangle + \langle\Psi'_{\mathrm{gs}}|\hat{H} - \hat{H}'|\Psi'_{\mathrm{gs}}\rangle \\ &= E'_{\mathbf{gs}} + \int \mathrm{d}r[v_{ext} - v'_{ext}]\rho_{\mathrm{gs}}. \end{aligned} \tag{2.2}$$

However, analogously, for $\hat{H}'$ we also have that

$$\begin{aligned} E'_{\mathrm{gs}} = \langle\Psi'_{\mathrm{gs}}|\hat{H}'|\Psi'_{\mathrm{gs}}\rangle < \langle\Psi_{\mathrm{gs}}|\hat{H}'|\Psi_{\mathrm{gs}}\rangle &= \langle\Psi_{\mathrm{gs}}|\hat{H}|\Psi_{\mathrm{gs}}\rangle - \langle\Psi_{\mathrm{gs}}|\hat{H} - \hat{H}'|\Psi_{\mathrm{gs}}\rangle \\ &= E_{\mathbf{gs}} - \int \mathrm{d}r[v_{ext} - v'_{ext}]\rho_{\mathrm{gs}}. \end{aligned} \tag{2.3}$$

Adding Eqns. 2.2 and 2.3 we have the contradiction

$$E_{\mathrm{gs}} + E'_{\mathrm{gs}} < E_{\mathrm{gs}} + E'_{\mathrm{gs}}, \tag{2.4}$$

The second theorem of HK postulates the existence of a universal energy functional $E[\rho]$[AF11; Mar04; HK64]

$$E[\rho] = E_{\mathrm{HK}}[\rho] + \int \rho(r)v(r)\mathrm{d}r = T[\rho] + V_{\mathrm{ee}}[\rho] + \int \rho(r)v(r)\mathrm{d}r, \tag{2.5}$$

whose minimum is the ground state energy of a system with external potential v_{ext}. In Eqn. 2.5 $T[\rho]$ is the kinetic energy

$$T[\rho] = \sum_i f_i \left\langle \Psi_i(x_1, ..., x_n)\right| - \frac{1}{2}\nabla^2 \left|\Psi_i(x_1, ..., x_n)\right\rangle, \tag{2.6}$$

V_{ee} the total electron-electron repulsion energy

$$V_{ee} = \int\int \frac{\rho(r)\rho(r')}{|r-r'|}\mathrm{d}r\mathrm{d}r', \tag{2.7}$$

and E_{HK} is defined independently of $v(r)$ and thus is a universal functional of ρ [PW94]. Universality refers to the fact that E_{HK} is the same for both a single atom or a large molecule. While the HK theorem shows that any property of a molecule can be computed using the gs electron density ρ_{gs}, to actually find ρ_{gs} one applies the HK variational theorem that states that an energy functional $E_{gs}[\rho']$ with the corresponding trial density ρ' cannot be less than the true gs energy $E_0[\rho]$[AF11]. To arrive at the gs electron density ρ_{gs} then, we can apply the variational theorem for an arbitrary wave function and determine the corresponding energy using

$$\rho(r) = \sum_n f_n \langle\Psi_n|r\rangle \langle r|\Psi_n\rangle \tag{2.8}$$

or in terms of a single Slater determinant constructed from N orbitals ϕ_n as

$$\rho(r) = \sum_n f_n|\phi_n|^2, \tag{2.9}$$

where f_n is the occupation of the state. The variation of the above trial density then must satisfy the stationary principle[AF11; PW94]

$$\delta\{E[\rho] - \mu\int\rho(r)\mathrm{d}r\}|_{\int\rho(r)\mathrm{d}r-N=0} = 0, \tag{2.10}$$

where we constrained the density to the number of electrons N in the system and the Lagrange multiplier μ is the chemical potential, also called the *Fermi energy* in the zero-temperature limit. ρ_{gs} thus must satisfy the Euler-Lagrange equation

$$\mu = \frac{\delta E[\rho]}{\delta\rho(r)} = v(r) + \frac{\delta E_{HK}[\rho]}{\delta\rho(r)}, \tag{2.11}$$

which presents the basis of the density-functional theory. It is to note here that the HK theorems were dealing with systems at temperature T=0. For the theorems of HK to carry over to systems of non-zero temperatures we have to construct the density associated with the thermal ensemble. This was done by Mermin [Mer65] in 1965. Given a system of N electrons and density matrices $\rho^{(N)}$, Mermin constructed a grand potential as a functional of the latter given by [Mer65; Mar04]

$$\Omega[\rho^{(N)}] = \mathrm{Tr}\,\rho^{(N)}[(\hat{H} - \mu\hat{N}) + \frac{1}{\beta}\ln\rho^{(N)}]. \tag{2.12}$$

He found the minimum to be the equilibrium grand potential

$$\Omega = \Omega[\rho_0^{(N)}] = -\frac{1}{\beta}\ln\mathrm{Tr}\exp(-\beta(\hat{H} - \mu\hat{N})), \tag{2.13}$$

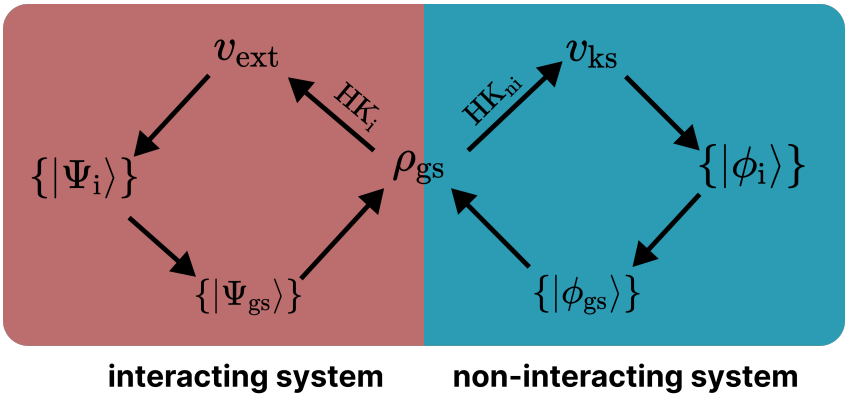

Fig. 2.1.: A schematic overview of the HK and KS theorems showing that a non-interacting system can be constructed that shares the same ground state density ρ_{gs} as the interacting system and, thus, the non-interacting KS representation of the full many-body problem can determine all properties of the latter. $\mathrm{HK_i}$ and $\mathrm{HK_{ni}}$ indicate the application of the HK theorems for the interacting and non-interacting systems, respectively, and the $|\phi\rangle$ refer to the wave functions of the non-interacting system (in Sec. 2.2, however, still denoted as $|\Psi\rangle$).

where $\rho_0^{(N)}$ is the grand canonical density matrix

$$\rho_0^{(N)} = \frac{\exp(-\beta(\hat{H} - \mu\hat{N}))}{\mathrm{Tr}\exp(-\beta(\hat{H} - \mu\hat{N}))}. \tag{2.14}$$

While the extensions of the HK theorems by Mermin are more compelling in the sense that they also allow for example for the formulation of the entropy as a functional of the equilibrium density, the Mermin functional has not been widely used - in particular due to the added difficulty and complexity when it comes to constructing approximate functionals of the entropy[Mar04].

2.2 From Kohn-Sham to Exchange-Correlation Functionals

Although the theorems established by Hohenberg and Kohn provide an exact theoretical structure, the complexity of many-body interactions compels the need for approximations for practical applications. It was Kohn and Sham (KS) [KS65] that developed an approximate approach to DFT that retains exactness for systems with slowly varying or high densities. The proposition for the KS method is to reframe the complexity of the many-body problem of interacting electrons into a system of noninteracting particles, see Fig. 2.1. The main idea being that it is feasible to reproduce the exact gs density ρ_{gs} of the original interacting many-electron system using a noninteracting system whilst keeping the same external potential. Note here

that the noninteracting character of the method stems from the KS expression of the kinetic energy functional [PW94]

$$T_s[\rho] = \sum_i \langle\psi_i| -\frac{1}{2}\nabla^2|\psi_i\rangle\,, \tag{2.15}$$

in which any interaction is ignored by setting $f_i = 1$, see Eqn. 2.6, for N orbitals ψ_i and $f_i = 0$ for the rest. The total energy in the KS system is defined as [PW94; AF11]

$$E[\rho] = T_s[\rho] + \int v_{\text{ext}}(r)\rho(r)\mathrm{d}r + \frac{1}{2}\int\int \frac{\rho(r)\rho(r')}{|r-r'|}\mathrm{d}r\mathrm{d}r' + E_{\text{XC}}[\rho], \tag{2.16}$$

where $E_{\text{XC}}[\rho]$ is the exchange-correlation energy. It contains the difference between T, the kinetic energy of the original interacting system, and T_s, as well as the non-classical part of V_{ee}[Pau94]. The Euler equation in Eqn. 2.11 can now be written as

$$\begin{aligned}\mu &= \frac{\delta E[\rho]}{\delta\rho(r)} = v_{\text{ext}}(r) + \int \frac{\rho(r')}{|r-r'|}\mathrm{d}r' + \underbrace{\frac{\delta E_{\text{XC}}[\rho]}{\delta\rho(r)}}_{v_{\text{exc}}} + \frac{\delta T_s[\rho]}{\delta\rho(r)} \\ &= v_{\text{eff}}(r) + \frac{\delta T_s[\rho]}{\delta\rho(r)}.\end{aligned} \tag{2.17}$$

To obtain the density $\rho(r)$ for a given $v_{\text{eff}}(r)$, that satisfies Eqn. 2.17 we need to solve the N one-electron equations

$$[-\frac{1}{2}\nabla^2 + v_{\text{eff}}(r)]\psi_i = \epsilon_i\psi_i, \tag{2.18}$$

where

$$\hat{H}_{ni} = -\frac{1}{2}\nabla^2 + v_{\text{eff}}(r) \tag{2.19}$$

is the Hamiltonian of the non-interacting system. Because v_{eff} depends on $\rho(r)$, the above equations must be solved self-consistently, i.e. to start with an initial guess for $\rho(r)$ to construct v_{eff} with Eqn. 2.17 and then find a new $\rho(r)$ using Eqn. 2.18 and

$$\rho(r) = \sum_i \langle\psi_i|r\rangle\,\langle r|\psi_i\rangle\,. \tag{2.20}$$

Because the complexity of the electron-electron interactions of an N-electron system are contained in the exchange-correlation functional $\mathrm{E_{XC}}[\rho]$, the latter forms a crucial component of the KS scheme. For practical calculations, the density functional has to be approximated, and thus the task becomes to find the $\mathrm{E_{XC}}[\rho]$ functional and its corresponding exchange-correlation potential $\mathrm{v_{exc}}(r)$. The main source for errors

arising in DFT comes to be from the attempts to approximate $\mathrm{E_{XC}}[\rho]$[1]. To account for exchange and correlation contributions separately, $\mathrm{E_{XC}}[\rho]$ can be separated into

$$E_{\mathrm{XC}}[\rho] = E_{\mathrm{X}}[\rho] + E_{\mathrm{C}}[\rho]. \tag{2.21}$$

The origin of the exchange energy in Eqn. 2.21 is the Pauli exclusion principle[Pau94; httb]. In particular, because in Quantum Mechanics we don't know the exact position of electrons, when it comes to calculating the energy of an orbital, what we actually compute is the average of the energy taken over all possible positions of the electron with the corresponding configuration weighting. The exchange energy $\mathrm{E_X}[\rho]$ is then simply the difference between that particular average energy accounting for the exclusion principle and one in which it is ignored. The exchange energy for electrons is thus always negative, because the (average) energy conforming to the Pauli principle is the energetically preferred state[Pau94].

On the other hand, given the Hartree-Fock (HF) energy $\mathrm{E_{HF}}$ within a complete basis $\{\phi\}$, the correlation energy is defined as the difference between the exact energy E and $\mathrm{E_{HF}}$ [PW94]

$$E_{\mathrm{C}} = E - E_{\mathrm{HF}} \tag{2.22}$$

Given Eqn. 2.22 the correlation energy can be construed as the shortcomings of the HF approach[HG11; htta]. These shortcomings are conventionally referred to as static and dynamic correlation. The latter refers to the fact that the HF approach does not account for the instantaneous interactions of the electrons with each other, but rather treats each electron as if it's interacting with the average created by the remaining N-1 electrons. The static correlation comes to be because the choice of a single Slater determinant for the representation of the wave function in the HF approach is a lacking representation. Static correlation is then the difference between the single Slater determinant and a linear combination of Slater determinants that would otherwise be necessary to give a good description of a many-electron state[HG11; htta]. Because both correlation effects stem from the same interaction it is near impossible to keep them separate, and are rather additively referred to as $\mathrm{E_C}$, see Eqn. 2.21.

The research on finding new and better approximations of the exchange-correlation functional is very active. In the following we will mention a few classes of these approximations.

[1] Due to the approximate nature of $\mathrm{E_{XC}}[\rho]$ it cannot be regarded as an upper bond for the true energy.

In the *Local Density Approximation* (LDA) we assume that the exchange-correlation energy per particle $\epsilon_{\mathrm{XC}}(\rho(r))$ is only dependent on the local density. Thus, we can express the exchange-correlation energy as

$$E_{\mathrm{XC}}^{\mathrm{LDA}}[\rho] = \int \rho(r)\epsilon_{\mathrm{XC}}(\rho(r))dr. \tag{2.23}$$

Note in Eqn. 2.23 that we also assume the electron distribution of the system to be homogeneous. To account for inhomogeneities in $\rho(r)$ we go into *Generalized Gradient Approximation* (GGA) functionals that, in addition to the local density, also consider its gradient $\nabla\rho(r)$

$$E_{\mathrm{XC}}^{\mathrm{GGA}}[\rho, \nabla\rho] = \int f(\rho(r), \nabla\rho(r))dr. \tag{2.24}$$

The most widely used PBE [PBE96] functional falls into this category of functionals. *Meta-GGA* functionals improve on that further by incorporating the kinetic energy density

$$\tau = \sum_i n_i |\nabla\phi_i|^2, \tag{2.25}$$

where ϕ_i and n_i are the orbitals and their occupation numbers, respectively. Thus, we have

$$E_{\mathrm{XC}}^{\mathrm{meta-GGA}}[\rho, \nabla\rho, \tau] = \int f(\rho(r), \nabla\rho(r), \tau(r))dr. \tag{2.26}$$

An example of such a meta-GGA functional is the SCAN functional by Perdew et al. [SRP15b], which satisfies all known exact meta-GGA constraints.

Another class of exchange-correlation functionals are called *Hybrid Functionals*. They incorporate a part of exact exchange from Hartree-Fock theory with a DFT functional

$$E_{\mathrm{XC}}^{\mathrm{hybrid}}[\rho] = \alpha E_{\mathrm{X}}^{\mathrm{HF}}[\rho] + (1-\alpha)E_{\mathrm{X}}^{\mathrm{DFT}}[\rho], \tag{2.27}$$

where α is a mixing parameter. See Sec. 4.4 for more details and examples.

The proper choice of the exchange-correlation functional critically affects the accuracy of DFT calculations. Although LDA and GGA functionals strike a good balance between accuracy and computational efficiency, higher level functionals like meta-GGA and hybrids offer improved accuracy for numerous systems. With the development and implementation of these functionals, as has been done for the SCAN functional into the CP-PAW code in this work, advances to the application of DFT to various complex systems can be made.

2.3 The Levy constrained-search formulation

Having shown the existence of the one-to-one mapping between the ground-state electron density ρ_{gs} and the ground-state wave function $|\Psi_{gs}\rangle$, in this section we want to highlight the constrained search formulation by Levy [Lev79a; Lev82; Mar04; PW94] to determine $|\Psi_{gs}\rangle$ from a given ground-state density. Let S_i be the subset of the full N-electron Hilbert Space, where we have

$$\{|\Psi\rangle \in S_i | \, |\Psi\rangle \to \rho_i\}, \tag{2.28}$$

i.e. the subset of all wave functions integrating to a density ρ_i, see Fig. 2.2. Because there is an infinite number of antisymmetric wave functions in Eqn. 2.28 that give the same density, we have that $|\Psi_{\rho_{gs}}\rangle$ is not necessarily equal to $|\Psi_{gs}\rangle$, $|\Psi_{\rho_{gs}}\rangle$ being any wave function whose quadrature is the ground-state density ρ_{gs}. Thus, given the minimum-energy principle for the ground-state of an N-electron system we have that [PW94; Mar04]

$$E_{gs} = \langle\Psi_{gs}|\hat{T} + \hat{V}_{ee} + \sum_i^N v(r_i)|\Psi_{gs}\rangle \leq \langle\Psi_{\rho_{gs}}|\hat{T} + \hat{V}_{ee} + \sum_i^N v(r_i)|\Psi_{\rho_{gs}}\rangle \tag{2.29}$$

Because the potential energy caused by $v_{ext}(r)$ is a functional of ρ, see Sec. 2.1, we can rewrite the above equation as

$$\langle\Psi_{gs}|\hat{T} + \hat{V}_{ee}|\Psi_{gs}\rangle + \int v_{ext}(r)\rho_{gs}\mathrm{d}r \leq \langle\Psi_{\rho_{gs}}|\hat{T} + \hat{V}_{ee}|\Psi_{\rho_{gs}}\rangle + \int v_{ext}(r)\rho_{gs}\mathrm{d}r. \tag{2.30}$$

Thus, we have that

$$\langle\Psi_{gs}|\hat{T} + \hat{V}_{ee}|\Psi_{gs}\rangle \leq \langle\Psi_{\rho_{gs}}|\hat{T} + \hat{V}_{ee}|\Psi_{\rho_{gs}}\rangle\,, \tag{2.31}$$

and we can identify the ground state $|\Psi_{gs}\rangle$ of any set such as in Eqn. 2.28 as the one that minimizes the right-hand side of Eqn. 2.31. Note here that at the minimum of the total energy of the system in a given external potential $v_{ext}(r)$ the Levy functional must equal the HK functional

$$\begin{aligned} E_{\mathrm{HK}}[\rho_{gs}] &= \langle\Psi_{gs}|\hat{T} + \hat{V}_{ee}|\Psi_{gs}\rangle \\ &= \min_{\Psi\to\rho_{gs}} \langle\Psi|\hat{T} + \hat{V}_{ee}|\Psi\rangle \end{aligned} \tag{2.32}$$

since the density of the minimum is v-representable, i.e. can be generated by the given external potential. Eqn. 2.32 searches over all wave functions of the N-electron Hilbert Space that integrate into a desired ρ_{gs} and thus finds the minimum of $\langle\hat{T} + \hat{V}_{ee}\rangle$. This defines Levy's *constrained-search* for $E_{\mathrm{HK}}[\rho_{gs}]$. This is different than the "constrained" formulation in HK, which only exerted a normalization

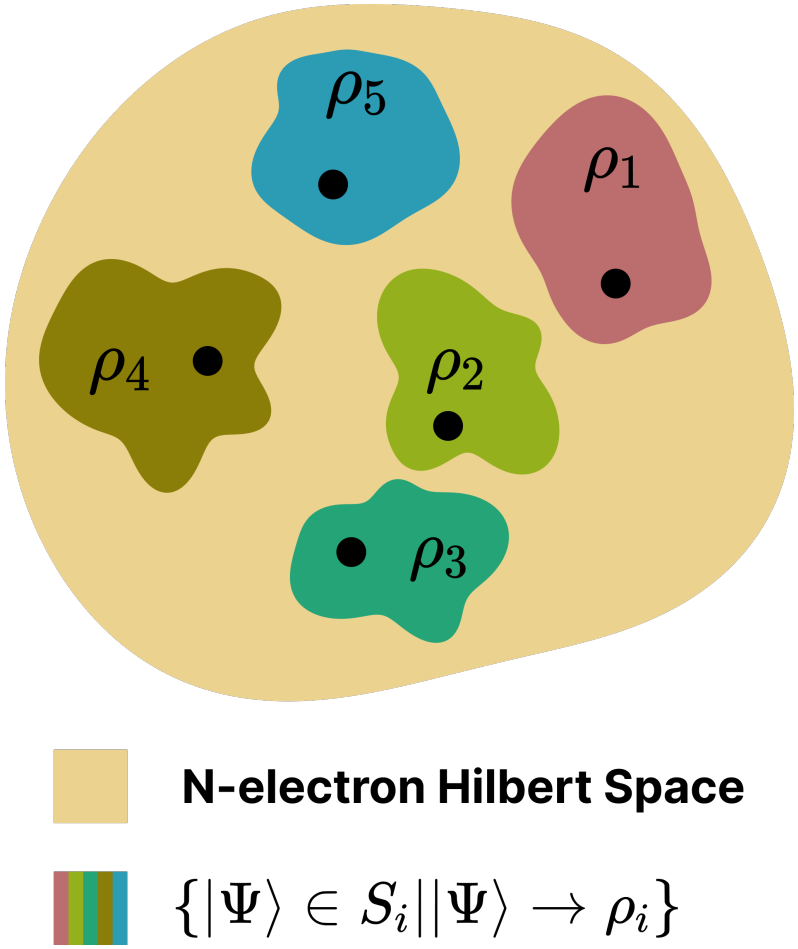

Fig. 2.2.: Partition of the full N-electron Hilbert Space in the Levy Constrained Search Formulation. Each colored area depicts the set of all Ψ that integrate to a particular ρ_i. The search for the minimum in Eqn. 2.32 for a ρ_i is constrained to the associated set S_i with this ρ_i and all its wave functions, i.e. $\{\Psi \in S_i | \Psi \rightarrow \rho_i\}$. The minimum is established by only one such point in each subset (black dot).

constraint, see Eqn. 2.10, but still searched the entirety of the N-electron Hilbert Space. Additionally, unlike in HK, the Levy constrained search lifts the requirement of v-representable densities and allows the densities to be searched over instead to fulfil only the weaker constraint of N-representability, i.e. any density that is non-negative, normalizes to the total number of electrons N and is square-integrable (continuous)[PW94; Lev79a].

3

Projector Augmented Wave Method

Following the introduction on DFT in the previous chapter and the difficulties it encounters, in particular when dealing with singularities at the positions of the atomic nuclei in the KS equations, we turn our attention to a method that addresses these issues - the Projector Augmented Wave (PAW) method [Blö94a]. The main premise of the PAW method is to generalize both the pseudo-potential (PP) and the linear augmented plane-wave (LAPW) methods. To solve the Kohn-Sham equations and the above mentioned problem that the potential has singularities at the atomic nuclei, there are different ways to deal with this. One option is to apply the PP approximation to get rid of the singularities and make descriptions of the Kohn-Sham states with simple basis sets possible. Alternatively, a sophisticated basis set can be utilized to get a representation on the basis of a potential including the singularities.

In addition to bridging the gap between the PP and LAPW methods, the PAW method also provides the full wave function (WF) because it is an all-electron (AE) method and this wave function is not accessible in pure PP methods. Furthermore, the PAW method enables energy-conserving molecular dynamics (MD) simulations which are done using the original fictitious Lagrangian approach by Car-Parrinello[CP85a].

As the present work is not concerned with MD simulations, interested readers may refer to the original paper by Bloechl [Blö94a] for further details.

The wave function of real compounds has distinct signatures in different regions of space. It is smooth in the bonding region and oscillating near the nucleus due to the strong attractions by the nucleus. The difficulty for electronic structure methods is to do well in both regions. In augmented wave methods the idea is to split the wave function into parts: (i) some partial wave expansion within an atom centered sphere and (ii) envelope functions expanded in either plane-waves or some other convenient basis set. Values and derivatives are matched at interfaces of the atom-centered and bonding regions.

Consider the Hilbert space of all wave functions orthogonal to the core states

$$|\Psi^c\rangle \perp |\Psi_n\rangle \in \mathcal{H}. \tag{3.1}$$

The physically relevant wave functions in this particular Hilbert Space exhibit strong oscillations, which make a numerical treatment very difficult. The objective is to transform these wave functions into so-called pseudo (PS) wave functions that live in a PS Hilbert space, i.e.

$$|\tilde{\Psi}_n\rangle \in \mathcal{H}^{PS}. \tag{3.2}$$

This will be a linear transformation of the physically relevant AE wave functions into computationally convenient PS wave functions. By AE wave functions we are referring to a full one-electron wave function, not a many-electron wave function.

To follow the original notation of the paper, we refer to the density as $n(r)$, as opposed to $\rho(r)$, as has been done in the rest of this thesis.

3.1 Transformation

Given an explicit expression of the linear transformation $\mathcal{T}$ from $|\tilde{\Psi}\rangle$ to $|\Psi\rangle$

$$|\Psi\rangle = \mathcal{T}\,|\tilde{\Psi}\rangle\,, \tag{3.3}$$

the relevant physical observables can be obtained as

$$\langle A\rangle = \langle\tilde{\Psi}|\,A\,|\Psi\rangle \tag{3.4}$$

after the transformation or simply as

$$\langle A\rangle = \langle\tilde{\Psi}|\,\tilde{A}\,|\tilde{\Psi}\rangle = \langle\tilde{\Psi}|\,\mathcal{T}^\dagger A\mathcal{T}\,|\tilde{\Psi}\rangle \tag{3.5}$$

in $\mathcal{H}^{PS}$. Similarly, the total energy can be evaluated as a functional of the PS wave function and the ground state PS wave function can be obtained using the derivative of the energy with respect to the PS wave function, i.e.

$$\frac{\partial E[\mathcal{T}\,|\tilde{\Psi}\rangle]}{\partial\,\langle\tilde{\Psi}|} = \epsilon\mathcal{T}^\dagger\mathcal{T}\,|\tilde{\Psi}\rangle\,. \tag{3.6}$$

The objective is to select a linear transformation that will exploit the characteristics of particular atom types. As such only transformations that differ from identity by some local sum centered around atoms are considered, i.e.

$$\mathcal{T} = 1 + \sum_R \hat{\mathcal{T}}_R, \tag{3.7}$$

where $\hat{\mathcal{T}}_R$ only acts within some augmentation region Ω_R and is otherwise 0. This indicates that AE and PS wave functions are identical outside the augmentation regions, because outside, the transformation is equivalent to the identity, see Eqn. 3.7.

The present question then is: How do we define these local $\hat{\mathcal{T}}_R$? This is done by having a set of initial, smooth functions $|\tilde{\phi}_i\rangle$, so-called PS partial waves (PW), and specifying $\hat{\mathcal{T}}_R$ in such a way that a specific target AE partial wave $|\phi_i\rangle$ is attained:

$$|\phi_i\rangle = (1 + \hat{\mathcal{T}}_R)\,|\tilde{\phi}_i\rangle\,. \tag{3.8}$$

In his original paper Blöchl refers to the solutions of the Schrödinger equation of each particular isolated atom as a good and natural choice for the AE WFs. Note here, that the index i in Eqn. 3.8 is a onverted index that refers to the atomic site R, the angular momentum quantum numbers $L = (l, m)$ and an additional label n that differentiates partial waves on the same site and with the same angular momentum, thus

$$i = (R, L = (l, m), n). \tag{3.9}$$

The PS PWs $|\tilde{\phi}_i\rangle$ of Eqn. 3.8 must fulfill two conditions: (i) they must be identical to the AE PWs outside the augmentation region

$$|\phi_i\rangle = |\tilde{\phi}_i\rangle \;\textit{,if}\; |\tilde{\phi}_i\rangle \notin \Omega_R \tag{3.10}$$

and (ii) they should form a complete set $\{|\tilde{\phi}_i\rangle\}$ within the augmentation region. Within Ω_R every PS wave function can be expanded into PS partial waves

$$|\tilde{\Psi}\rangle = \sum_i |\tilde{\phi}_i\rangle\, c_i. \tag{3.11}$$

Using Eqn. 3.8 we have

$$|\Psi\rangle = \mathcal{T}\,|\tilde{\Psi}\rangle = \sum_i |\phi_i\rangle\, c_i \tag{3.12}$$

where the coefficients c_i in Eqns. 3.11 and 3.12 are identical within Ω_R. Appending a zero term to Eqn. 3.12 we can rewrite the equation as

$$|\Psi\rangle = |\tilde{\Psi}\rangle - \sum_i |\tilde{\phi}_i\rangle\, c_i + \sum_i |\phi_i\rangle\, c_i. \tag{3.13}$$

Given the requirement of the transformation $\mathcal{T}$ to be linear, the coefficients must be linear functionals of the PS WFs. This is analogous to stating that the coefficients are scalar products

$$c_i = \langle \tilde{p}_i | \tilde{\Psi} \rangle \tag{3.14}$$

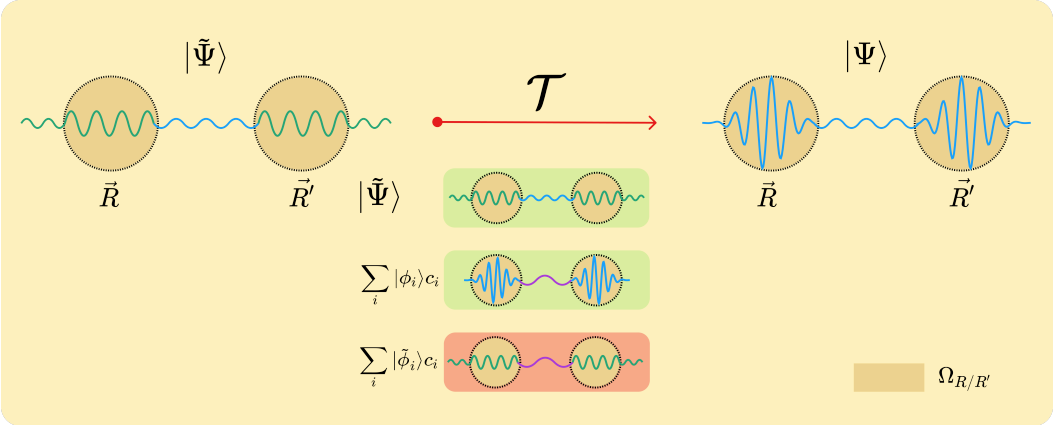

Fig. 3.1.: Simplified macro overview of the transformation process in the PAW method. $\Omega_{R,R'}$ is referring to the augmentation region of each site.

of the PS WFs, where $\langle\tilde{p}_i|$ are fixed functions, called projector functions. It follows from Eqn. 3.14 that there is exactly one projector function for each PS PW. Using Eqn. 3.14 in 3.11 gives us

$$|\tilde{\Psi}\rangle = \sum_i |\tilde{\phi}_i\rangle \langle\tilde{p}_i|\tilde{\Psi}\rangle \,. \tag{3.15}$$

$\langle\tilde{p}_i|$ must fulfill

$$\sum_i |\tilde{\phi}_i\rangle \langle\tilde{p}_i| = 1, \tag{3.16}$$

so that the one-center expansion

$$|\tilde{\Psi}\rangle = \sum_i |\tilde{\phi}_i\rangle \langle\tilde{p}|\tilde{\Psi}\rangle \tag{3.17}$$

is equal to the PS WF itself. It follows from this that

$$\langle\tilde{p}_i|\tilde{\phi}_j\rangle = \delta_{i,j}, \tag{3.18}$$

with $\delta_{i,j}$ as the Kronecker-Delta. This is easily seen by multiplying Eqn. 3.16 with $|\tilde{\phi}_j\rangle$.

Lastly, using Eqns. 3.3, 3.8, 3.11 and 3.14 the one-electron wave function can be expressed as

$$|\Psi\rangle = \mathcal{T}|\tilde{\Psi}\rangle = |\tilde{\Psi}\rangle + \sum_i |\phi_i\rangle c_i - \sum_i |\tilde{\phi}_i\rangle c_i \tag{3.19}$$

$$= |\tilde{\Psi}\rangle + \sum_i |\phi_i\rangle \langle\tilde{p}_i|\tilde{\Psi}\rangle - \sum_i |\tilde{\phi}_i\rangle \langle\tilde{p}_i|\tilde{\Psi}\rangle \tag{3.20}$$

$$= |\tilde{\Psi}\rangle + \sum_i (|\phi_i\rangle - |\tilde{\phi}_i\rangle) \langle\tilde{p}_i|\tilde{\Psi}\rangle \,, \tag{3.21}$$

see Fig. 3.1 for a graphical representation of the transformation. This results in an

expression of the transformation of the following form:

$$\mathcal{T} = 1 + \sum_i (|\phi_i\rangle - |\tilde{\phi}_i\rangle) \langle \tilde{p}_i| \,. \tag{3.22}$$

Based on Eqn. 3.22 the issue of the operators can be addressed next.

3.2 Operators

The aim is to obtain observable quantities as the expectation values of the PS WFs. Similarly to Eqn. 3.21 in which a representation of the wave function in the PS Hilbert space has been defined, a pseudo representation of the operators is given in the following. The expectation value of any operator A can be expressed as

$$\langle A \rangle = \sum_n f_n \langle \Psi_n | A | \Psi_n \rangle \,. \tag{3.23}$$

Using Eqn. 3.21 the same can be expressed in the PS Hilbert space as

$$\langle A \rangle = \sum_n f_n \langle \tilde{\Psi}_n | \underbrace{\mathcal{T}^\dagger A \mathcal{T}}_{\tilde{A}} | \tilde{\Psi}_n \rangle \,, \tag{3.24}$$

which directly gives a representation of the PS operator $\tilde{A}$ as

$$\tilde{A} = \mathcal{T}^\dagger A \mathcal{T} = A + \sum_{i,j} |\tilde{p}_i\rangle \left(\langle \phi_i | A | \phi_j \rangle - \langle \tilde{\phi}_i | A | \tilde{\phi}_j \rangle \right) \langle \tilde{p}_j | \,, \tag{3.25}$$

with

$$\sum_i |\tilde{\phi}_i\rangle \langle \tilde{p}_i| = 1 \tag{3.26}$$

inside Ω_R and

$$|\tilde{\phi}_i\rangle = |\phi_i\rangle \tag{3.27}$$

outside Ω_R. Eqn. 3.25 contains three parts: (i) the first part contains an operator that directly acts on the PS wave function and is evaluated in either real or reciprocal space and (ii-iii) the last two parts contain the projectors and the expectation value of the operator either between the AE or PS partial waves.

In addition to the general form of the PS operator $\tilde{A}$, another degree of freedom can be utilized by extending Eqn. 3.25 with a zero-term

$$\langle B - \sum_{i,j} |\tilde{p}_i\rangle \langle \tilde{\phi}_i | B | \tilde{\phi}_j \rangle \langle \tilde{p}_j | \rangle = 0, \tag{3.28}$$

where B is an arbitrary operator localized in the augmentation region. Eqn. 3.28 can be utilized in situations where the operator A cannot be easily evaluated in a plane-

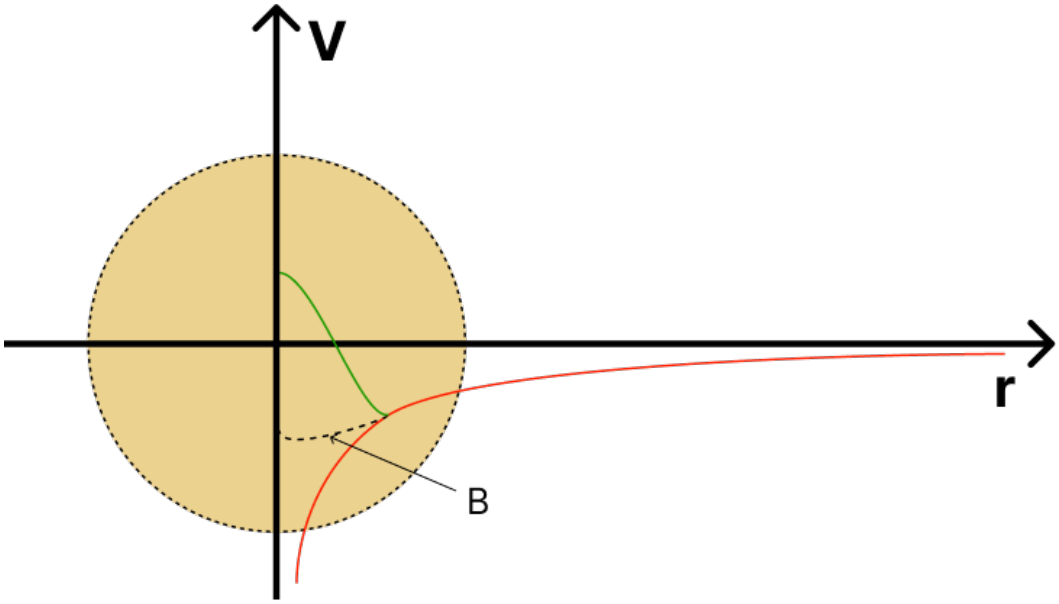

Fig. 3.2.: Construction of a localized operator B (dashed) in the case of the Coulomb Potential (red) and a new potential (green) that is identical to the Coulomb potential but smooth and continuous within the augmentation region.

wave expansion. One such example is the Coulomb potential with its singularity near the nucleus. In this case a new potential can be constructed that is identical to the true potential but is smooth and continuous inside the augmentation region, see Fig. 3.2. The difference between the new potential and true potential will be localized within Ω_R and can act as the operator B in Eqn. 3.28. Adding a potential with characteristics of the potential B to Eqn. 3.25 essentially cancels the singularity and results in an expression less sensitive to the truncation of the number of plane-waves.

Using the pseudo operator representation of Eqn. 3.25 all observables can be computed. In the case of the charge density $n(r)$, which is the expectation value of the real-space projection operator $|r\rangle\langle r|$ for any point r, we get an expression of $n(r)$ as

$$n(r) = \sum_n f_n \langle \tilde{\Psi}_n | r \rangle \langle r | \tilde{\Psi}_n \rangle = \tilde{n}(r) + n^1(r) - \tilde{n}^1(r), \tag{3.29}$$

where $\tilde{n}(r)$ is the contribution from the pseudo WF and $n^1(r)$ and $\tilde{n}^1(r)$ are the contributions from the expectation values with the AE and PS partial waves, respectively. It is important to remember that all of the charge density contributions also contain contributions from the core states $\sum_n \langle \phi_n^c | r \rangle \langle r | \phi_n^c \rangle$, $\sum_n \langle \tilde{\phi}_n^c | r \rangle \langle r | \tilde{\phi}_n^c \rangle$ and $\sum_n \langle \tilde{\Psi}_n^c | r \rangle \langle r | \tilde{\Psi}_n^c \rangle$. In practice, however, instead of getting the contribution from each core state a PS core density is constructed.

3.3 Total Energy

Similar to other expectation values, see Eqn. 3.29, the expression for the total energy can be split into smooth parts and one-center contributions. Thus, we have

$$\begin{aligned} E &= \sum_n f_n \langle \Psi_n | -\frac{1}{2}\nabla^2 | \Psi_n \rangle + \frac{1}{2}\int \mathrm{d}r \int \mathrm{d}r' \frac{(n+n^z)(n+n^z)}{|r-r'|} + \int \mathrm{d}r n \epsilon_{\mathrm{xc}}(n) \\ &= \tilde{E} + E^1 - \tilde{E}^1, \end{aligned} \tag{3.30}$$

where $\tilde{E}$ is the smooth part evaluated on regular grids in either Fourier or real-space and two one-center contributions evaluated on radial grids in an angular momentum representation. n^z is denoting the point charge density of the nucleus and ϵ_{xc} the energy per electron from exchange and correlation. Using atomic units the total energy contributions are given as

$$\begin{aligned} \tilde{E} &= \sum_n f_n \langle \tilde{\Psi}_n | -\frac{1}{2}\nabla^2 | \tilde{\Psi}_n \rangle + \frac{1}{2}\int \mathrm{d}r \int \mathrm{d}r' \frac{(\tilde{n}+\hat{n})(\tilde{n}+\hat{n})}{|r-r'|} \\ &+ \int \mathrm{d}r \tilde{n} \bar{v} + \int \mathrm{d}r \tilde{n} \epsilon_{\mathrm{xc}}(\tilde{n}) \end{aligned} \tag{3.31}$$

$$\begin{aligned} E^1 &= \sum_{n,i,j} f_n \langle \tilde{\Psi}_n | \tilde{p}_i \rangle \langle \phi_i | -\frac{1}{2}\nabla^2 | \phi_j \rangle \langle \tilde{p}_j | \tilde{\Psi}_n \rangle \\ &+ \frac{1}{2}\int \mathrm{d}r \int \mathrm{d}r' \frac{(n^1+n^z)(n^1+n^z)}{|r-r'|} + \int \mathrm{d}r n^1 \epsilon_{\mathrm{xc}}(n^1) \end{aligned} \tag{3.32}$$

$$\begin{aligned} \tilde{E}^1 &= \sum_{n,i,j} f_n \langle \tilde{\Psi}_n | \tilde{p}_i \rangle \langle \tilde{\phi}_i | -\frac{1}{2}\nabla^2 | \tilde{\phi}_j \rangle \langle \tilde{p}_j | \tilde{\Psi}_n \rangle \\ &+ \frac{1}{2}\int \mathrm{d}r \int \mathrm{d}r' \frac{(\tilde{n}^1+n^z)(\tilde{n}^1+n^z)}{|r-r'|} + \int \mathrm{d}r \tilde{n}^1 \bar{v} + \int \mathrm{d}r \tilde{n}^1 \epsilon_{\mathrm{xc}}(\tilde{n}^1). \end{aligned} \tag{3.33}$$

In Eqns. 3.31 and 3.33 $\bar{v}$ is an arbitrary potential localized within Ω_R. Additionally, we have that $\tilde{n} = \tilde{n}^1$ in Ω_R, so that the contribution of $\bar{v}$ to the total energy vanishes. It only contributes if the partial wave expansion is not complete to minimize truncation errors. $\hat{n}$ is a compensation charge density and it is expressed as a sum of generalized Gaussians and chosen such that it is localized in the augmentation region.

All the expressions derived so far have been exact - at least in the frozen core approximation. But to go from an exact formalism to a practical implementation requires the use of some approximations. Since the formalism requires certain completeness conditions of basis sets Blöchl introduced two approximations: (i) a plane-wave cutoff E_{PW} defined as the maximum of $G^2/2$ and (ii) truncating the sum of partial waves and projector functions to a finite number. Typical values for the above approximations are (i) 30Ry for the cutoff energy and (ii) one or two partial waves per site and angular momentum and a maximum angular momentum of

maybe $l = 1$ or $l = 2$. These approximations result in a new total energy functional E' and values are chosen in such a way that the new functional is sufficiently close to the exact functional E.

3.4 Notes on a practical implementation

To evaluate the exchange and correlation energy in Eqns. 3.32 and 3.33 Blöchl employs a technique from full-potential LMTO calculations, in which the corresponding energy density is expanded in the charge density with respect to its spherical part $n^1_{R,l=0}$:

$$\begin{aligned}\int \mathrm{d}r n^1_R \epsilon_{\mathrm{xc}}(n^1_R) &= \int \mathrm{d}r n^1_{R,l=0} \epsilon_{\mathrm{xc}}(n^1_{R,l=0}) \\ &+ \frac{1}{2} \sum_{L,l\neq 0} \int \mathrm{d}r \frac{\partial \mu_{\mathrm{xc}}(n^1_{R,l=0}}{\partial n^1_R} (n^1_{R,L})^2 \\ &+ \mathcal{O}((n^1_{R,L})^3), \end{aligned} \tag{3.34}$$

where $\mu_{\mathrm{xc}} = \frac{\mathrm{d}n\epsilon_{\mathrm{xc}}(n)}{\mathrm{d}n}$. $n^1_{R,L}$ denotes the angular momentum components of the one-center charge density. One-center contributions from the PS charge density are treated analogously to Eqn. 3.34. The Taylor expansion in Eqn. 3.34 introduces the necessity to define second and third order derivatives of the exchange and correlation energy. This has been done for the implementation of the SCAN functional [SRP15b] of Perdew et al. into the CP-PAW code base using the PAW formalism and the respective derivatives can be found in the Appendix.

4 Structural Analysis of C_3O_2 using the local hybrid functional PBE0r

Previously, we examined the Projector Augmented Wave method, investigating its effectiveness in dealing with the singularities at the atomic nuclei within the KS method. By closing the gap between pseudo-potential and LAPW methods, the PAW formalism has become an essential tool in computational chemistry. Expanding on this premise, we now transition to a detailed structural analysis of the C_3O_2 monomer, utilizing the local hybrid functional PBE0r within the CP-PAW framework. Here, we aim to explore the complexities of C_3O_2, making use of advanced computational techniques to provide insights into the characteristics of its electronic structure and bonding. Carbon suboxide, a molecule of considerable historical and chemical interest, presents particular challenges and opportunities for computational studies. It establishes itself as a suitable candidate for applications in organic electronics and photovoltaics due to its extended π-conjugated systems and its proclivity to form polymers. Thus, understanding its structure and electronic properties is pivotal in optimizing its performance in these applications. To enable such an analysis, we utilize the Carr-Parrinello approach [CP85b], integrating the PAW method with the PBE0r functional.

4.1 Car-Parrinello Lagrangian

Within the Carr-Parrinello method, introduced by Carr and Parrinello in 1985, we can concurrently evolve the electronic and ionic degrees of freedom, thus supplying a dynamic view on the structural attributes of both, molecules and materials. The Carr-Parrinello Lagrangian is a fundamental ingredient in molecular dynamics simulations, allowing for the simultaneous solution of the classical equations of motion for nuclei and the KS equations for electrons. This dual evolution is expressed by the following Lagrangian

$$\begin{aligned}\mathcal{L}_{\text{CP}} = \quad & \frac{1}{2}\sum_{I}^{N_n} M_I \dot{R}_I^2 + \sum_{i}^{N_e} \langle \dot{\phi}_i(t) | m_\psi | \dot{\phi_i}(t) \rangle \\ & - E_{\text{KS}}[\phi_i, R_I] \end{aligned} \tag{4.1}$$

where E_{KS} is the Kohn-Sham energy of the system and m_ψ is the fictitious mass of the wave function. m_ψ is not a mass in the same sense that m_e is, i.e. m_ψ is not simply used instead of the electron mass. For one, they have different dimensions as is evident from eqn. (4.1), [μ]=energy·time^2. Effectively though, μ takes on the same role as the mass, which is to say it controls the acceleration of the degrees of freedom of the KS wave functions[Mar04; Gio].

4.2 Wave Function Dynamics

As hinted at above, to solve the electronic problem and achieve the electronic ground state we use *Car-Parrinello Molecular Dynamics*[CP85b], i.e. propagating the orbitals as if they are particles and finding their minimum instead of repeatedly solving the electronic problem.

The total energy can be expressed as

$$\begin{aligned} E_{\text{tot}} = \quad & \sum_n f_n \langle \dot{\tilde{\Psi}}_n | \, m_\Psi \, | \dot{\tilde{\Psi}}_n \rangle + E_{\text{DFT}} \\ & - \sum_{n,m} \Big(\langle \tilde{\Psi} |_n \, \tilde{O} \, | \tilde{\Psi} \rangle_m - \delta_{n,m} \Big) \Lambda_{m,n}, \end{aligned} \tag{4.2}$$

with $\tilde{\Psi}$ as the pseudo wave functions of the PAW method, $\Lambda_{n,m}$ as the Lagrange parameters for the wave function orthonormality constraint and

$$\begin{aligned} E_{\text{DFT}} \quad = \quad & \sum_n \langle \Psi_n | - \frac{1}{2} \Delta^2 \, | \Psi_n \rangle \\ + \quad & \frac{1}{2} \int dr \int dr' \frac{(n(r) + n^Z(r))(n(r') + n^Z(r'))}{|r - r'|} \\ + \quad & \int dr n(r) \epsilon_{xc}(n_\sigma(r), \Delta n_\sigma(r)), \end{aligned} \tag{4.3}$$

where $n^Z(r) = -\sum_R Z_R \delta(r - R)$ is the density of the nuclei point charges. The minimization of (4.2) is performed with a Car-Parrinello-like constrained minimization to ensure the orthonormality of the wave functions, i.e. $\langle \psi_n | \psi_m \rangle = \delta_{n,m}$ and $\sum_i f_i = N$, the constraint for the number of particles, have to be fulfilled. The equation of motion for the wave functions is

$$m_\Psi \, | \ddot{\tilde{\Psi}}_n \rangle = -\tilde{H} \, | \tilde{\Psi}_n \rangle + \sum_m \tilde{O} \, | \tilde{\Psi}_m \rangle \, \Lambda_{m,n} - m_\Psi \, | \dot{\tilde{\Psi}}_n \rangle \, f_\Psi, \tag{4.4}$$

which is solved by discretizing the time coordinate and choosing the Lagrange multipliers in every propagation such that the constraints are fulfilled in the next iteration. For small values of the kinetic energy of the wave functions the fictitious

mass m_Ψ is close to the Born-Oppenheimer surface and thus Eqn. (4.4) describes the classical motion of the nuclei.

4.3 Damped Nuclear Dynamics

Leveraging the Carr-Parrinello approach of the previous section, we can now discuss the Damped Nuclear Dynamics (DND) approach. In the latter, we can extend the Carr-Parrinello method to include damping mechanisms that help in the optimization of nuclear configurations. This section presents an introduction to the DND approach - an important tool for reaching ground state configurations by quenching excess kinetic energy from the system. The DND method introduces frictional forces to dissipate kinetic energy, and thus pushing the system towards a stable, low-energy configuration, i.e. either a local or global minimum. This technique ensures that the system relaxes efficiently to its ground state, which is especially useful in simulations that seek the equilibrium structure of a molecule or material. We can express the equation of motion (EOM) for damped dynamics as

$$m\ddot{x} = F(x) - m\alpha\dot{x}, \tag{4.5}$$

where m is the mass, $F(x)$ is the force acting on the nuclei and α is the friction coefficient. $\dot{x}$ and $\ddot{x}$ are the velocity and acceleration, respectively. The damping term $-m\alpha\dot{x}$ defines the frictional force which is proportional to the velocity. A common algorithm used to discretize the EOM of Eqn. 4.5 is given by Verlet[Ver67]. The simplicity and numerical stability of the Verlet algorithm makes it especially suited for molecular dynamics simulations. Setting $a = \frac{\alpha\Delta t}{2}$ the EOM can be written as

$$\begin{aligned} x(t+\Delta t) = \quad & \tfrac{2}{1+a}x(t) - \tfrac{1-a}{1+a}x(t-\Delta t) \\ & + \tfrac{1}{m}F(x)\tfrac{\Delta t^2}{1+a} \end{aligned} \tag{4.6}$$

In the absence of damping ($a = 0$), this simplifies to the original Verlet algorithm

$$x(t+\Delta t) = 2x(t) - x(t-\Delta t) + \frac{1}{m}F(x)\Delta t^2, \tag{4.7}$$

whose dynamics over long time scales is energy conserving and independent of the step size due to time inversion symmetry. For steepest descent dynamics, which are analogous to infinite damping ($a = 1$), we have for the equation of motion

$$x(t+\Delta t) = x(t) - \frac{1}{m}F(x)\frac{\Delta t^2}{2}, \tag{4.8}$$

where $\frac{\Delta t^2}{2m}$ is the mixing parameter. While Eqn. (4.8) describes dynamics with infinite friction, the motion does not come to rest in this limit because the time step is scaled

inversely proportional[Blö20]. By using friction dynamics in the structural analysis of molecules, such as C_3O_2, we need to repeatedly damp the nuclear motion until the system reaches its energetically preferred state. This enables an accurate description of structural parameters and potential energy surfaces. We can utilize DND to refine structures obtained from any prior MD simulations. This is particularly useful for hybrid functionals, such as PBE0r, that blend in a fraction of exact exchange from Hartree-Fock theory with the PBE exchange-correlation functional, largely due to the efficiency and accuracy provided by DND. Hence, we have a powerful framework for the structural analysis and optimization of molecular systems, comprising of the integration of damped nuclear dynamics with the Carr-Parrinello method and local hybrid functionals.

4.4 Local hybrid functional PBE0r

The Kohn-Sham (KS) method - based on the density functional theory in the local-spin-density approximation (LSDA) - gives insight into the physical and chemical properties[GAE03] of many materials. To achieve a reduction in the computational complexity and load in solving the KS equations or minimising the DFT energy an efficient representation of the KS wave functions must be used. This is done employing the projector augmented wave formalism[Blö94b]. Additionally, while KS DFT is in theory exact, approximations of the exchange-correlation functional E_{XC} need to be used.

In this work in particular calculations were done with the local hybrid functional PBE0r by Blöchl et. al. [Sot+17] that is based on the PBE0 [AB99] functional. The PBE0r tries to alleviate the difficulties of conventional density functionals with strongly correlated transition metal oxides in an efficient manner. It borrows ideas from range-separated hybrid functionals and from the LDA+U [Kuo+17] method. Like other hybrid functionals ([AB99; HSE03; HSE06; Kru+06] it combines local DF approximation of the exchange-correlation functional with an exact contribution from the Hartree-Fock (HF) approximation E_x^{HF}. The original PBE0 on which PBE0r leans on does this by replacing 25% of the exchange contribution from the PBE functional with exact HF exchange [AB99; EBB20]

$$E_{\mathrm{XC}}^{\mathrm{PBE0}} = E_{\mathrm{XC}}^{\mathrm{PBE}} + 0.25(E_{\mathrm{X}}^{\mathrm{HF}} - E_{\mathrm{X}}^{\mathrm{PBE}}). \tag{4.9}$$

While the inclusion of the HF exchange is followed by an increase in computational cost, this has been remedied by replacing the Coulomb interaction in the exchange by a screened interaction. For the HSE06 functional[HSE03; HSE06; Kru+06], another

functional derived from the PBE0 functional, this is done using a screened Coulomb interaction separated into short and long range of the form

$$\frac{1}{r} = \underbrace{\frac{1-\mathrm{erf}(\omega r)}{r}}_{\textit{short range}} + \underbrace{\frac{\mathrm{erf}(\omega r)}{r}}_{\textit{long range}}, \tag{4.10}$$

where ω is the screening parameter determining the separation range. A fitting to experimental properties [Kru+06] resulted in an empirical value of $\omega = 0.11a_0$, where a_0 is the Bohr radius. Effectively, this means that the HF exchange is only calculated for the short range and not the long range, reducing the computational cost considerably.

In the hybrid functionals, the average of the exchange hole as function of the interaction strength is interpolated between the exchange hole at zero interaction and the exchange correlation hole at full interaction. The interaction-strength average with this interpolation can be represented as an average of the exchange energy and the exchange correlation energy.

Screening is strong at large distances, while it is small in the core region of the atom, where the kinetic energy is large. This can be described by a range-separated hybrid functional, which limits the Fock term to short distances. This principle is one reason for using only the onsite interaction in the Hubbard model. While functionals such as HSE use a distance criterion, see Eqn. 4.10, for the saparation of weakly vs strongly screened regions, the LDA+U method limits the interaction to a subset of orbitals for each atom.

In the PBE0r functional we decompose the Kohn-Sham wave functions $|\psi_n\rangle$ into atom-centered orbitals $|\chi_{R,\alpha}\rangle$ and we restrict the admixture of explicit exchange to the onsite terms.

$$|\psi_n\rangle = \sum_{R,\alpha} |\chi_{R,\alpha}\rangle\langle\tilde{\pi}_{R,\alpha}|\tilde{\psi}_n\rangle \tag{4.11}$$

The projector functions $\langle\pi_{R,\alpha}|$ for the local orbitals are constructed as superpositions of the partial-wave projector functions $\langle\tilde{p}_{R,i}|$.

The exchange term [BWP11a; BPP13a] being

$$\begin{aligned} E_X \;=\; & \sum_R \sum_{\alpha,\beta,\gamma,\delta} \Theta_{\delta,\beta}\Theta_{\gamma,\alpha} W_{R,\alpha,\beta,\gamma,\delta} \\ & \cdot \sum_{\sigma,\sigma'\in\{\uparrow,\downarrow\}} \int d^3r \int d^3r' \, \frac{e^2 \chi^*_{R,\alpha}(\vec{r},\sigma)\chi^*_{R,\beta}(\vec{r'},\sigma')\chi_{R,\delta}(\vec{r},\sigma)\chi_{R,\gamma}(\vec{r'},\sigma')}{4\pi\epsilon_0|\vec{r}-\vec{r'}|}. \end{aligned} \tag{4.12}$$

In the latter, a fraction of the PBE exchange energy E_x^{PBE} is replaced by the explicit non-local HF exchange energy E_x^{HF}, i.e.:

$$E^{\text{PBE0r}} = E^{\text{PBE}} + \sum_n a_{x,n}(E_{x,n}^{\text{HF}} - E_{x,n}^{\text{PBE}}) \tag{4.13}$$

The Kohn-Sham wave functions in the PBE0r are mapped onto local tight-binding orbitals (LTBO) and the off-site terms are excluded from the exchange correction. This restriction on the exchange correction enables a sort of range separation bearing similarities to the long-range screening of the interaction in the GW approximation. This exclusion of off-site terms is appropriate for materials such as transition metal oxides which have strongly localized d orbitals whereas it is not suitable for the description of systems containing strong covalent bonds[Sot+17]. The admixture $a_{x,n}$[PEB96; Sot+17] is a freely adjustable parameter in PBE0r and can be set to fit experimentally observed spectral features. The mixing parameter can be chosen individually for each atom and thus, essentially, describes a local dielectric constant[EBB20].

While traditional GGA or other hybrid functionals face challenges when dealing with systems that show strong electronic localization, PBE0r has been proven to be effective dealing with the latter. Recent benchmark studies on materials like Li-Mn oxides show PBE0r to do well in predicting electronic and structural properties that agree well with experimental values, while keeping the computational effort similar to that of GGA functionals [EBB20].

4.5 How to analyse bonds

Going from an overview on Damped Nuclear Dynamics and PBE0r, we now consider techniques involved in analysing chemical bonding in molecular systems. Understanding the properties and strength of the bonds is critical in also understanding structural and electronic properties of molecules, such as e.g. C_3O_2, which we have been investigating. An essential indicator for bonding is the band structure energy, defined as

$$E_{\text{B}} = \sum_n f_n \epsilon_n \tag{4.14}$$

where ϵ_n are the orbital energies and f_n the corresponding occupations. Eqn. 4.14 can also be written in terms of the density of states (DOS)[Pet18]

$$E_{\mathrm{B}} = \int_{-\infty}^{\infty} d\epsilon f(\epsilon-\mu)\epsilon \sum_n \delta(\epsilon-\epsilon_n) \tag{4.15}$$

$$= \int_{-\infty}^{\infty} d\epsilon D(\epsilon)\epsilon f(\epsilon-\mu), \tag{4.16}$$

where $f(\epsilon-\mu)$ refers to the fermi-distribution. At temperature T=0K the chemical potential μ is the Fermi Energy of the system and lies between the highest occupied and lowest unoccupied state. The density of states provides a detailed local and energy-resolved perspective on the binding properties of materials.

Using projector functions, the wave functions can be decomposed into local orbitals[1] χ_i [Blö94b]

$$|\psi_n\rangle = \sum_i |\chi_i\rangle \langle p_i|\psi_n\rangle \tag{4.17}$$

For this to hold the basis functions must form a complete set and be mutually orthonormal with the projector functions. Assuming the wave functions are normalized and using Eqn. (4.17), the total DOS D(ϵ) can be expressed by a local basis set

$$\begin{aligned} D(\epsilon) &= \sum_n \delta(\epsilon-\epsilon_n) \langle\psi_n|\psi_n\rangle \\ &= \sum_{i,j}\sum_n \delta(\epsilon-\epsilon_n) \langle\psi_n|p_i\rangle \langle\chi_i|\chi_j\rangle \langle p_j|\psi_n\rangle \\ &= \sum_{i,j} D_{j,i}(\epsilon) \langle\chi_i|\chi_j\rangle \end{aligned} \tag{4.18}$$

The diagonal elements $D_{j,j} \langle\chi_j|\chi_j\rangle$ are called the *projected density of states*[Pet18]. The off-diagonal elements, or the hopping terms, are the Crystal Orbital Overlap Populations [HH83]. The COOPs give an additional layer of information by providing insight into the bonding information. Positive values indicate a charge accumulation in the bond, *bonding* states, while negative values indicate antibonding states. The sum of the overlap population over all states is a measure for the strength of the bond. However, COOPs are basis set dependent quantities and thus in general are no absolute bonding indicators.

[1] Which can be non-orthogonal.

Strictly speaking the COOPs do not contribute to the total energy of the system. Multiplying Eqn. (4.18) by the energy we have

$$\begin{aligned} D(\epsilon)\epsilon &= \sum_n \delta(\epsilon-\epsilon_n)\epsilon \langle\psi_n|\psi_n\rangle \\ &= \sum_n \delta(\epsilon-\epsilon_n)\epsilon \langle\psi_n| \hat{H} |\psi_n\rangle \\ &= \sum_{i,j}\sum_n \delta(\epsilon-\epsilon_n) \langle\psi_n|p_i\rangle \\ &\quad \cdot \langle\chi_i| \hat{H} |\chi_j\rangle \langle p_j|\psi_n\rangle \\ &= D_{j,i}(\epsilon) \langle\chi_i| \hat{H} |\chi_j\rangle \end{aligned} \tag{4.19}$$

where the last term in (4.19) is the *Crystal Orbital Hamilton Population* (COHP) [DB93]. Eqn. (4.19) contains information about bonding, nonbonding and antibonding energy regions within a specified energy range, while integrating the COHP reveals the contributions of an atom or bond to the distribution of one-particle energies[DB93]. The sign convention is opposite to that of the COOPs, i.e. bonding states are negative off-site terms and antibonding states are positive.

The local decomposition of the DOS in Eqn. 4.18 not only accounts for the contribution of individual atomic orbitals to the entire electronic structure, but, as mentioned above, also gives insights into the nature of the chemical bonding. In the case of C_3O_2 for example, we can analyse the bonding between the carbon and its associated oxygen by simply checking the projected DOS and assessing the contributions from different atomic orbitals. The COOP and COHP methods are especially useful in this regard. As indicated above, these methods allow us to quantify interactions between specifics pairs of atoms, i.e. to what degree these interactions are bonding, antibonding and non-bonding. This can provide a deeper look into the electronic structure and stability of the molecule.

Using these analytical techniques alongside the structural and electronic properties we acquire from DFT and post-DFT calculations, we get a more complete understanding of the bonding characteristics in complex molecular structures. In addition to improving and complementing theoretical models, this approach can also guide experimental research to synthesize materials with desired properties.

4.6 Results and Discussion

Building on the previous discussion of the theoretical framework and methodologies employed in this study, we now transition to the results section, which merges

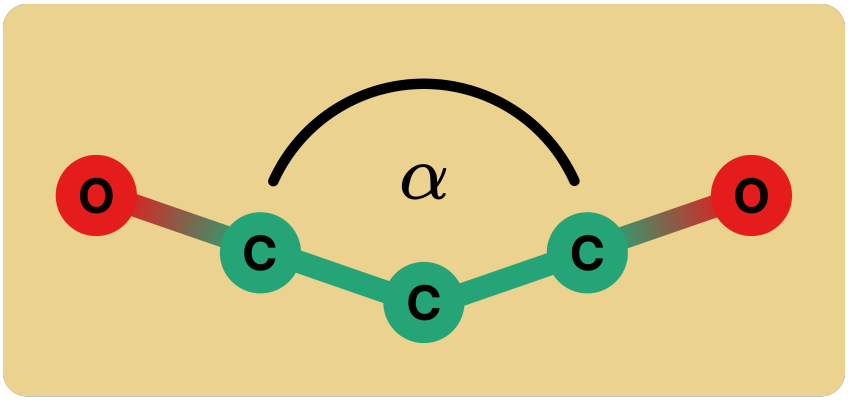

Fig. 4.1.: Structural overview of the C_3O_2 monomer with angle α(C-C-C).

the computational details and findings from the use of the local hybrid functional PBE0r.

The Car-Parrinello PAW code was utilized to perform the PBE0r calculations. Here, the augmentation of the PAW method included the physically relevant valence electrons of Carbon and Oxygen, i.e. the 2s and 2p orbitals of C and O, respectively. The construction of the auxiliary partial waves was done by setting the matching radii (in terms of the covalent radii) to 0.75 for all orbitals. The auxiliary wave functions were constructed as nodeless partial waves[BF12]. The tight-binding orbitals included the 2s and 2p orbitals of Carbon and Oxygen, respectively. Calculations are done in a 15Å×15Å×15Å unit cell, the plane wave cutoff value for the wave functions is set to 30Ry and the contribution of the non-local HF exchange energy is set to 10%. Finally, the number of projector functions and partial waves was set to 5 for each atom type.

The structure of C_3O_2 can be seen in Fig. 4.1, while Fig. 4.2 shows the single point energies of both PBE and PBE0r at different angles α(C-C-C). While PBE results indicate a clear linear structure for C_3O_2, PBE0r results have an energetic minium at around 170°, indicating that the molecule has a slight bent around its center Carbon atom. As discussed in sec. 4.5 the off-site terms of the overlap matrix give insight into the electron correlation and chemical bonding properties of materials and as such also to the physics and chemistry that lead to the bent structure.

Fig. 4.3 shows the total DOS as well as the projected DOS of the individual orbitals for Oxygen and Carbon. While the mixed state at -30eV has contributions from the Carbon s and p orbitals, it exhibits a predominant Oxygen s character. The state at -22eV can be identified as a bonding state between the s orbital of the center Carbon atom with the s and p orbitals of the two neighbouring Carbon atoms. Analogously,

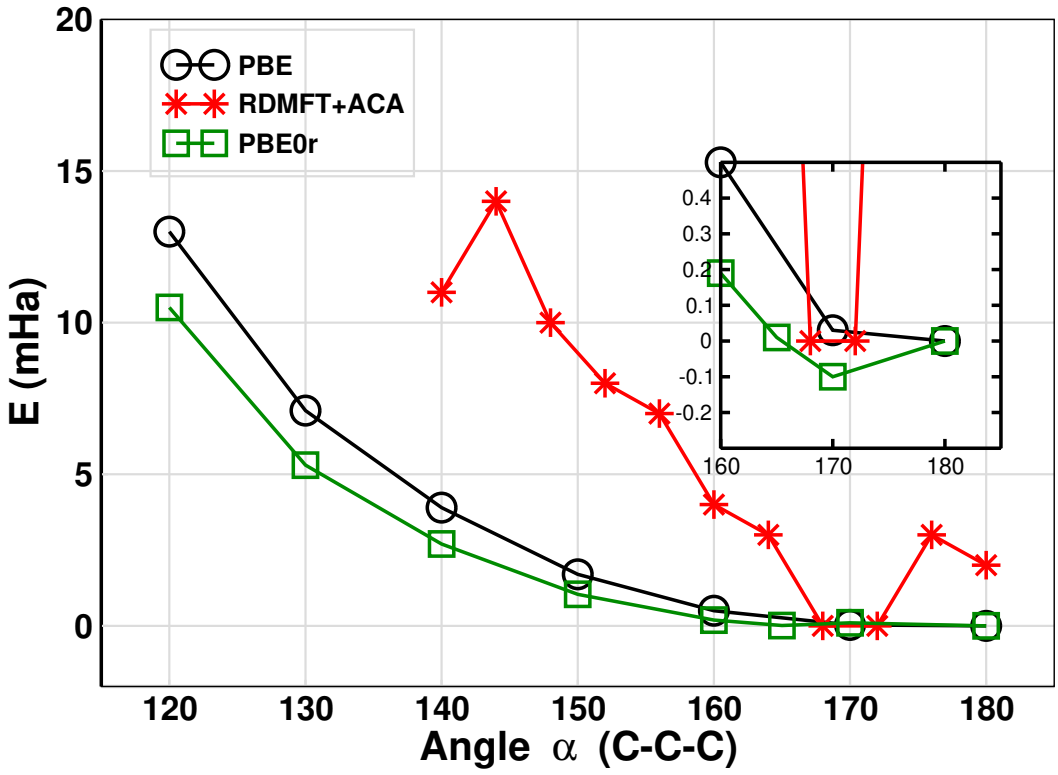

Fig. 4.2.: Results from static calculations using PBE, the hybrid functional PBE0r and results from the RDMFT+ACA approach. Unlike PBE, both PBE0r and RDMFT+ACA indicate a bent structure of the C_3O_2 molecule at around 170°. See Sec. 5.5 for a discussion of the RDMFT+ACA results.

the state at -18eV is the mixed antibonding state between the p orbitals of the center Carbon with the s and p orbitals of its neighbours. The orbital character in both states is dominated by the contribution from the central Carbon, i.e. the states at -22eV and -18eV are of primarily s and p character, respectively. The final state before the Fermi Energy starting at [-13eV,-11eV] is a bonding state between the p orbitals of both Oxygen and the two outer Carbons.

The projected DOS of both atom types approximately shows an energetic separation of the s and p orbitals at lower energies, while this is not the case for states above $\approx$-13eV and close to the Fermi Energy.

The valence state at the Fermi level, see Fig. 4.3, contains contributions of p orbitals of both Oxygen and Carbon. The contribution from the central Carbon to the valence state is significantly higher than that of its neighbours and is similar to that of the Oxygen. The partial charge on the center Carbon was calculated to be -0.23e. According to the Valence Shell Electron Pair Repulsion (VSEPR)[GN57] theory, this partial charge will exhibit a repulsive force on the neighbouring atoms of the center Carbon, which explains the slight bend observed in the PBE0r results. This

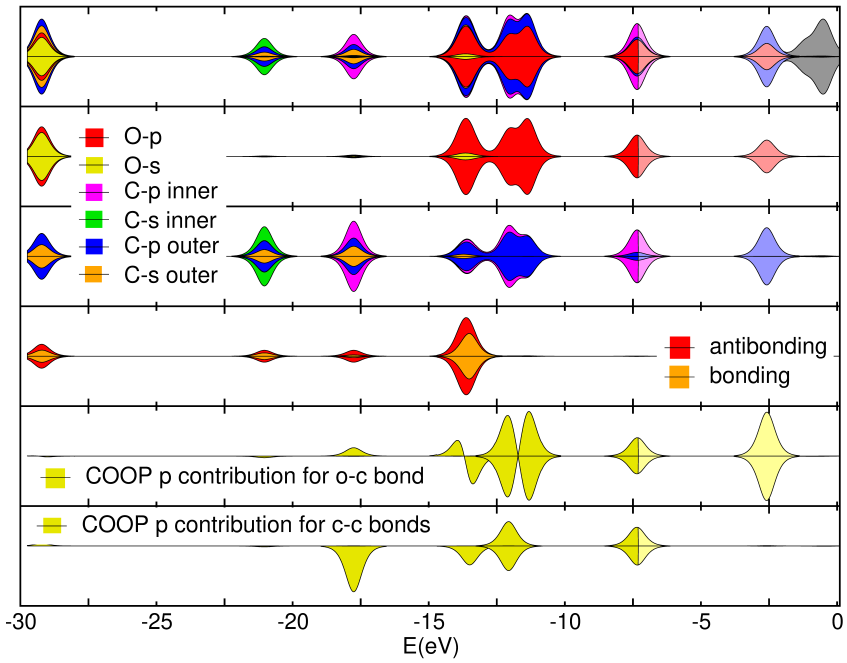

Fig. 4.3.: First row: Total DOS including projected DOS of oxygen s, p and carbon s, p orbitals (due to negligible contribution of d orbitals to the total DOS these were not included in the DOS calculations). Second and Third Row: Projected DOS of oxygen and carbon, respectively. Fourth Row: Bonding (orange) and antibonding (red) states. Fifth and Sixth Row: COOP for the p contribution of the $O-C$ and $C-C$ bond, respectively. Note: *inner* here refers to contributions from the center Carbon atom and *outer* to the two neighbouring Carbon atoms.

observation aligns with prior experimental and theoretical studies[Tor+95; VJP91; JJ86; Kop00; HKS14; DMR76; Bun80; MS99].

5

Reduced Density Matrix Functional Theory

In the field of quantum chemistry, electronic structure calculations are largely done using either wave function or density functional theory (DFT)-based methods. Although the former offers high accuracy, due to the unfavourable scaling of the computational cost it is usually limited to small systems. And while the latter achieves a good compromise between cost and accuracy, most of the approximations in that field have their own set of problems arising from the use of a strictly local object - the electron density[PG15]. Replacing DFT with the less investigated density-matrix functional theory (RDMFT)[Gil75] for the description of strong electronic correlations offers two advantages[Sch19]: (i) While the density-matrix functional has no contributions from the kinetic energy and only contains contributions from the interaction and the entropy, the kinetic energy is known exactly in terms of the one-electron reduced density-matrix (1RDM). (ii) The strong correlation effects can be directly derived from the fractional occupations of the above mentioned and readily available 1RDM of the physical system.

5.1 Formalism

Consider the probability distribution

$$\Psi_N(x^N)\Psi_N^*(x^N), \tag{5.1}$$

where

$$x^N = x_1 x_2 \cdots x_N \tag{5.2}$$

and

$$x_i = (r_i, s_i)\ ,\ i \in \{1...N\}. \tag{5.3}$$

The above distribution is associated with a solution of the Schrödinger equation with Hamiltonian of form 2.1. Eqn. 5.1 is a special case of the more general form [PW94]

$$\rho^{(N)}(x'^N, x^N) = \Psi_N(x'^N)\Psi_N^*(x^N), \tag{5.4}$$

$\rho^{(N)}(x'^N, x^N)$ being an element of a matrix, the density matrix. For Eqn. 5.1 we have $x_i' = x_i$, i.e. a diagonal element of the density matrix. Eqn. 5.1 is referred to as the Nth order density matrix . Given a binomial coefficient $\binom{N}{p}$ we can then define the reduced density matrix of order p by [PW94]

$$\rho^{(p)}(x'^p, x^p) = \binom{N}{p} \int \cdots \int \rho^{(N)}(x_1' x_2' \cdot\cdot x_p' x_{p+1} \cdot\cdot x_N, x_1 x_2 \cdot\cdot x_N) \mathrm{d}x_{p+1} \cdot\cdot \mathrm{d}x_N \tag{5.5}$$

In this chapter we are interested in the one-particle case

$$\rho^{(1)}(x_1', x_1) = N \int \cdot\cdot \int \Psi(x_1' x_2 \cdot\cdot x_N)\Psi^*(x_1 x_2 \cdot\cdot x_N) \mathrm{d}x_2 \cdot\cdot \mathrm{d}x_N, \tag{5.6}$$

in particular the spinless one particle reduced density matrix (1-RDM)

$$\rho^{(1)}(r_1', r_1) = \int \rho^{(1)}(r_1' s_1, r_1 s_1) \mathrm{d}s_1. \tag{5.7}$$

With having established a formulation for the basic variable of RDMFT in Eqn. 5.7, we can now work on an expression for the energy in the RDMFT representation. To simplify the notation and reduce clutter let

$$\rho^{(1)}_{\alpha,\beta} = \rho^{(1)}(\alpha, \beta) \tag{5.8}$$

The primary focal point for an interacting N-particle system is the grand potential[SKB17]

$$\Omega_{T,\mu}(\hat{h} + \hat{W}) = -k_B T \ln[\mathrm{Tr}\{\exp(-\frac{1}{k_B T}(\hat{h} + \hat{W} - \mu\hat{N})\}], \tag{5.9}$$

where T is the temperature, k_B the Boltzmann constant, μ the chemical potential and $\hat{N}$ the total particle number operator. Given the density-matrix functional $\mathrm{F}_\beta^W[\rho^{(1)}]$ with respect to the one-particle reduced density-matrix $\rho^{(1)}$ we can apply the Legendre-Fenchel transformation [Leg87; Fen49] to represent the grand potential within RDMFT as

$$\Omega_{\beta,\mu}[h] = \min_{\rho^{(1)}: 0 \leq \rho^{(1)} \leq \mathbb{1}} \{\mathrm{Tr}[\rho^{(1)}(h - \mu\mathbb{1})] + F_\beta^W[\rho^{(1)}]\} \tag{5.10}$$

The minimization is performed over all ensemble-representable 1-RDMs $\rho^{(1)}$, i.e. the $\rho^{(1)}$ have the form[1]

$$\rho^{(1)}_{\alpha,\alpha'} = \sum_i P_i \left\langle \Psi_i | \hat{c}^\dagger_{\alpha'} \hat{c}_\alpha | \Psi_i \right\rangle , \tag{5.11}$$

where P_i is the probability of finding the system in state $|\Psi_i\rangle$, and $\hat{c}^\dagger_{\alpha'}$ and $\hat{c}_\alpha$ are the creation and annihilation operators, respectively. Similarly, we can write the Helmholtz potential as

$$\begin{aligned} H_{\beta,N}[h] &= \min_{\rho^{(1)}:0\leq\rho^{(1)}\leq\mathbb{1},\mathrm{Tr}[\rho^{(1)}]=N} \{\mathrm{Tr}[\rho^{(1)}h] \\ &\quad + F^W_\beta[\rho^{(1)}]\}. \end{aligned} \tag{5.12}$$

Thus, the ground-state energy is

$$\begin{aligned} E_N[h] &= \min_{\rho^{(1)}:0\leq\rho^{(1)}\leq\mathbb{1},\mathrm{Tr}[\rho^{(1)}]=N} \{\mathrm{Tr}[\rho^{(1)}h] \\ &\quad + F^W[\rho^{(1)}]\}. \end{aligned} \tag{5.13}$$

with $\mathrm{F}^W[\rho^{(1)}]$ as the zero-temperature density-matrix functional in the limit $\beta \to \infty$. Setting the chemical potential to zero we can express the density-matrix functional as the Legendre-Fenchel transformation of the grand potential, i.e.

$$F^W_\beta[\rho^{(1)}] = \max_h \left[\Omega_{\beta,\mu=0}[h] - \mathrm{Tr}[\rho^{(1)}h]\right] \tag{5.14}$$

The h refer to the matrix elements of the one-particle Hamiltonian. The matrix elements of the one-particle Hamiltonian and the one-particle reduced density-matrix are conjugate quantities and we have the relations[Sch19]

$$\frac{\partial \Omega_{\beta,\mu}[h]}{\partial h_{\alpha,\beta}} = \rho^{(1)}_{\beta,\alpha} \tag{5.15}$$

$$\frac{\partial F^W_\beta[\rho^{(1)}]}{\partial \rho^{(1)}_{\alpha,\beta}} = -h_{\beta,\alpha} \tag{5.16}$$

It has been shown[Lev79b; Val80] that the density-matrix functional can be obtained from a constrained minimization over an ensemble of orthonormal fermionic many-particle wave functions $|\Psi_i\rangle$ and ensemble probabilities P_i with $0 \leq \mathrm{P}_i \leq 1$ and $\sum_i P_i = 1$ with a given 1-RDM $\rho^{(1)}$ according to Eqn. 5.11 as

$$\begin{aligned} F^W_\beta[\rho^{(1)}] &= \min_{\{P_i,|\Psi_i\rangle\}\to\rho^{(1)}} \Big[\sum_i P_i \left\langle \Psi_i | W | \Psi_i \right\rangle \\ &\quad + \frac{1}{\beta}\sum_i P_i \ln P_i\Big] \end{aligned} \tag{5.17}$$

[1] Eqn. 5.11 is the ensemble generalization of Eqn. 5.7.

Oftentimes the density-matrix functional is decomposed into four contributions[Hel06; BPP13b; BCG15]: the Hartree energy $F_H^W[\rho^{(1)}]$, Fock energy $F_x^W[\rho^{(1)}]$, an entropy contribution of a non-interacting system $F_\beta^0[\rho^{(1)}]$ and correlation energy $F_{c,\beta}^W[\rho^{(1)}]$ as

$$\begin{aligned} F_\beta^W[\rho^{(1)}] &= F_H^W[\rho^{(1)}] + F_x^W[\rho^{(1)}] + F_\beta^0[\rho^{(1)}] + F_{c,\beta}^W[\rho^{(1)}] \\ F_H^W[\rho^{(1)}] &= \frac{1}{2}\sum_{\alpha,\beta,\gamma,\delta} U_{\alpha,\beta,\delta,\gamma}\rho^{(1)}_{\beta,\alpha}\rho^{(1)}_{\gamma,\beta}, \qquad (5.18) \\ F_x^W[\rho^{(1)}] &= -\frac{1}{2}\sum_{\alpha,\beta,\gamma,\delta} U_{\alpha,\beta,\delta,\gamma}\rho^{(1)}_{\gamma,\alpha}\rho^{(1)}_{\delta,\beta}, \qquad (5.19) \\ F_\beta^0[\rho^{(1)}] &= \frac{1}{\beta}\,\mathrm{Tr}[\rho^{(1)}\ln\rho^{(1)} - (\mathbb{1}-\rho^{(1)})\ln(\mathbb{1}-\rho^{(1)})]. \qquad (5.20) \end{aligned}$$

The correlation energy $F_{c,\beta}^W[\rho^{(1)}]$ contains both interaction and entropy contributions and has to be approximated[SKB17]. The RDMFT energy minimization of (5.13) can be rewritten in a DFT-like expression as

$$\begin{aligned} E_N[h] &= \min_{\{f_i\},\{|\phi_i\rangle\}:0\le f_i\le 1,\mu,\Lambda_{i,j}} \mathrm{stat}\{E_{\mathrm{RDMFT}}(\{f_i\},\{|\phi_i\rangle\}) \\ &- \mu(\sum_i f_i - N) - \sum_{i,j}\Lambda_{i,j}(\langle\phi_i\rangle\,\phi_j - \delta_{i,j})\} \qquad (5.21) \end{aligned}$$

with

$$\begin{aligned} E_{\mathrm{RDMFT}}(\{f_i\},\{|\phi_i\rangle\}) &= \mathrm{Tr}[\rho^{(1)}(\{f_i\},\{|\phi_i\rangle\})h] \\ &+ F_\beta^W[\rho^{(1)}(\{f_i\},\{|\phi_i\rangle\})]. \qquad (5.22) \end{aligned}$$

For a list of properties of the RDMF refer to [Sch19].

5.2 General DF+RDMF approach

The following sections describe an approach to combine density functions and reduced density-matrix functionals in a hybrid theory geared towards the description of strong local electronic correlations in solids. We begin this by defining the general starting point for an approach that contains DFs and RDMFs. The premise is to define the interaction Hamiltonian

$$W = \frac{1}{2}\sum_{\alpha,\beta,\gamma,\delta} U_{\alpha,\beta,\gamma,\delta}\hat{c}_\alpha^\dagger\hat{c}_\beta^\dagger\hat{c}_\delta\hat{c}_\gamma \qquad (5.23)$$

that is given in a one-particle basis $|\chi_\alpha\rangle$ as a decomposition into two terms

$$W = W_{\mathrm{DF}} + W_{\mathrm{RDMF}}. \qquad (5.24)$$

The density-matrix functional $F_\beta^W[\rho^{(1)}]$ is then approximated as

$$F^W[\rho^{(1)}] \approx F^{W_{\mathrm{DF}}}[\rho^{(1)}] + F^{W_{\mathrm{RDMF}}}[\rho^{(1)}]. \tag{5.25}$$

The first and second term are then later evaluated by an approximate density-functional and a density-matrix functional, respectively, i.e.

$$F^W[\rho^{(1)}] \approx F_{\mathrm{DF}}^{W_{\mathrm{DF}}}[\rho^{(1)}] + F_{\mathrm{RDMF}}^{W_{\mathrm{RDMF}}}[\rho^{(1)}]. \tag{5.26}$$

A similar starting point can be reached by extending the original density-matrix functional with a zero-term

$$F^W[\rho^{(1)}] = F^W[\rho^{(1)}] + (F^{W'}[\rho^{(1)}] - F^{W'}[\rho^{(1)}]). \tag{5.27}$$

The first and last density-matrix functional can be approximated with a density functional

$$F^W[\rho^{(1)}] \approx F_{\mathrm{DF}}^W[\rho^{(1)}] + \underbrace{(F^{W'}[\rho^{(1)}] - F_{\mathrm{DF}}^{W'}[\rho^{(1)}])}_{\text{correction}} \tag{5.28}$$

to have a hybrid expression of the original density-matrix functional whose last term obtains the form of a correction contribution. The local hybrid functional PBE0r as described in Sec. 4.4 can be used as an additional approximation for Eqn. 5.28, because it approximates the RDMF part in the above correction by a scaled Fock Energy[SKB17]. The first hybrid expression in (5.26) is identical to (5.28) for the choice $W' = W_{\mathrm{RDMF}}$ if the approximate density functional $F_{\mathrm{DF}}^W[\rho^{(1)}]$ is linear in the interaction, i.e.

$$F_{\mathrm{DF}}^W[\rho^{(1)}] = F_{\mathrm{DF}}^{W_{\mathrm{DF}}}[\rho^{(1)}] + F_{\mathrm{DF}}^{W_{\mathrm{RDMF}}}[\rho^{(1)}]. \tag{5.29}$$

This is for instance the case if it is evaluated for a fixed hole function. The rest of the chapter is derived with (5.28) as the chosen starting point[Sch19]. Due to the availability of exact results, the qualitative analysis of the above decomposition in the DF+RDMF scheme has been done on Hubbard chains[BWP11b; Sch19] and among other things has been proven to properly deal with static and spin correlations[SKB17].

5.3 Real-Space-Decomposition DF+RDMF approach

In a hybrid theory approach Blöchl et al. [BWP11c] proposed combining DFT and RDMFT adapted towards the description of the local physics in materials with strong

electronic correlations. Let $\chi = \{\chi_\alpha\}$ denote the complete one-particle basis set. Bloechl et al. chose the interaction W' as the interaction of a subset $C = \{\chi_\alpha\} \subset \chi$ of one-particle states as

$$W' = \frac{1}{2} \sum_{\alpha,\beta,\gamma,\delta \in C} U_{\alpha,\beta,\gamma,\delta} c_\alpha^\dagger c_\eta^\dagger c_\delta c_\gamma \tag{5.30}$$

$$U_{\alpha,\beta,\gamma,\delta} = \int d^4\vec{x} \int d^4\vec{x'} \frac{e^2}{4\pi\epsilon_0 |\vec{r} - \vec{r'}|} \cdot \chi_\alpha^*(\vec{x}) \chi_\beta^*(\vec{x'}) \chi_\gamma(\vec{x}) \chi_\delta(\vec{x}) \tag{5.31}$$

In their original publication the local one-particle states in C have been chosen such that the corresponding interaction W' contains the strongly interacting states responsible for the strong electronic correlations. It is easy to see that in the limit of $C = \chi$ - a complete one-particle basis set - W' becomes the full interaction W.

However, the above *orbital-based* approach has an inconsistency of the double-counting that is remedied by the following real-space modification. As mentioned, we start from Eqn. (5.28) as in the original approach but propose to redefine the interaction W'. It will now be defined as the decomposition of the full Coulomb interaction $w(\vec{r}, \vec{r'})$ in real-space, i.e.

$$w(\vec{r}, \vec{r'}) = \frac{e^2}{4\pi\epsilon_0 |\vec{r} - \vec{r'}|} \tag{5.32}$$

$$= (1 - \lambda(\vec{r}, \vec{r'})) w(\vec{r}, \vec{r'}) + \lambda(\vec{r}, \vec{r'}) w(\vec{r}, \vec{r'}) \tag{5.33}$$

$$\Rightarrow w'(\vec{r}, \vec{r'}) = \lambda(\vec{r}, \vec{r'}) w(\vec{r}, \vec{r'}) \tag{5.34}$$

and thus

$$W' = \frac{1}{2} \int d^4\vec{x}_1 \int d^4\vec{x}_2 \int d^4\vec{x}_3 \int d^4\vec{x}_4 w'(\vec{x}_1, \vec{x}_2) \cdot \delta(\vec{x}_1 - \vec{x}_4) \delta(\vec{x}_2 - \vec{x}_3). \tag{5.35}$$

Here, $\lambda(\vec{r}, \vec{r'})$ is some function with $0 \leq \lambda(\vec{r}, \vec{r'}) \leq 1$ and sets the decomposition of the interaction. The choice of the interaction function will be discussed in Sec. 5.5. The key advantage of the real-space definition of the interaction is that the density functional $F_{\mathrm{DF}}^{W'}[\rho^{(1)}]$ can be evaluated without having to introduce an approximate model interaction as was done in the original publication[BWP11c]. This change of definition allows evaluating the correction term

$$F^{W'}[\rho^{(1)}] - F_{\mathrm{DF}}^{W'}[\rho^{(1)}] \tag{5.36}$$

in a consistent way by using the exact same interaction for the density-matrix functional and the density functional. Additionally, and in contrast to Blöchl et al., the density-matrix functionals F_{DF} are evaluated without the kinetic energy

contribution from the exchange-correlation functional[Sch19]. The hole function is used at full interaction strength ($\lambda = 1$) and we have

$$\begin{aligned} F^W[\rho^{(1)}] &= \frac{1}{2}\int d^3\vec{r} n(\vec{r}) \int d^3\vec{r}'(h_{\lambda=1}(\vec{r}', \vec{r}) + n(\vec{r}))w(\vec{r}, \vec{r}') \\ &= U_{\text{XC}} + E_{\text{H}}[n] \end{aligned} \tag{5.37}$$

Schade [Sch19] defined the local density functional $F_{\text{DF}}^{W'}[\rho^{(1)}]$ for the interaction W' as

$$\begin{aligned} F_{\text{DF}}^{W'}[\rho^{(1)}] &= \frac{1}{2}\int d^3\vec{r} n(\vec{r}) \int d^3\vec{r}' \\ &\quad \cdot h_{\lambda(\vec{r},\vec{r}')}(\vec{r}', \vec{r})\lambda(\vec{r}, \vec{r}')w(\vec{r}, \vec{r}') \end{aligned} \tag{5.38}$$

Because of the hole function's dependence on the interaction decomposition function $\lambda(\vec{r}, \vec{r}')$ Eqn. (5.38) is the hole function of a system with interaction $\lambda(\vec{r}, \vec{r}')w(\vec{r}, \vec{r}')$. This is given rise by Schade's assumption of a local dependency of (5.38) on the local strength $\lambda(\vec{r}, \vec{r}')$ of the interaction. Finally, although the minimization problem in the real-space-decomposition based DF+RDMF scheme

$$\begin{aligned} E[h] &= \min_{\rho^{(1)}:0\leq\rho^{(1)}\leq 1, \text{Tr}\,\rho^{(1)}=N} \{\text{Tr}[\rho^{(1)}h] + U_{\text{XC}}[n] + E_{\text{H}}[n] \\ &\quad + (F^{W'}[\rho^{(1)}] - F_{\text{DF}}^{W'}[\rho^{(1)}]\} \end{aligned} \tag{5.39}$$

is identical to the one proposed by Bloechl et al., the functionals are defined differently. Similar to them however Schade proposes a local approximation for the real-space decomposition based DF+RDMF approach. To this end the decomposition function $\lambda(\vec{r}, \vec{r}')$ is defined as a sum of localized contributions λ_{R} as

$$\lambda(\vec{r}, \vec{r}') = \sum_{\text{R}} \lambda_{\text{R}}(\vec{r}, \vec{r}'), \tag{5.40}$$

where every local contribution λ_{R} is localized in the vicinity of the position $\vec{R}_{\text{R}}$. Given the above local approximation a decomposition of the interaction W' into local terms W_{R} is obtained, where the latter are defined as

$$\begin{aligned} W_{\text{R}} &= \frac{1}{2}\int d^4\vec{x}_1 \int d^4\vec{x}_2 \int d^4\vec{x}_3 \int d^4\vec{x}_4 \\ &\quad \cdot w(\vec{x}_1, \vec{x}_2)\lambda_{\text{R}}(\vec{r}_1, \vec{r}_2)\delta(\vec{x}_1 - \vec{x}_4)\delta(\vec{x}_2 - \vec{x}_3). \end{aligned} \tag{5.41}$$

The minimization in Eqn. (5.39) thus becomes

$$\begin{aligned} E[h] &= \min_{\rho^{(1)}:0\leq\rho^{(1)}\leq 1, \text{Tr}\,\rho^{(1)}=N} \{\text{Tr}[\rho^{(1)}h] + U_{\text{XC}}[n] + E_{\text{H}}[n] \\ &\quad + \sum_{\text{R}} (F^{W_{\text{R}}}[\rho^{(1)}] - F_{\text{DF}}^{W_{\text{R}}}[\rho^{(1)}]\}, \end{aligned} \tag{5.42}$$

where the density functional $F_{\mathrm{DF}}^{W_{\mathrm{R}}}$ is evaluated with the interaction $w(\vec{r},\vec{r}')\lambda_{\mathrm{R}}(\vec{r},\vec{r}')$ as

$$\begin{aligned} F_{\mathrm{DF}}^{W_{\mathrm{R}}}[\rho^{(1)}] &= \frac{1}{2}\int d^3\vec{r} n(\vec{r}) \int d^3\vec{r}' (h_{\lambda_{\mathrm{R}}(\vec{r},\vec{r}')}(\vec{r},\vec{r}') + n(\vec{r}')) \\ &\quad \cdot\lambda(\vec{r},\vec{r}')w(\vec{r},\vec{r}') \end{aligned} \tag{5.43}$$

Possible choices for λ_{R} include

$$\lambda_{\mathrm{sym,R}}(\vec{r},\vec{r}') = f(|\vec{r}-\vec{R}|)f(|\vec{r}'-\vec{R}|) \tag{5.44}$$

for the symmetric choice and

$$\lambda_{\mathrm{non-sym,R}}(\vec{r},\vec{r}') = f(|\vec{r}-\vec{R}|) \tag{5.45}$$

for the non-symmetric choice. Other expressions are also possible and can be chosen in a way to best fit the physical situation.

5.4 Adaptive Cluster Approximation

The computational complexity and effort in evaluating the necessary density-matrix functionals $F^{W'}[\rho^{(1)}]$ approach that of the exact functional. Using the local approximation of the density-matrix functional and calculating $F^{W'}[\rho^{(1)}]$ as one would calculate the exact functional will grant no reduction to computational time[Sch19]. Instead we require a way to reduce the number of non-interacting one-particle states in $F^{W'}[\rho^{(1)}]$. The main idea of the ACA is to apply a unitary rotation on the one-particle basis before performing a cluster approximation, i.e. neglecting some one-particle states. This unitary transformation is constructed in such a way that the following neglect of orbitals affects the density-matrix functional only minimally. The ACA can be seen as a generalization of Töws and Pastor's two-step approximation[TP11; TP12] .

Let $|\chi_\alpha\rangle$ be an N_χ-dimensional one-particle basis and $\rho^{(1)} \in \mathrm{C}^{N_\chi \times N_\chi}$ the corresponding one-particle reduced density-matrix. Additionally, assuming that the interaction is limited to the first N_{imp} one-particle orbitals, we have[2]

$$W_{\mathrm{loc}} = \frac{1}{2}\sum_{\alpha,\beta,\gamma\,\delta \leq N_{\mathrm{imp}}} U_{\alpha,\beta,\gamma\,\delta} c_\alpha^\dagger c_\beta^\dagger c_\delta c_\gamma. \tag{5.46}$$

[2]This can always be achieved by reordering the one-particle basis.

N_{imp} and the remaining $N_{\text{bath}} = N_\chi - N_{\text{imp}}$ are called the interacting one-particle states and bath-states, respectively. In the simplest case of a block-diagonal one-particle reduced density matrix

$$\rho^{(1)} = \begin{pmatrix} \rho^{(1)}_{\text{imp,imp}} & 0 \\ 0 & \rho^{(1)}_{\text{bath,bath}} \end{pmatrix} \tag{5.47}$$

with $\rho^{(1)}_{\text{imp,imp}} \in \mathrm{C}^{N_{\text{imp}} \times N_{\text{imp}}}$ and $\rho^{(1)}_{\text{bath,bath}} \in \mathrm{C}^{N_{\text{bath}} \times N_{\text{bath}}}$, the density-matrix functional can be shown to have the separation property[Sch19]

$$F^{W_{\text{loc}}}[\rho^{(1)}] = F^{W_{\text{loc}}}_{\text{imp,imp}} + F^{0}_{\text{bath,bath}}. \tag{5.48}$$

From the above equation it follows that the density-matrix functional $F^{W_{\text{loc}}}[\rho^{(1)}]$ with a complexity of $\mathcal{O}(2^{N_\chi})$ can be evaluated by calculating the functional $F^{W_{\text{loc}}}_{\text{imp,imp}}$ with a computational complexity of $\mathcal{O}(2^{N_{\text{imp}}})$ and a non-interacting functional $F^{0}_{\text{bath,bath}}$, which is given by[Sch19]

$$F^0_\beta[\rho^{(1)}] = \frac{1}{\beta}\,\mathrm{Tr}[\rho^{(1)} \ln \rho^{(1)} - (1-\rho^{(1)}) \ln(1-\rho^{(1)})]. \tag{5.49}$$

For a general one-particle reduced density-matrix

$$\rho^{(1)} = \begin{pmatrix} \rho^{(1)}_{\text{imp,imp}} & \rho^{(1)}_{\text{imp,bath}} \\ (\rho^{(1)}_{\text{imp,bath}})^\dagger & \rho^{(1)}_{\text{bath,bath}} \end{pmatrix} \tag{5.50}$$

a unitary transformation of the form

$$U = \begin{pmatrix} \mathbb{1} & 0 \\ 0 & U_{\text{bath,bath}} \end{pmatrix} \tag{5.51}$$

with $U_{\text{bath,bath}} \in \mathrm{C}^{N_{\text{bath}} \times N_{\text{bath}}}$, that only acts on the bath-states and hence does not spread out the localized interaction over all one-particle states, can be constructed. The density-matrix functional is independent of the unitary transform, i.e.

$$F^W[\rho^{(1)}] = F^W[U^\dagger \rho^{(1)} U]. \tag{5.52}$$

The idea of the unitary transformation is to transform the general one-particle reduced density matrix of Eqn. 5.50 into a band-like shape onto which the separation property 5.48 can be applied.

The unitary transform is constructed such that the transformed one-particle reduced density-matrix obtains the banded form

$$\tilde{\rho}^{(1)} = U^\dagger \rho^{(1)} U = \tag{5.53}$$

$$\begin{pmatrix} \rho^{(1)}_{\text{imp,imp}} & \tilde{\rho}^{(1)}_{\text{imp,bath}_1} & 0 & \dots \\ (\tilde{\rho}^{(1)}_{\text{imp,bath}_1})^\dagger & \tilde{\rho}^{(1)}_{\text{bath}_1,\text{bath}_1} & \tilde{\rho}^{(1)}_{\text{bath}_1,\text{bath}_2} & 0 \\ 0 & (\tilde{\rho}^{(1)}_{\text{bath}_1,\text{bath}_2})^\dagger & \tilde{\rho}^{(1)}_{\text{bath}_2,\text{bath}_2} & \tilde{\rho}^{(1)}_{\text{bath}_2,\text{bath}_3} \\ \vdots & 0 & (\tilde{\rho}^{(1)}_{\text{bath}_2,\text{bath}_3})^\dagger & \tilde{\rho}^{(1)}_{\text{bath}_3,\text{bath}_3} \end{pmatrix} \tag{5.54}$$

The transformation of the one-particle basis introduces no approximation. Further, Eqns. 5.51-5.54 have shown that a unitary transformation, that limits the dimension of the off-diagonal matrices $\tilde{\rho}^{(1)}_{\text{imp,bath}_1}$ and $\tilde{\rho}^{(1)}_{\text{bath}_i,\text{bath}_{i+1}}$ to at most $N_{\text{imp}} \times N_{\text{imp}}$, exists. Thus, the transformed one-particle reduced density matrix has a bandwidth of at most $2N_{\text{imp}} - 1$. See Appendix of [Sch19] for the detailed proof.

Due to the banded form of the density matrix, neglecting one of the off-diagonal matrices $\tilde{\rho}^{(1)}_{\text{bath}_i,\text{bath}_{i+1}}$ results in a block-diagonal one-particle reduced density-matrix. If we neglect the coupling between the first level and second level effective bath, i.e. $\tilde{\rho}^{(1)}_{\text{bath}_1,\text{bath}_2}$, we obtain

$$\tilde{\rho}^{(1)} \approx \tilde{\rho}^{(1)}_{M=1} = \tag{5.55}$$

$$\left(\begin{array}{cc|cc} \rho^{(1)}_{\text{imp,imp}} & \tilde{\rho}^{(1)}_{\text{imp,bath}_1} & 0 & \dots \\ (\tilde{\rho}^{(1)}_{\text{imp,bath}_1})^\dagger & \tilde{\rho}^{(1)}_{\text{bath}_1,\text{bath}_1} & 0 & 0 \\ \hline 0 & 0 & \tilde{\rho}^{(1)}_{\text{bath}_2,\text{bath}_2} & \tilde{\rho}^{(1)}_{\text{bath}_2,\text{bath}_3} \\ \vdots & 0 & (\tilde{\rho}^{(1)}_{\text{bath}_2,\text{bath}_3})^\dagger & \tilde{\rho}^{(1)}_{\text{bath}_3,\text{bath}_3} \end{array}\right). \tag{5.56}$$

Eqn. 5.56 represents the adaptive cluster approximation at the first level, i.e. with one effective bath level (ACA(M=1))

$$F^{W'}[\rho^{(1)}] \approx F^{W'}_{\text{ACA(M=1)}}[\rho^{(1)}] = F^{W'}[\rho^{(1)}_{M=1}] \tag{5.57}$$

and we can use the separation property Eqn. 5.48 on a block matrix such as Eqn. 5.56 to obtain a density-matrix functional of the i-bath level and the non-interacting functional of the remainder. Numerical evidence suggests that the difference of the exact density-matrix functional and the ACA(M)-approximation

$$|F^{W}[\rho^{(1)}] - F^{W}_{\text{ACA(M)}}[\rho^{(1)}]| \tag{5.58}$$

is a monotonically decreasing function of M. Properties and convergence tests of the ACA on different bath levels can be found in [Sch19].

5.5 Application to C_3O_2

Previously, using the local hybrid functional PBE0r, we found that the energetically preferred state of the C_3O_2 monomer is taken when the structure is in a bent configuration with a main angle α of about 170°. Because the RDMFT+ACA method offers a more accurate description of strong electronic correlations due to its inherent use of fractional occupations of the 1RDM, we aim to apply the former in a complementary manner to confirm the results, ensuring that our findings are reproducible and reliable.

Similarly to locally approximating the interaction W in Sec. 5.1 we can apply a local approximation on the decomposition function $\lambda(\vec{r},\vec{r}')$ and define it as a sum of localized contributions λ_R in the form

$$\lambda(\vec{r},\vec{r}') = \sum_R \lambda_R(\vec{r},\vec{r}'). \tag{5.59}$$

Every local contribution λ_R is supposed to be localized in the vicinity of the position $\vec{R}_R$. Given the symmetry of the molecule Eqn. 5.59 can be written as

$$\lambda_{sym,\vec{R}}(\vec{r},\vec{r}') = f(|\vec{r}-\vec{R}|)f(|\vec{r}'-\vec{R}|) \tag{5.60}$$

and select the positions of the center carbon atom as the centers $\vec{R}$. We choose the function $f(r)$ as a sum of five Gaussians

$$\begin{aligned} f(r) &= e^{-1.5609r^2} + 564.35\cdot(e^{-1.5606r^2} - e^{-1.6503r^2}) \\ &\quad +3729.03\cdot(e^{-1.6641r^2} - e^{-1.65083r^2}), \end{aligned} \tag{5.61}$$

approximating a smoothened step function.

With this choice, we obtain a decomposition of the interaction W' into local terms W_R that are defined as

$$\begin{aligned} W_R &= \frac{1}{2}\int d^4\vec{x}_1 \int d^4\vec{x}_2 \int d^4\vec{x}_3 \int d^4\vec{x}_4 w(\vec{x}_1,\vec{x}_2) \\ &\quad \cdot\lambda_R(\vec{r},\vec{r}')\delta(\vec{x}_1-\vec{x}_4)\delta(\vec{x}_2-\vec{x}_3). \end{aligned} \tag{5.62}$$

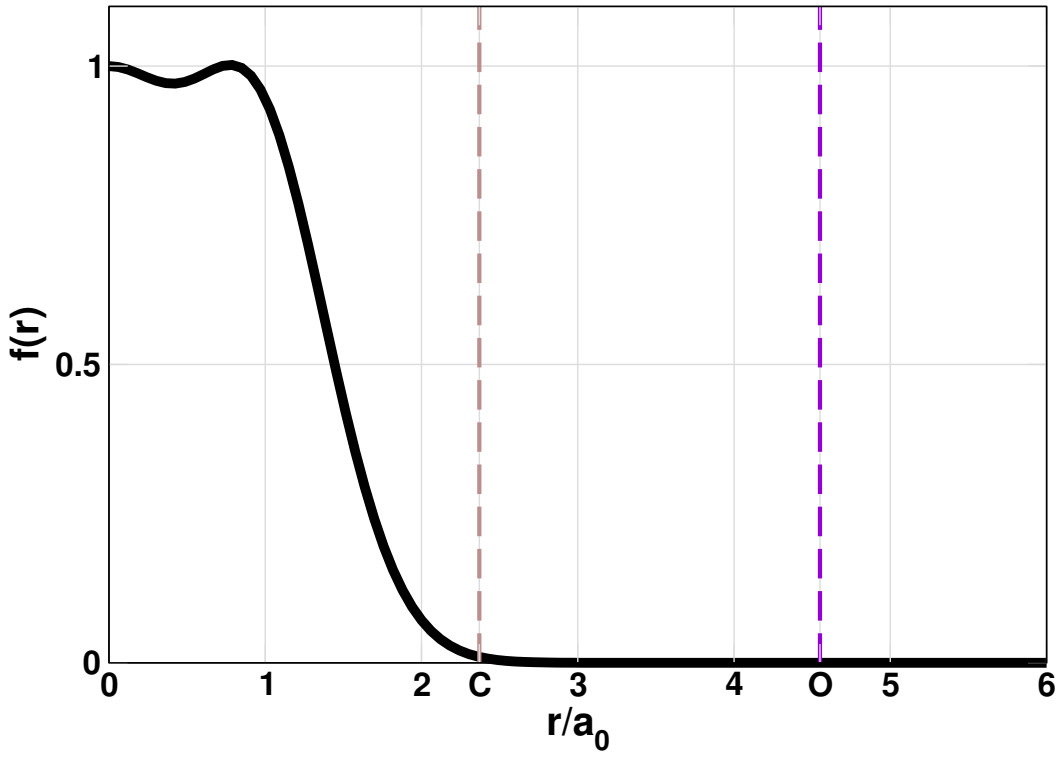

Fig. 5.1.: The function f(r) given by Eqn. 5.61. The center carbon of C_3O_2 is located at the origin. The vertical arrows indicate the distances to the neighbouring carbon atoms and oxygen atoms at $r = 2.37a_0$ (brown dashed line) and $r = 4.55a_0$ (violet dashed line), respectively.

Due to the shape of C_3O_2 - i.e. of a molecule consisting of a chain of 5 atoms - the density-matrix functional of the full interaction is divided into the sum of interactions around the individual atoms, i.e.

$$\begin{aligned} F^W[\rho^{(1)}] \approx\ & F_{DFT}^{W_{C_1}}[\rho^{(1)}] + F_{DFT}^{W_{C_2}}[\rho^{(1)}] \\ & + F_{CI}^{W_{C_3}}[\rho^{(1)}] \\ & + F_{DFT}^{W_{O_1}}[\rho^{(1)}] + F_{DFT}^{W_{O_2}}[\rho^{(1)}]. \end{aligned} \tag{5.63}$$

To determine the minimum bath level for sufficiently accurate results static calculations at all bath levels with varying number of determinants were done, see Fig. 5.2. The results indicate that a bath level of 2 gives sufficiently accurate results (within 0.3kcal/mol). The density-matrix functionals of the interactions around C_1,C_3,O_1 and O_2 are evaluated by an approximate density-functional and the interaction of the remaining center carbon atom C_3 with a density-matrix functional on an ACA(1) level. As shown in Fig. 4.2, the single-point energies of C_3O_2 at different angles α(C-C-C) indicate a minimum around 170°, in good agreement with the PBE0r results. This reinforces the conclusion that the C_3O_2 molecule has a slight bend around its central Carbon atom, validating the observations made with the PBE0r functional and highlighting the consistency between the different computational approaches. All in all, both PBE0r and RDMFT+ACA calculations indicate a bent structure for the

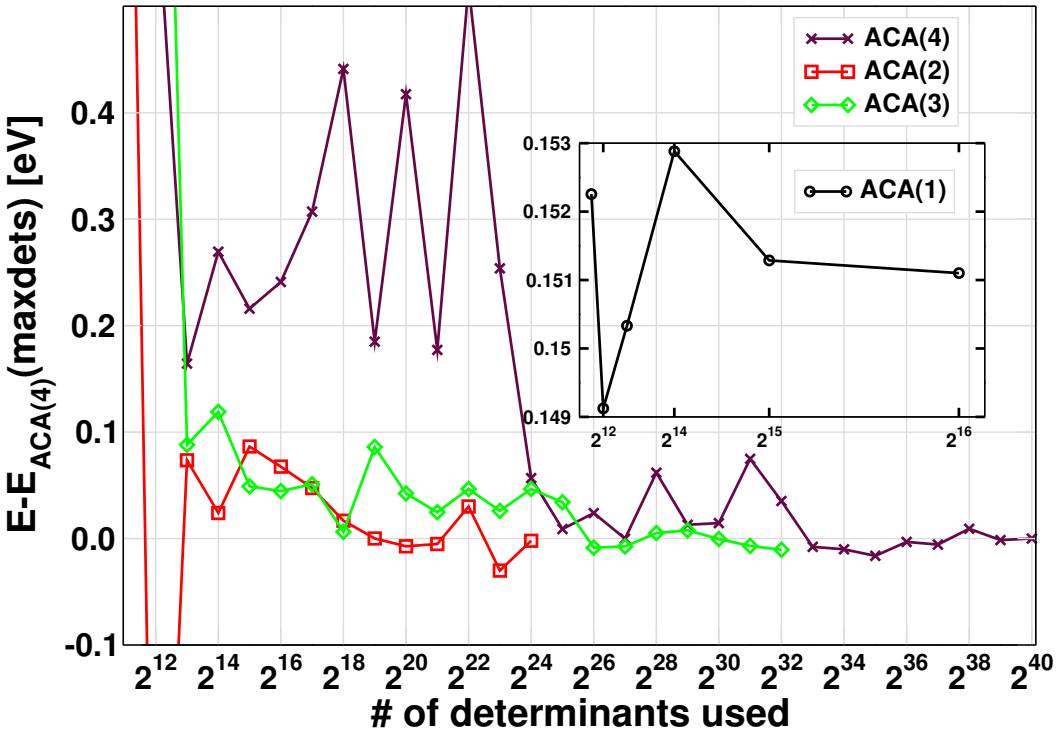

Fig. 5.2.: Energy convergence on different ACA levels. With an estimated error of less than 0.3kcal/mol the ACA(2) results of the level of the second bath give sufficiently accurate results. Inset: ACA(1) results.

C_3O_2 molecule, with an angle of roughly 170° around the central Carbon atom. The computational moethods used provide a comprehensive understanding of the molecular characteristics, contributing relevant insights into the structural and electronic properties of C_3O_2.

6 Nanostructure Growth Mechanisms in CIGS Thin Films

Having discussed the structural and electronic properties of C_3O_2 in the previous chapters, we now look at CIGS thin films as a means of studying nanostructure growth. Understanding the early stages of growth of such thin films is crucial for improving the performance and scalability of the latter for various applications, e.g. for high-efficiency photovoltaic systems. In this chapter, we employ TBMD simulations, in particular the eXtended Tight-Binding method developed by Grimme et al.[BEG19; GBS17], to investigate the initial stages of CIGS thin-film growth on a $MoSe_2$ substrate. By examining the mechanics of single atom adsorption, diffusion paths and energy barriers, we seek to provide insights into the kinetic and thermodynamic processes that govern the formation of these nanostructures. The understanding of these early stages of growth mechanisms can be applied to other thin-film growth processes as well.

First, we review the methods and computational details of the static and MD calculations in Sec. 6.1. And lastly, we discuss our results in Sec. 6.2, where we elaborate on the above mentioned processes.

6.1 Methods and Computational Details

The total energy calculations are performed using the Vienna Ab-Initio Simulation Package (VASP) [KH93; KH94b; Kre96; Kre+96; KH94a; KJ99]. The exchange and correlation interactions are described within the generalized gradient approximation (GGA) using the optB86b-vdW [KBM09] functional. The plane-wave (PW) basis set cut-off energy is set to 400eV and convergence criteria for the forces and the relaxation are set to 0.01eV/Å and 10^{-4}eV, respectively. Table 6.1 lists the lattice parameters obtained by various exchange-correlation functionals, indicating that optB86b-vdW predicts the lattice parameters very close to the experimental ones.

The k-points are generated using the Monkhorst-Pack scheme [MP76] in a $4\times4\times4$ and a $4\times4\times1$ mesh on a Γ-centered grid for the single and multi layer systems, respectively. The climbing image nudged elastic band method (CI-NEB) [HUJ00] is used to gain an insight into the diffusion dynamics of In and Se adatoms on

the $MoSe_2$(0001) surface. The multilayered system consists of a 4 layered 3×3 $MoSe_2$ supercell whose 2 bottom layers are fixed to simulate the bulk. To avoid any interactions between periodic images of the system, an optimized vacuum gap of 13Å along the z-direction is employed.

The TBMD calculations are done with the xTB method as implemented in the CP2K [Küh+20] software package. In order to model the growth of In_2Se_3 films on $MoSe_2$ (0001) using a TBMD method, a 2-layered 8×8 $MoSe_2$ supercell with dimensions 26.62×26.62×40$Å^3$ is chosen. A vacuum gap of 27Å is chosen along the z-direction to ensure that (1) there is no interactions between adsorbants and their periodic images and (2) the growth film has sufficient space to form.

All processes that can appear on a growing crystal surface are considered. These include atom depositions, surface diffusion, evaporation, bulk diffusion, defect depositions and more, see Fig. 6.1. Starting from a clean $MoSe_2$ surface, In and Se atoms are deposited at randomly chosen surface sites after regular intervals. In our growth model, deposition flux and ratio of In and Se atoms can be controlled. Here we consider systems with In:Se ratios of 1:1 and 2:3. After each deposition, the system is allowed to equilibrate for about 5ps. The substrate temperature is 300K.

6.2 Results and Discussion

6.2.1 Mechanics of Single Atom Adsorptions

The (0001) surface of $MoSe_2$[Mir+16] is energetically most favorable and is thus used as the substrate for all given growth simulations. The (0001) $MoSe_2$ surface is terminated with an Se layer, therefore it exhibits an inert surface character, i.e. it's highly non-reactive like e.g. pure Si or mica [Gao+20]. The adsorption of single atoms on the clean $MoSe_2$ surfaces and $MoSe_2$ surfaces with Se or Na atoms present above the top-most layer were considered, see Fig. 6.2 a) and b). Table 6.2 shows a summary of adsorption energies for single adatoms on different $MoSe_2$

Tab. 6.1.: Bulk lattice parameters obtained from different XC functionals used in our study and their deviation from experimental values, a=3.299Å, and c=12.938Å

Functional	Δ a	Δ c
BEEF-VdW	+1.24%	+8.76%
DFT-D3-BJ	-0.73%	-1.58%
SCAN	-1.18%	+19.15%
rVV10+SCAN	-0.27%	+1.92%
optB86b-VdW	-0.06%	+0.88%

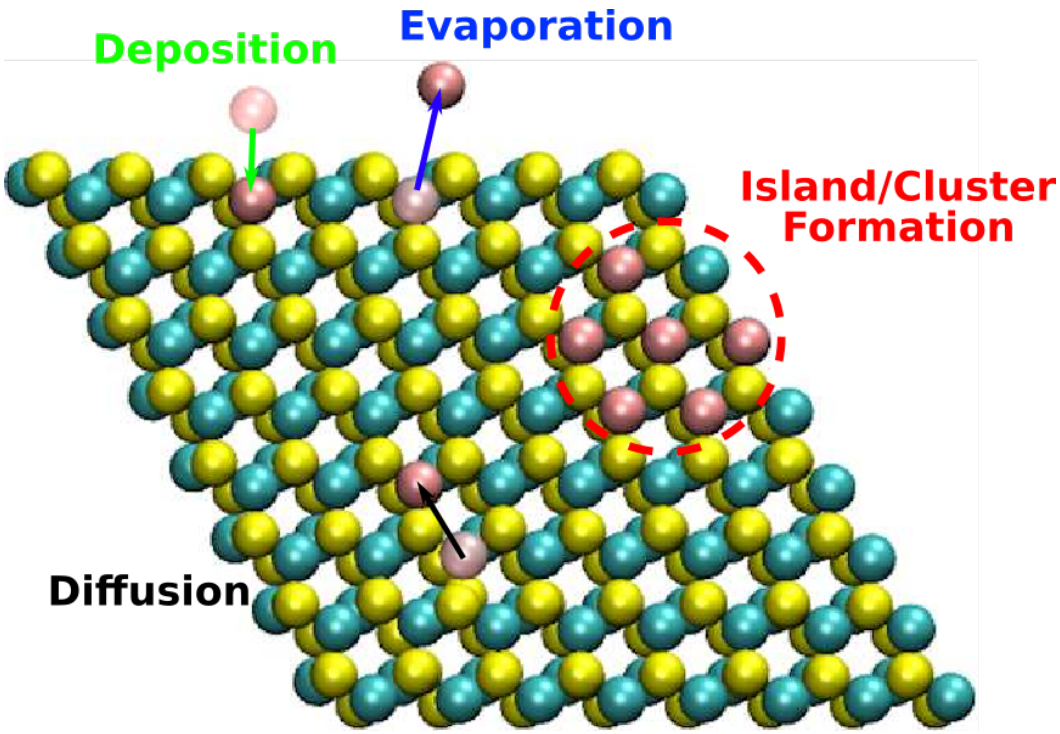

Fig. 6.1.: Schematic picture of the processes taking place on the substrate - among them adsorption, desorption, diffusion on the surface and cluster/island formation.

surfaces. Adsorption of In and Se is endothermic on a clean substrate, while Na is adsorbing exothermically on the surface. It's assumed to be due to the differences in electronegativity of the adatoms - the greatest difference being between Se[1] and Na.

Since both Na and Se are readily available, due to the diffusion of Na from the lime glass and the Se vapor in the chamber, adsorption calculations of In and Se were

[1]The $MoSe_2$ surface is terminated into an Se layer and thus only the difference to Se is relevant.

	E^{ads} in eV
In^{ads} on clean $MoSe_2$	+3.07
In^{ads} on Na/$MoSe_2$	+2.91
In^{ads} on 3Na/$MoSe_2$	+2.08
In^{ads} on 2Na/$MoSe_2$	+2.07
In^{ads} on Se/$MoSe_2$	+1.81
Se^{ads} on clean $MoSe_2$	+1.56
Se^{ads} on Na/$MoSe_2$	+0.9
Se^{ads} on In/$MoSe_2$	+0.28
Na^{ads} on clean $MoSe_2$	-0.29
In^{ads} on 2Se/$MoSe_2$	-0.38
Se^{ads} on 2Na/$MoSe_2$	-2.0

Tab. 6.2.: Adsorption energies of atoms on clean $MoSe_2$ and on an $MoSe_2$ surface with previously adsorbed atoms.

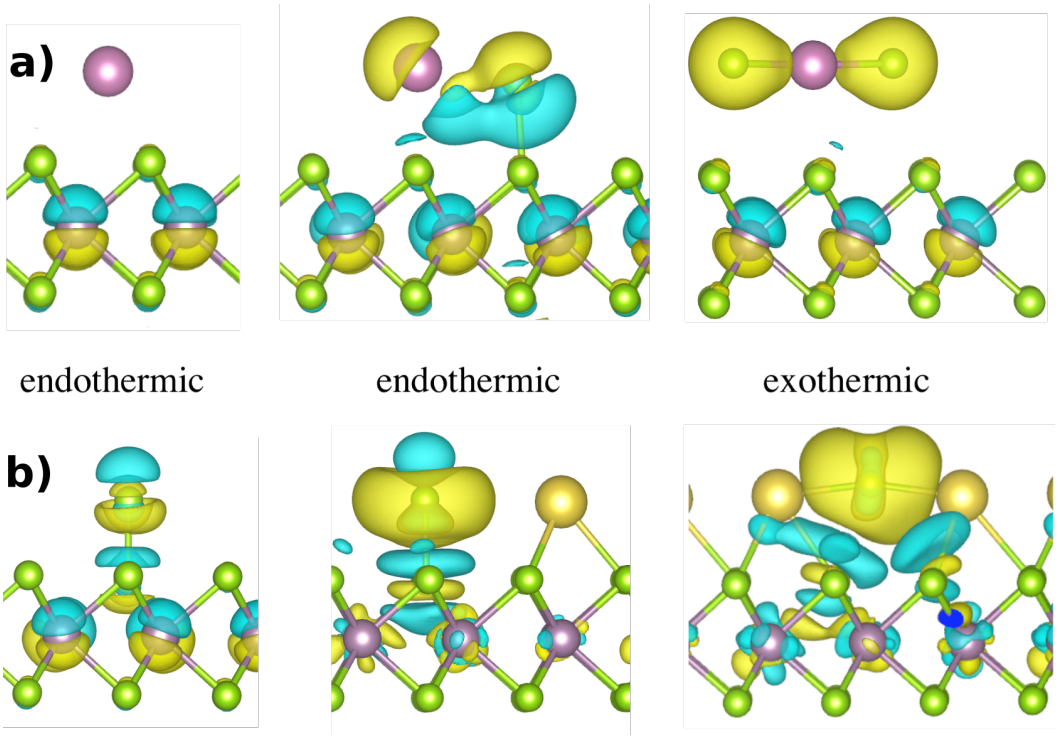

Fig. 6.2.: a) Se facilitates an exothermic adsorption of In on-top of the $MoSe_2$ surface, while b) the availability of Na enables an exothermic adsorption for Se. Mo: purple, Se: green, In: pink, Na: yellow. Yellow shaded areas refer to charge accumulation, while blue shaded areas refer to the opposite.

undertaken with either Na and Se already being on the surface. The presence of two Se or Na atoms on the $MoSe_2$ surface facilitates an electrostatic interaction with In and Se, respectively, and thus allows for an exothermic adsorption with adsorption energies of E_a=-0.38eV in case of In and -2.0eV for Se. Fig. 6.3 shows the Density of States (DOS) and band structure (BS) of a clean $MoSe_2$ surface. The band structure exhibits a metallic behavior and the only contributions are coming from the d- and p-orbitals of Mo and Se, respectively.

Fig. 6.4 and A.1 (see Appendix) show BS and DOS corresponding to the systems shown in Fig. 6.2. The adsorption of In onto the $MoSe_2$ surface does not create any new bands in the BS of the system (see Fig. 6.4 (top) and corresponds to the electron density figure which does not show any perturbation of the electronic structure, indicating a physiosorption. Having Se atoms present on the surface prior to In adsorption introduces new bands close and below the Fermi energy coming from the p orbitals of the Se atoms, see Fig. 6.4 mid and bottom. Indium can interact with these newly formed valence electrons and enable a purely electrostatic adsorption of the former.

The situation with Se and Na on the other hand is more interesting. Here, the addition of Na prior to Se adsorption brings the bands from the Se p-orbitals closer

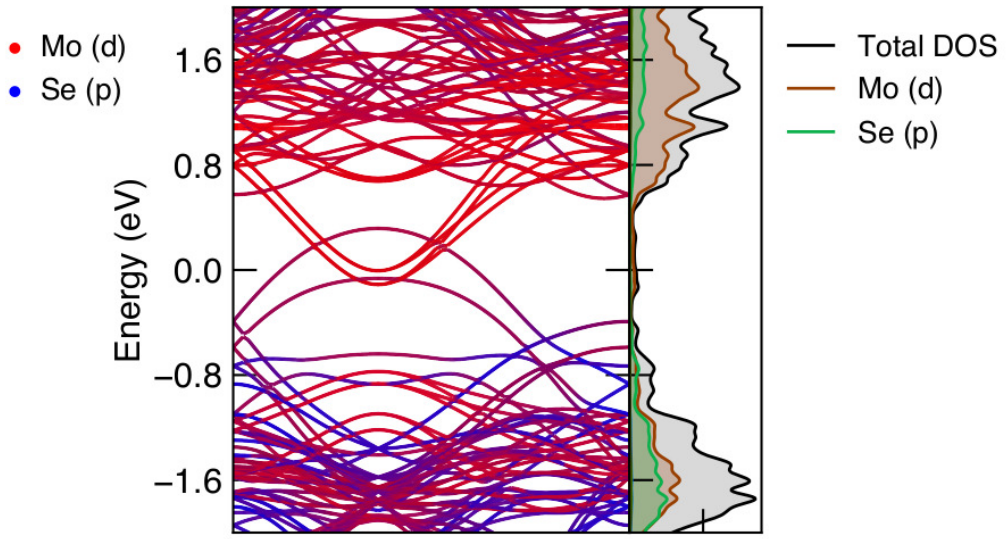

Fig. 6.3.: Band structure and DOS for clean MoSe2. Parentheses refer to the respective orbitals of the atoms.

towards the Fermi level and makes them available as valence electrons. These can now form bonds with the Na, enabling an exothermic adsorption of Se.

6.2.2 Diffusion Paths & Energy Barriers

To understand the energetics and dynamics of isolated atoms and clusters of the constituent elements, ab-initio total energy calculations for isolated In and Se adsorbants as well as various molecular formations of In_xSe_y on $MoSe_2$ are performed. In and Se adatoms are most stable when they are directly on-top of the surface Mo and Se sites, respectively. Adsorption calculations of (In, Se) on the other hand indicate the energetic minimum to be over a hollow region with a bond length of 2.768 ± 0.001Å , see Fig. 6.5. Diffusion paths and barriers for In and Se on $MoSe_2$ are obtained using the NEB method. Fig. 6.6 shows that the diffusion path is taken along a hollow region for both In and Se diffusions, while In protrudes more strongly into the hollow region than Se. The energy barrier of the In diffusion between two adjacent Mo sites is $E_a = 0.11$eV, while the energy barrier of Se for a diffusion between adjacent Se sites is $E_a = 1.08$eV. Due to its large energy barrier the latter is not observed in the MD simulations (see Sec. 6.2.3 for more details).

6.2.3 Kinetic Thermodynamics

Adatom diffusion on a surface is described as a chain of thermally activated uncorrelated events, called a Markovian chain[Gag17; AE10], a random walk on a substrate if you will. Using Arrhenius Law

$$D = D_0 \cdot \exp\left(-E_a/k_B T\right), \tag{6.1}$$

where D is the diffusion rate and D_0 a pre-exponential factor, we can - given a diffusion rate D - estimate D_0 by providing energy barriers from the NEB calculations. An adatom spends most of its time at specific surface sites and only occasionally takes random hops between adjacent adsorption sites. In addition to Eq. 6.1 the level of diffusivity of an adatom hopping between surface sites can be expressed using the Einstein's equation expressed in the continuous time random walk formalism

$$D = MSD(\tau)/(2d\tau^{\alpha}), \tag{6.2}$$

where MSD(τ) refers to the adatom's mean square displacement with lag time τ. d refers to the dimensionality of the diffusion path which in case of a surface diffusion is 2. α defines the dominant diffusion type to account for possible non-linearities of MSD(τ) vs τ. $\alpha = 1$ (linear) indicates normal diffusion (random walk), while $\alpha < 1$ and $1 < \alpha < 2$ correspond to subdiffusive and superdiffusive regimes, respectively. Finally, $\alpha \geq 2$ corresponds to ballistic diffusion [Ger+20]. Using Eqn. 6.1 the energy barrier E_a of any observed diffusion can be computed as

$$E_a = -k_B T \ln(D/D_0), \tag{6.3}$$

where D can be calculated using Eqn. 6.2. Unlike Se, which with its rather large energy barrier of E_a=1.08eV was not observed in any of the MD simulations, the easily observed diffusion path of In with E_a=0.11eV can be used to get an estimate for the pre-exponential factor D_0. The latter can be taken to be constant - a valid assumption for solids [YKR07]. Fig. 6.7 shows a selected In adatom diffusion on $MoSe_2$ vs lag time τ for its MSD and diffusion coefficient for up to 4ps of lag time. The linear variation of MSD(τ) vs τ indicates that the given system is in the diffusive regime ($\alpha = 1$) [Gio19]. Since the process of In diffusion is in the diffusive regime, diffusion barriers can be obtained using Eq. 6.2.[2] Using Eq. 6.1 this results in $D_0 \approx 64 \cdot 10^3 Å^2/ns$. Thus, the energy barrier of any process, given only its diffusion coefficient in the diffusive regime, can be derived. Other diffusions, such as e.g. InSe dimers, can be observed. The energy barriers extracted for various such dimers fall in the range of 0.124-0.138eV$\pm k_B T$, which is in good agreement with previously done adaptive kinetic Monte Carlo (aKMC) calculations for InSe on $MoSe_2$[Mir21].

[2]The diffusion coefficients for different lag times are obtained using Toni Giorgino's VMD plugin[Gio19] which utilizes Eqns. 6.1 and 6.2.

The diffusion barriers for other observed clusters and their respective dominant type of motion can be gleaned from Table 6.3. The general assumption that clusters of two or more atoms diffuse slower than the isolated atom does not hold true here as any of these systems have a lower energy barrier than isolated Se at 1.08eV. The addition of rotation as an aiding mechanism for diffusion in dimers/clusters of two or more atoms is likely to be a large contributor for the energy barrier decrease.

6.2.4 Film growth dynamics for different ratios of In:Se

This section deals with In_xSe_y growth on $MoSe_2$ for deposition ratios of In:Se of 1:1 and 2:3. Fig. 6.8 shows the deposition process of In and Se on the $MoSe_2$ (0001) surface given a 1:1 deposition rate. In the low coverage range the atoms are evenly distributed on the surface, which gradually transitions into a layer formation (Se_{sub}-In-Se) at higher coverages. Once the initial two layers are consolidated (0.47-0.7ML), a new In layer starts forming at even higher coverage. These observations indicate a sequential layering of Se-In-Se which is further confirmed by the layers observed in the depth profile of the system at 1ML coverage in Fig. 6.9. This confirms experimentally observed layer formations in In_2Se_3 powder and poly-crystalline samples[Küp+18], respectively. The dynamics in the case of a 2:3 deposition rate of In:Se is similar to the one above at low coverages, i.e. initial depositions correspond to In and Se adsorbing on their individual stable sites. Due to additional Se available to the system, any excess Se interact with each other to form Se dimers and trimers on-top of the In layer. This excess Se seems to initiate the formation of a second In layer before the first In layer fully covers the $MoSe_2$ surface. However, at higher coverages, see Fig. A.2 (e) in the Appendix, a strong admixture between the adatoms and the surface $MoSe_2$ layer is observed. This leads to better adhesive effects between adatoms and $MoSe_2$, but possibly changes the phase of the (In, Se) compound. Another effect of the excess Se during deposition can be observed in scaled island size distribution (ISD) plots of both systems, see Fig. 6.10. In the case

Tab. 6.3.: Selected clusters and islands in our simulations at 300K, their average diffusion barrier and the exhibited type of motion: rotational (r) and translational (t). (Lower index 'In' indicates clusters/islands on the grown In layer)

Cluster/Island	Diffusion Barrier E_α	Type of motion
Se_2	E_α=0.16 eV	r,t
Se_3	E_α=0.20 eV	r
$(Se_2)_{In}$	E_α=0.20 eV	r,t
$(Se_3)_{In}$	E_α=0.17 eV	r,t
InSe	E_α=0.22 eV	t
In_2Se	E_α=0.17 eV	r
In_3Se_2	E_α=0.21 eV	r
$(InSe)_{In}$	E_α=0.13 eV	r

of the 1:1 deposition rate, it shows that the initially wide spread size of clusters becomes smaller with increasing coverage and thus, the deviation from the average sized cluster becomes very small. For the ratio of 2:3, however, the simultaneous layer formation described before doesn't allow for many larger clusters initially but instead forms many smaller clusters which are closer to the size of the average cluster. In general, though, it appears that the ISD follows the generalized scaling behavior, resembling an exponential function and observed previously in monolayer nucleation experiments [Zhe+08].

6.2.5 Discussion

The validity of our assumption of a constant diffusion factor for solids we set in Sec. 6.2.3 hinges on the question whether the process/transition under consideration is in the diffusive regime, i.e. whether $MSD(\tau)$ vs τ is linear in τ and whether the system had sufficient time to equilibrate. We confirmed the former when we made the initial statement while the latter can be seen by plotting the bond length vs simulation time. One such plot is shown in Fig. 6.11 for the bond-length and angles of In-Se in coordinated clusters. It can be seen that there is no large deviation in the bond-length after about 2ps (except due to vibrational effects). Thus, energy barriers for variously sized clusters or islands can be determined while growing the film. Such kind of estimates are important and useful. On one hand, the barriers for such clusters or small islands are needed as input parameters for large-scale Monte-Carlo simulations. On the other hand, it is not straightforward to calculate these barriers by *ab-initio* calculations.

A layer-by-layer growth of (In, Se) compound on $MoSe_2$ surface is observed, i.e. the growing film of (In, Se) first fully covers the substrate surface before forming an additional layer. This growth dynamics has been observed recently by Gao et al. [Gao+20], growing In_2Se_3 nanoplates on different substrates. They observed that the growth on inert substrates (no dangling bonds on the substrate surface), such as mica or $MoSe_2$ in this case which has become inert due to the cleavage of the crystal along the van der Waals gap [MPM12; CR93], leads to the formation of horizontal nanoplates while growing them on reactive surfaces such as SiO/Si leads to the formation of vertical nanoplates.

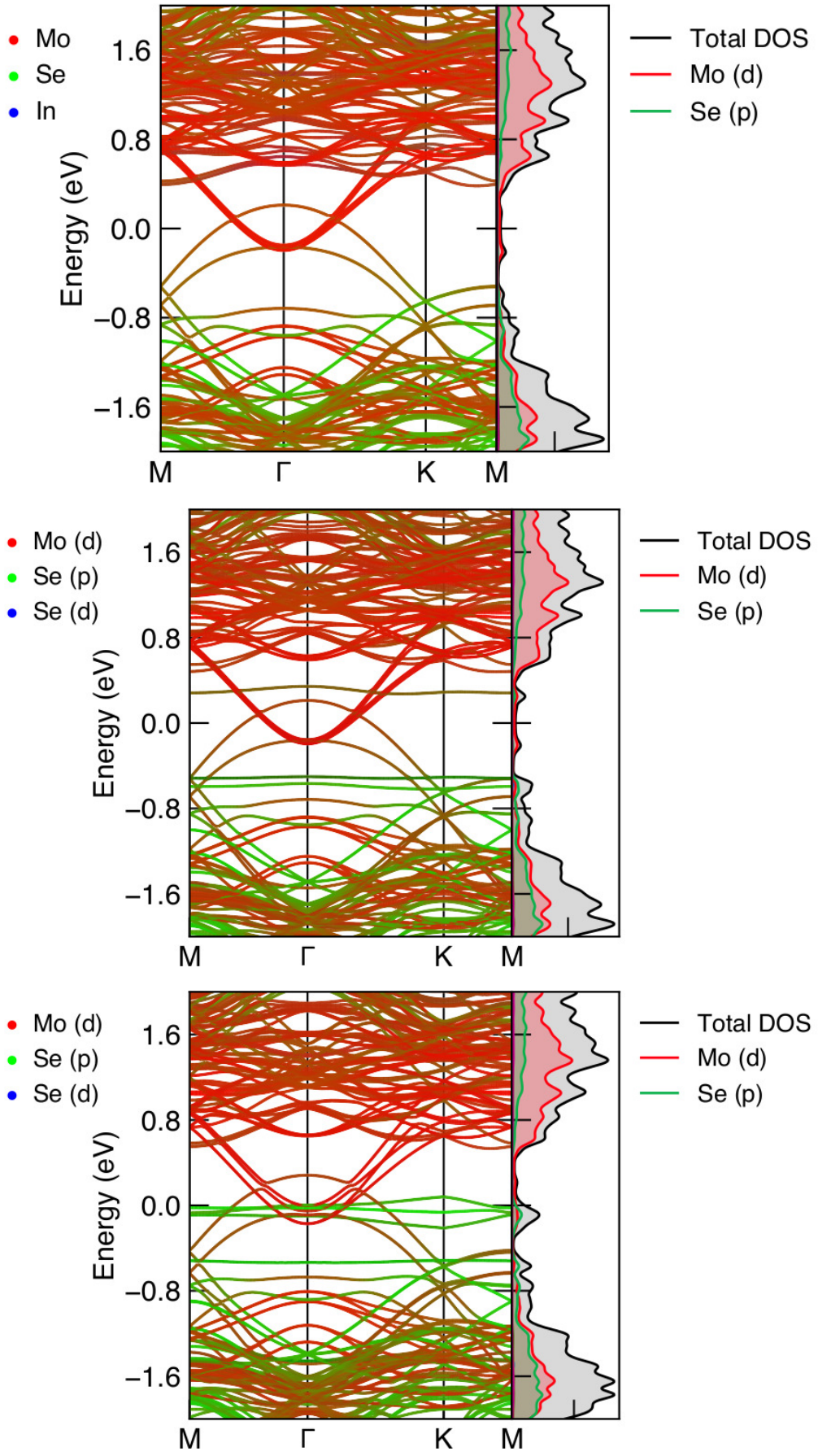

Fig. 6.4.: Band structure and DOS for In, InSe and InSe2 adsorbants. Parentheses refer to the respective orbitals of the atoms.

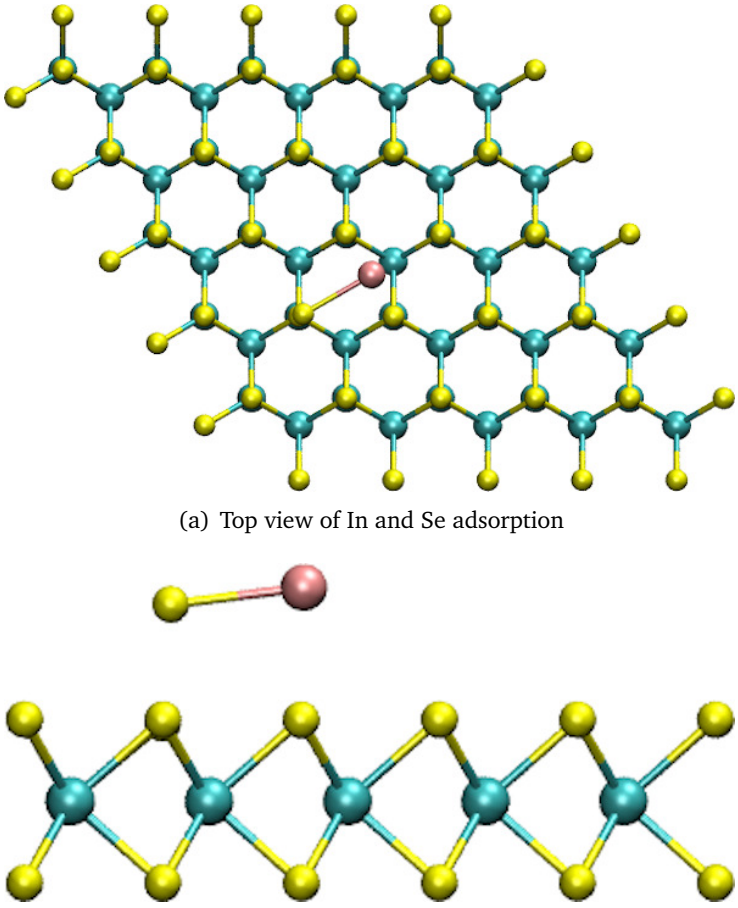

(a) Top view of In and Se adsorption

(b) Side view

Fig. 6.5.: Top (a) and side (b) views of $MoSe_2$ layer showing adsorbed In+Se pair. Mo, Se, and In atoms are represented as cyan, yellow and pink colored spheres, respectively.

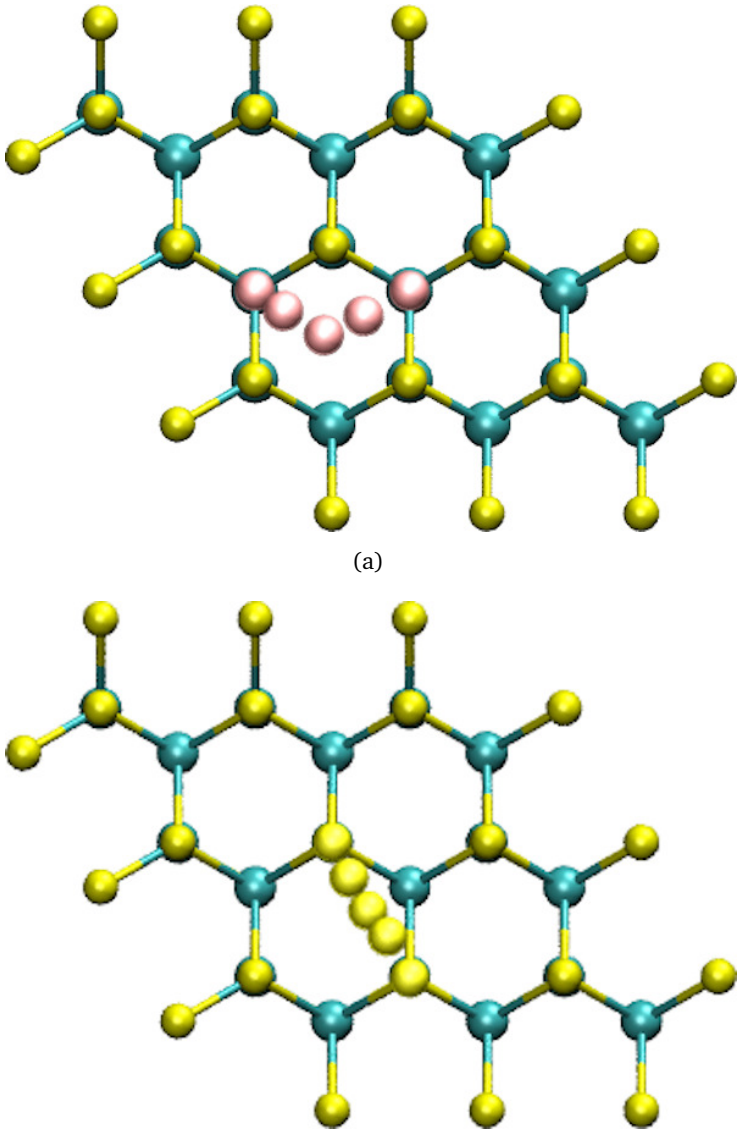

(a)

(b)

Fig. 6.6.: Diffusion paths of In (a) and Se (b) adatom on $MoSe_2$ surface. The diffusion paths are shown using diffused spheres connecting initial and final configurations. The energy barriers for In and Se are 0.11eV and 1.08eV, respectively. Mo, Se, and In atoms are represented as cyan, yellow and pink colored spheres, respectively.

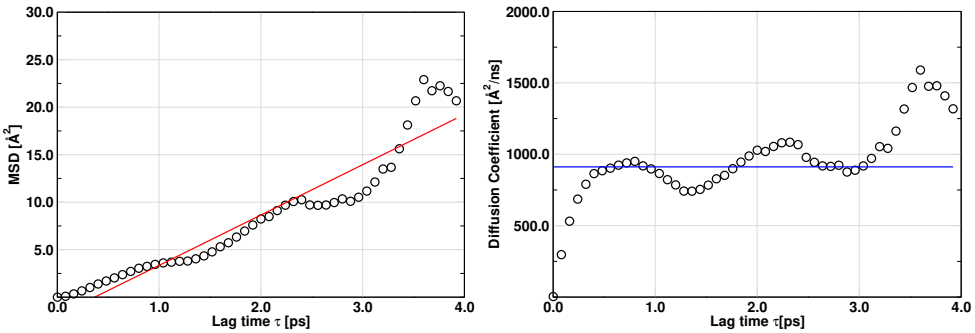

Fig. 6.7.: Left: MSD of In adatom diffusion on $MoSe_2$ surface. Right: Corresponding diffusion coefficient for Mo to Mo transition (for one particular trajectory has an average diffusion coefficient of D≈914Å^2/ns).

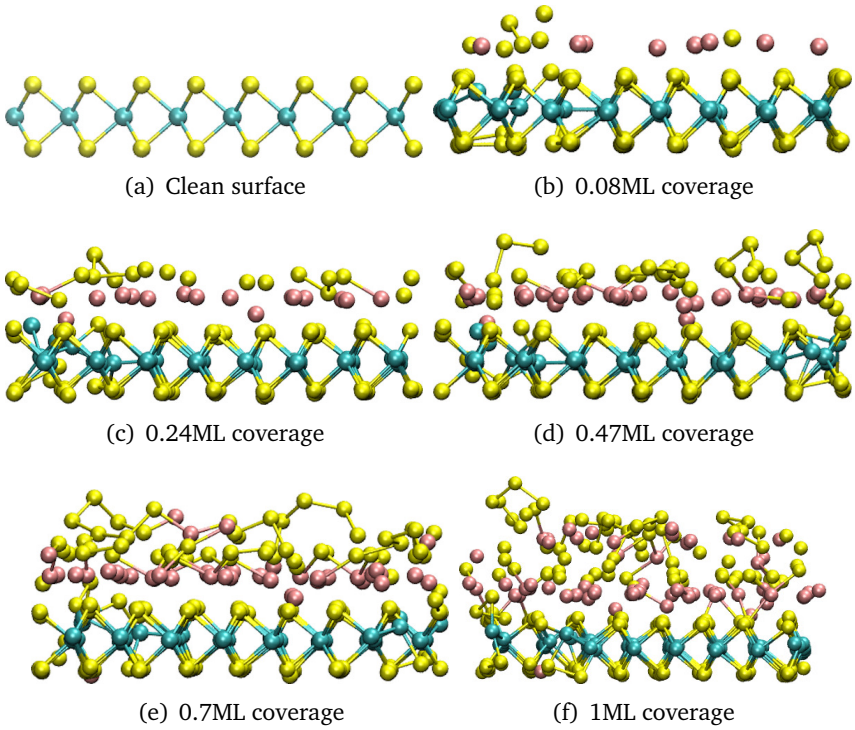

(a) Clean surface (b) 0.08ML coverage

(c) 0.24ML coverage (d) 0.47ML coverage

(e) 0.7ML coverage (f) 1ML coverage

Fig. 6.8.: Cross-sections of growing (In,Se) film on $MoSe_2$. Indium and selenium grow in a layer-by-layer fashion on $MoSe_2$ substrate under the given simulation conditions.

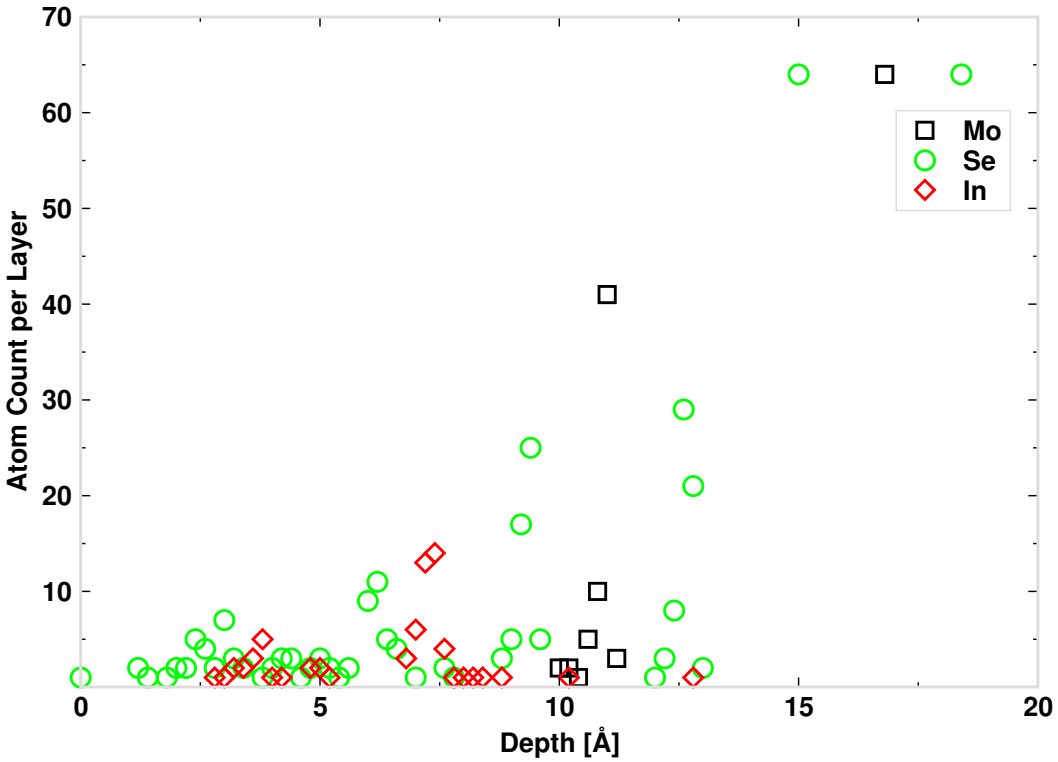

Fig. 6.9.: Depth profile for 1.0ML weighted by number of atoms per layer for the 1:1 case.

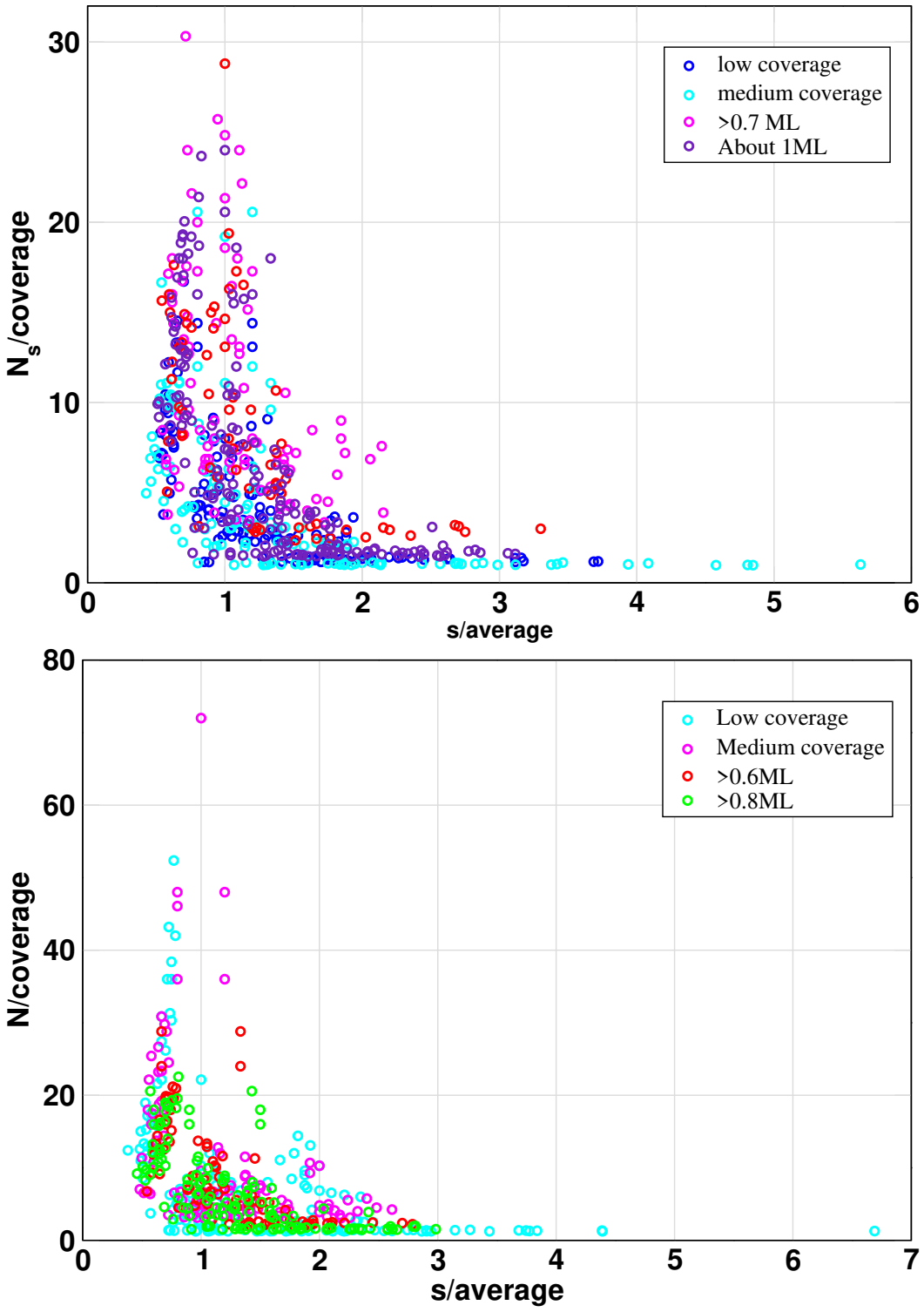

Fig. 6.10.: Coverage normalized size distributions for the cases with In:Se ratios of 1:1 and 2:3. With increasing coverage the size deviations decrease and get closer to the average at 1.

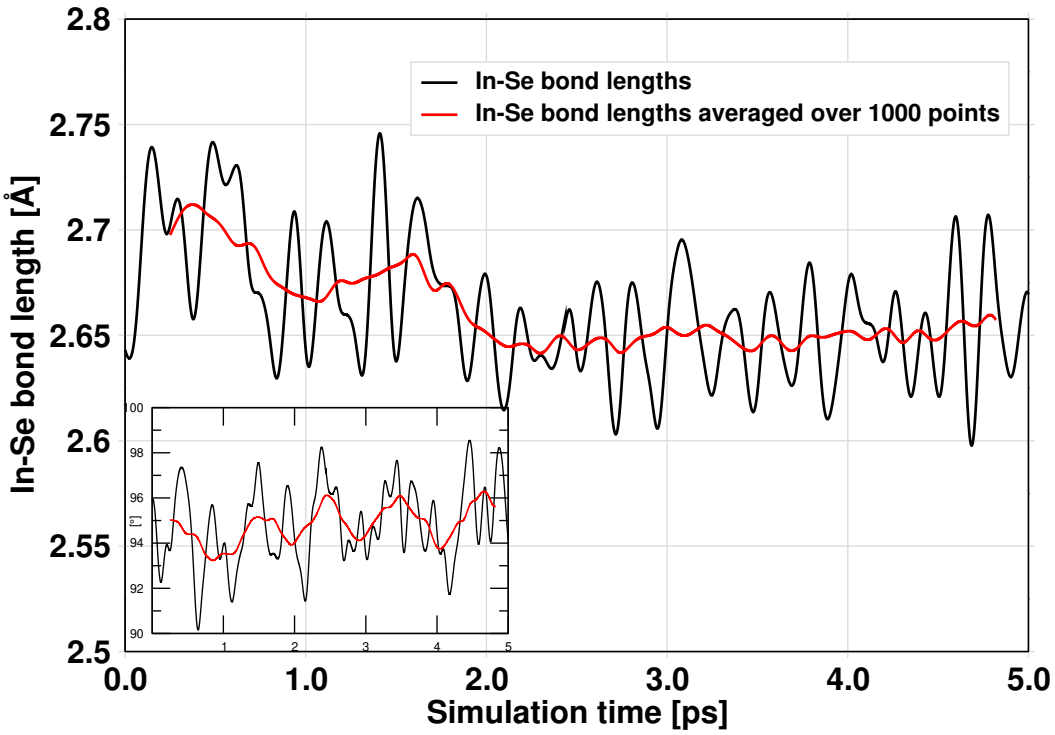

Fig. 6.11.: In-Se bond length variation in the complex (In,Se). Inset: Angles for threefold coordinated In clusters over time.

7 Conclusion

A notable part of the Thesis has been dedicated to the theoretical and practical implementation components of the PAW method - as a method designed to resolve issues arising from singularities from the potential at atomic nuclei sites when solving the Kohn-Sham equations and a formalism that bridges the gap between PP and LAPW methods while still giving access to the full one-electron wave function. The implementation of the SCAN functional by Perdew et al. within the original PAW framework of Blöchl in the CP-PAW code base while adhering to the necessity of second and third order derivatives as originally presented in [Blö94b], see Eqn. 3.34, provided insight to the inner workings of CP-PAW.

A detailed study of the C_3O_2 molecule was used to demonstrate an application of the methodologies presented within this Thesis. We have shown that the carbon suboxide in the gas phase minimizes into a bent geometry. This result conforms with calculations with higher-level methods but was achieved on a computationally much less demanding scope. We have shown that results from the use of a novel approach such as the real-space decomposed DF+RDMF approach and its reduction in computational effort by neglect of one-particle states are in accordance with results on the level of the local hybrid functionals. The bent structure goes contrary to our intuitive understanding of even such an apparently simple molecule. Not only does this suggest that C_3O_2 might exhibit the same properties as $g - C_3N_4$ does, e.g. for instance the possibility to synthesize C_3O_2 into a graphene-like substance, but it also opens up the possibility to gain new insight from other "ordinary" molecules and compounds from old chemistry that may have been overlooked due to our now seemingly faulty chemical intuition.

Furthermore, we looked into the growth mechanisms involved in the growth of CIGS thin films, as the latter has established itself as an essential component in the manufacturing of high-efficiency photovoltaic systems. *Ab-initio* based total energy calculations for adsorption of In and Se adatoms on an inert $MoSe_2$ substrate surface were performed. Diffusion paths and barriers of these adsorbates have been estimated using the NEB method. Utilizing the knowledge regarding the behavior of In and Se adsorption from first-principles calculations, we have established a tight-binding molecular dynamics based model for growth of (In, Se) film on $MoSe_2$. Many experimental growth parameters like temperature and deposition fluxes of incoming

atoms can be controlled in this model. At sufficient surface coverage, alternate layers of In-Se can be observed on the substrate surface. Formation of alternate In-Se layers indicates the formation of a crystalline phase of (In, Se) in the simulations. Further, it has been identified that diffusion of In adatoms on $MoSe_2$ surface falls under the diffusive regime. Altogether , we are now able to pick any atom or molecule in our system and partition them into individual processes they take on the surface and extract an energy barrier for all of them. This is important because doing NEB is exponentially difficult and, instead, with this approach the barriers are estimated from tight binding methods and this is useful for other methods, e.g. various Monte Carlo methods, which require these values as inputs.

By incorporating these computational approaches, we want to establish the importance of combining advanced theoretical methods with practical applications in Materials Science. We hope with this work to not only advance our insights into specific materials like C_3O_2 and CIGS, but also improve the theoretical tools available for a wider array of applications in molecular and nanostructure materials research.

Future research resulting from this thesis could investigate an extension of the RDMFT+ACA approach to a wider range of materials, such as those undergoing phase transitions or those displaying topological properties. Also, continued improvement and fine-tuning of the SCAN meta-GGA functional or other newly emerging functionals within the CPPAW framework could open new possibilities in the analysis of material properties, adding to the development of new materials with customizable mechanical and electronic properties.

Appendices

Supplementary Figures

A

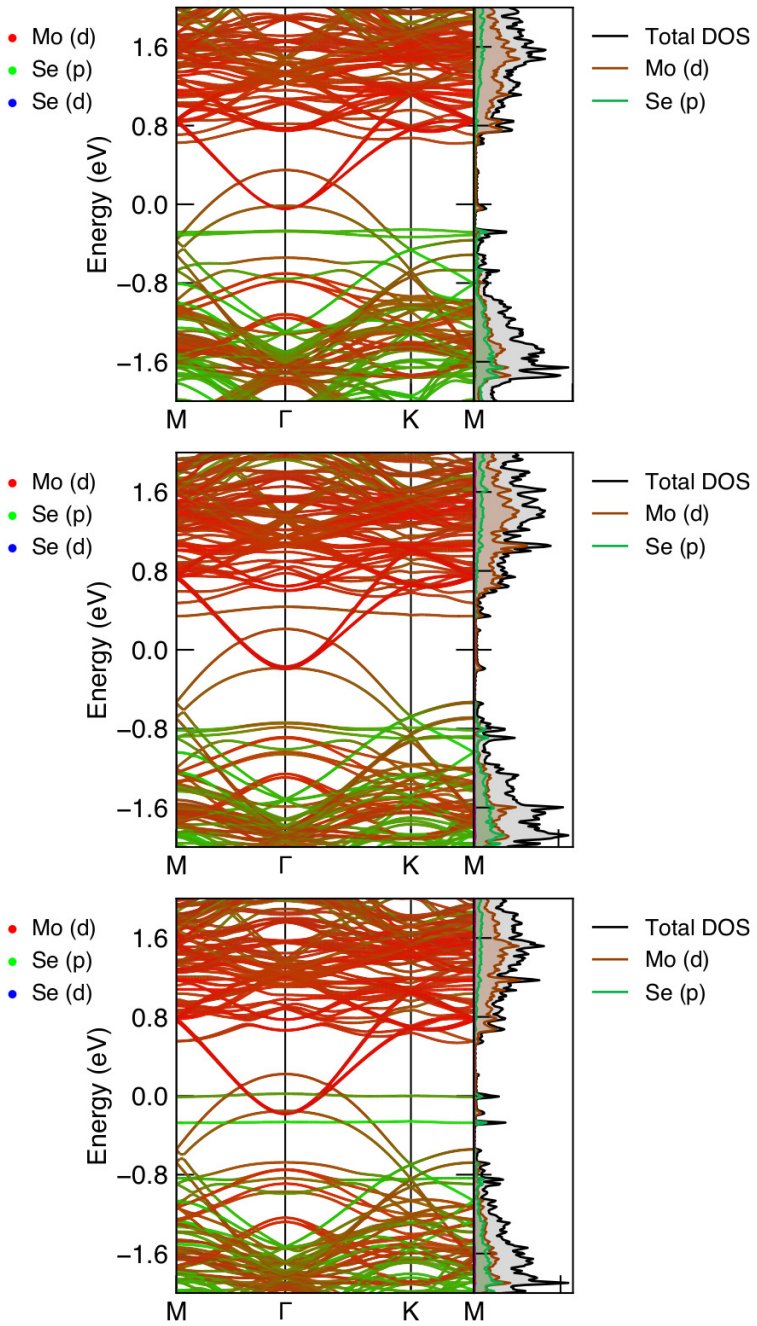

Fig. A.1.: Band structure and DOS for Se, SeNa and SeNa2 adsorbants.

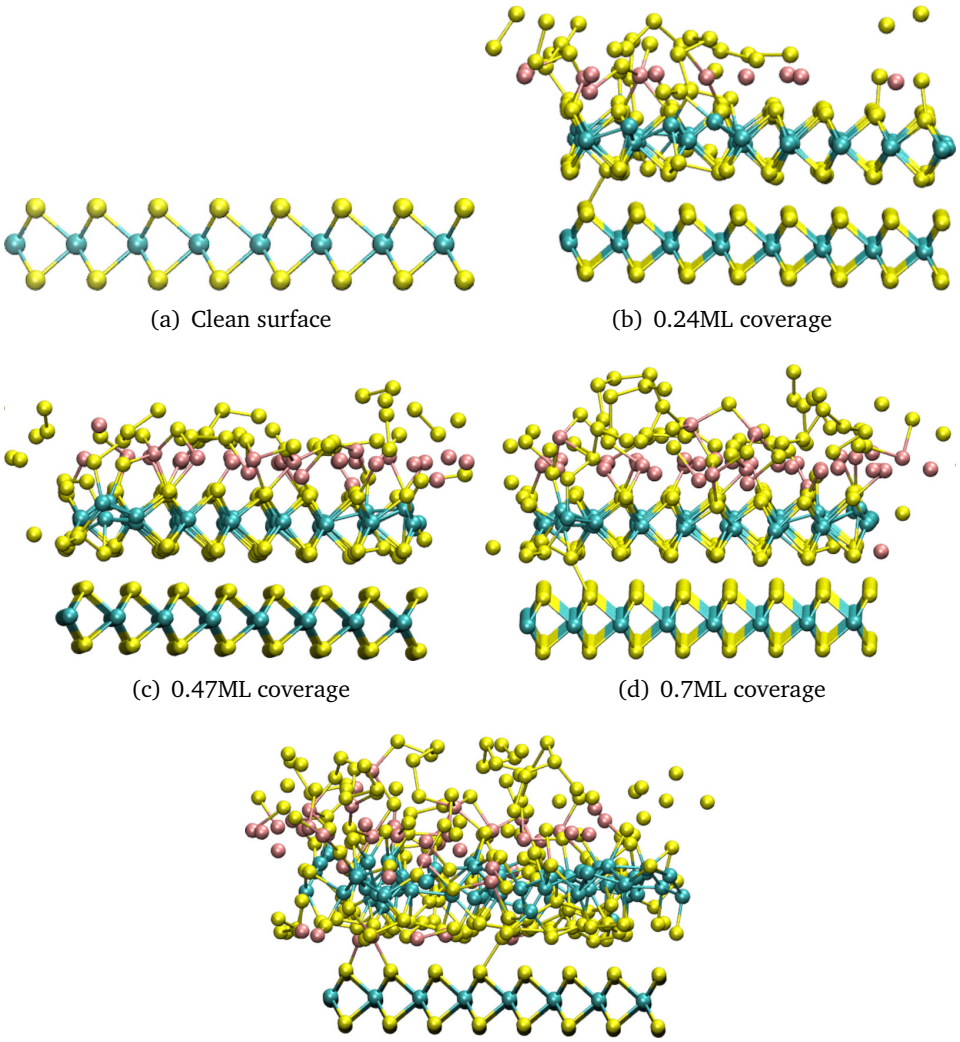

(a) Clean surface

(b) 0.24ML coverage

(c) 0.47ML coverage

(d) 0.7ML coverage

(e) 0.8ML coverage

Fig. A.2.: Crosssections of growing (In,Se) film on $MoSe_2$. Indium and selenium grow in a layer-by-layer fashion on $MoSe_2$ substrate under the given simulation conditions. Case: 2:3.

B Implementation of the SCAN functional

We want to calculate

$$E_{xc}[n_\uparrow, n_\downarrow] = \int d^3r n\epsilon_{xc}(n_\uparrow, n_\downarrow, \nabla n_\uparrow, \nabla n_\downarrow, \tau_\uparrow, \tau_\downarrow) \tag{B.1}$$

We can separate E_{xc} into E_x and E_c. For the SCAN functional the exchange energy is identical (except for a linear scaling) in both the restricted and unrestricted case. Thus, I will start with translation of the exchange part. Constants, not otherwise defined, can be found listed and tabled in the corresponding reference papers.

B.1 Exchange Energy for spin restricted and unrestricted scan

The exchange energy can be calculated as (see eqn. (3) of ref. [SRP15a])

$$E_x[n] = \int d^3r n\epsilon_x^{unif}(n)F_x(s,\alpha) \tag{B.2}$$

where n is simply the electron density[1] and

$$\begin{aligned}
\epsilon_x^{unif} &= -(3/4\pi)(3\pi^2 n)^{1/3} && \text{(B.3)}\\
F_x &= \{h_x^1(s,\alpha) + f_x(\alpha)[h_x^0 - h_x^1(s,\alpha)]\}g_x(s) && \text{(B.4)}\\
h_x^1 &= 1 + k_1 - k_1/(1 + x/k_1) = \frac{k_1 + x + k_1 x}{k_1 + x} && \text{(B.5)}\\
x &= \mu_{ak}s^2[1 + (b_4 s^2/\mu_{ak})\exp(-|b_4|s^2/\mu_{ak})]\\
&+ \{b_1 s^2 + b_2(1-\alpha)\exp[-b_3(1-\alpha)^2]\}^2 && \text{(B.6)}
\end{aligned}$$

α was nicely defined in the TPSS [Tao+03] paper as

$$\begin{aligned}
\alpha &= (\tau - \tau^w)/\tau^{unif} = (5p/3)(z^{-1} - 1) \geq 0 && \text{(B.7)}\\
\tau^w &= |\nabla n|^2/8n && \text{(B.8)}\\
\tau^{unif} &= (3/10)(3\pi^2)^{2/3}n^{5/3} && \text{(B.9)}
\end{aligned}$$

[1] which is given as an input along the with ∇n and τ

where $p = |\nabla n|^2/[4(3\pi^2)^{2/3}n^{8/3}] = s^2$ and $z = \tau^w/\tau \leq 1$. I'm going to use p instead of s^2 in eqn. B.6. For future purposes it is a good idea to have the derivations in regards to $n, \nabla n$ and τ on the ready. Thus:

$$\partial_n p = -8/3 \cdot |\nabla n|^2/[4(3\pi^2)^{2/3}n^{11/3}] = -\frac{8p}{3n} \tag{B.10}$$

$$\partial_{\nabla n} p = 2 \cdot p/\nabla n \tag{B.11}$$

```
! Exchange part which is the same for both restricted
! and unrestricted scan (except a linear scaling, see Oliver and Perdew
    1979)

subroutine scan_x()
implicit none !for the integer and real parameter differentiaion
********************
*INPUTS, OUTPUTS, and DECLARATIONS*
********************

p = ngr*ngr/(4.0d0*pi23*n**(8.0d0/3.0d0))
dp_dn = -8.0d0/3.0d0*p/n
dp_dngr = 2.0d0*p/ngr
```

While we are at it we can also do the derivatives for z and α:

$$\partial_n z = \partial_n \frac{|\nabla n|^2}{8n\tau} = -\frac{|\nabla|^2}{8\tau n^2} = -z/n \tag{B.12}$$

$$\partial_{\nabla n} z = 2 \cdot z/\nabla n \tag{B.13}$$

$$\partial_\tau z = -z/\tau \tag{B.14}$$

and

$$\partial_n \alpha = 5/3 \cdot (-p\partial_n z/z^2 + \partial_n p \cdot (1/z - 1)) \tag{B.15}$$

$$\partial_{\nabla n} \alpha = \frac{\alpha}{p}\partial_{\nabla n} p - \frac{5p}{3z^2}\partial_{\nabla n} z \tag{B.16}$$

$$\partial_\tau \alpha = 1/\tau^{unif} \tag{B.17}$$

This translates to:

```
tau_unif = 0.3d0*(3.0d0*pi**2)**(2.0d0/3.0d0)*n**(5.0d0/3.0d0)
tau_w = ngr*ngr/(8.0d0*n)

z = tau_w/tau
dz_dn = -z/n
dz_dngr = 2.0d0*z*/ngr
dz_dtau = -z/tau
```

```
alpha = (5.0d0*p/3.0d0)(1.0d0/z-1.0d0)
dalpha_dn = (5.0d0/3.0d0)*(-p*dz_dn/(z**2)+dp_dn*(1.0d0/z-1.0d0))
dalpha_dngr = (alpha/p)*dp_dngr - (5.0d0*p/(3.0d0*z**2))*dz_dngr
dalpha_dtau = 1.0d0/tau_unif
```

Analogously, x,h_x^1,f_x and g_x from eqn. B.4

$$\begin{aligned}
\partial_p x &= \mu_{ak} + b_4 p \exp(-b_4 p/\mu_{ak})[2 - p b_4/\mu_{ak}] \\
&+ 2b_1 \cdot (b_1 p + b_2(1-\alpha)\exp[-b_3(1-\alpha)^2]) \\
\partial_\alpha x &= 2b_2 \exp[-b_3(1-\alpha)^2] \\
&\cdot (b_1 p + b_2(1-\alpha)\exp[-b_3(1-\alpha)^2]) \\
&\cdot (2b_3(1-\alpha)^2 - 1) \\
\partial_x h_x^1 &= k_1^2/(k_1+x)^2 \\
\partial_p h_x^1 &= \partial_x h_x^1 \partial_p x \\
\partial_\alpha h_x^1 &= \partial_x h_x^1 \partial_\alpha x \\
\partial_\alpha f_x &= -\frac{c_{1x}\exp[-c_{1x}\alpha/(1-\alpha)] + d_x c_{2x}\exp[c_{2x}/(1-\alpha)]}{(1-\alpha)^2} \\
\partial_p g_x &= -\frac{a_1 \exp(-a_1/p^{1/4})}{4p^{5/4}}
\end{aligned}$$

Using the above derivatives we can now set on to get the derivatives of the enhancement factor F_x:

$$\begin{aligned}
\partial_p F_x &= \partial_p h_x^1 (1-f_x) g_x + (h_x^1 + f_x(h_x^0 - h_x^1))\partial_p g_x \\
\partial_\alpha F_x &= (\partial_\alpha h_x^1 + \partial_\alpha f_x \cdot (h_x^0 - h_x^1) - f_x \partial_\alpha h_x^1) g_x \\
\partial_n F_x &= \partial_\alpha F_x \partial_n \alpha + \partial_p F_x \partial_n p \\
\partial_{\nabla n} F_x = &= \partial_\alpha F_x \partial_\nabla \alpha + \partial_p F_x \partial_{\nabla n} p \\
\partial_\tau F_x &= \partial_\alpha F_x \partial_\tau \alpha
\end{aligned}$$

B.2 Correlation Energy for restricted spin

In the restricted case we have

$$\zeta = \frac{n_\uparrow - n_\downarrow}{n_\uparrow + n_\downarrow} = 0 \tag{B.18}$$

and the exchange scaling

$$\phi(\zeta) = [(1+\zeta)^{2/3} + (1-\zeta)^{2/3}]/2 = 1 \tag{B.19}$$

which simplifies some of the derivatives. The correlation energy density is defined as (see SI of [SRP15a])

$$\epsilon_c = \epsilon_c^1 + f_c(\alpha)(\epsilon_c^0 - \epsilon_c^1) \tag{B.20}$$

where

$$\begin{aligned} f_c(\alpha) &= \exp[-c_{1c}\alpha/(1-\alpha)]\theta(1-\alpha) \\ &- d_c \exp[c_{2c}/(1-\alpha)]\theta(\alpha-1)] \end{aligned}$$

and θ is the step function. ϵ_c^1 is defined as

$$\epsilon_c^1 = \epsilon_c^{LSDA1} + H_1, \tag{B.21}$$

where

$$\begin{aligned} H_1 &= \gamma\phi^3 \ln[1 + w_1(1 - g(At^2))] \\ \partial_{r_s} H_1 &= \frac{\gamma(\partial_{r_s} w_1(1 - g(At^2) + g(At^2)w_1(t^2\partial_{r_s} A + \partial_{r_s} t^2))}{(1 + 4At^2)} \\ \partial_p H_1 &= \frac{\gamma g(At^2) w_1 A \partial_p t^2}{(1 + 4At^2)(1 + w_1(1 - g(At)))} \\ t &= (3\pi^2/16)^{1/3} s/(\phi r_s^{1/2}) \\ &= (3\pi^2/16)^{1/3} p^{1/2}/(\phi r_s 1/2) \\ \partial_{r_s} t^2 &= -t^2/r_s \\ \partial_p t^2 &= t^2/(p r_s) \\ w_1 &= \exp[-\epsilon_c^{LSDA1}/(\gamma\phi^3)] - 1 \\ \partial_{r_s} w_1 &= -\exp[-\epsilon_c^{LSDA1}/\gamma] \cdot \partial_{r_s} \epsilon_c^{LSDA1} \\ A &= \beta(r_s)/(\gamma w_1) \\ \partial_{r_s} A &= \partial_{r_s}\beta/(\gamma w_1) - A/w_1 \partial_{r_s} w_1 \\ \beta &= 0.066725(1 + 0.1 r_s)/(1 + 0.1778 r_s) \\ \partial_{r_s}\beta &= -0.0052/(1 + +0.1778 r_s)^2 \\ g(At^2) &= 1/(1 + 4At^2)^{1/4} \end{aligned}$$

Let's start with the necessary derivatives for ϵ_c^1:

$$\partial_{r_s}\epsilon_c^1 = \epsilon_{r_s}\epsilon_c^{LSDA1} + \partial_{r_s} H_1 \tag{B.22}$$

$$\partial_p \epsilon_c^1 = \partial_p H_1 \tag{B.23}$$

Next up is the ϵ_c^0 in eqn. B.21

$$\epsilon_c^0 = (\epsilon_c^{LDA0} + H_0) G_c(\zeta) \tag{B.24}$$

where $G_c(\zeta) = \{1-2.3631[d_x(\zeta)-1]\}(1-\zeta^{12})$ and $d_x(\zeta) = [(1+\zeta)^{4/3}+(1-\zeta)^{4/3}]/2$, which is 1 in case of the restricted spin variant.

ϵ_c^{LDA0} here is defined as

$$\epsilon_c^{LDA0} = -b_{1c}/(1 + b_{2c}r_s^{1/2} + b_{3c}r_s) \tag{B.25}$$

$$\partial_{r_s}\epsilon_c^{LDA0} = \frac{b_{1c}(1/2 + b_{2c}/\sqrt{r_s} + b_{3c})}{(1 + b_{2c}\sqrt{r_s} + b_{3c}r_s)^2} \tag{B.26}$$

In analogy to H_1, we have

$$H_0 = b_{1c}\ln[1 + w_0(1 - g_\infty(\zeta = 0, s))] \tag{B.27}$$

$$\partial_{r_s}H_0 = b_{1c}\partial_{r_s}w_0(1 - g_\infty)/(1 + w_0(1 - g_\infty)) \tag{B.28}$$

$$\partial_p H_0 = -b_{1c}w_0\partial_p g_\infty/(1 + w_0(1 - g_\infty)) \tag{B.29}$$

$$w_0 = \exp[-\epsilon_c^{LDA0}/b_{1c}] - 1 \tag{B.30}$$

$$\partial_{r_s}w_0 = -\partial_{r_s}\epsilon_c^{LDA0}\exp(-\epsilon_c^{LDA0}/b_{1c})/b_{1c} \tag{B.31}$$

$$g_\infty = \lim_{r_s\to\infty} g(At^2) = 1/(1 + 4\chi_{\text{inf}}p)^{1/4} \tag{B.32}$$

$$\chi_\infty(\zeta) = (3\pi^2/16)^{2/3}\beta(r_s \to \infty)\phi/[c_x(\zeta) - f_0] \tag{B.33}$$

where $c_x(\zeta) = -(3/4\pi)(9\pi/4)^{1/3}d_x(\zeta)$ and f_0=0.9. At ζ=0 we have χ_∞=0.128026

The derivatives for ϵ_c^0 are then

$$\partial_{r_s}\epsilon_c^0 = \partial_{r_s}\epsilon_c^{LDA0} + \partial_{r_s}H_0 \tag{B.34}$$

$$\partial_p\epsilon_c^0 = \partial_p H_0 \tag{B.35}$$

Now we have all the ingredients to define ϵ_c in the code. Additionally I did the derivatives for E_c and E_x to get the potentials. The derivatives can be found in the code.

The correlation part for the unrestricted spin can be found in the code.

B.3 Second and Third Derivatives

B.3.1 Exchange part

Let

$$E_x[n] = \int d^3r n\epsilon_x^{unif}(n)F_x(p,\alpha) = \int d^3r A_x(n,p,\alpha) \tag{B.36}$$

We have for p:

$$\begin{aligned}
p &= |\nabla n|^2/[4(3\pi^2)^{2/3}n^{8/3}] = s^2 && \text{(B.37)}\\
\partial_n p &= -8/3\cdot|\nabla n|^2/[4(3\pi^2)^{2/3}n^{11/3}] = -\frac{8p}{3n} && \text{(B.38)}\\
\partial_n^2 p &= \frac{88p}{9n^2} && \text{(B.39)}\\
\partial_n^3 p &= -\frac{1232p}{27n^3} && \text{(B.40)}\\
\partial_{\nabla n} p &= 2\cdot p/\nabla n && \text{(B.41)}\\
\partial_{\nabla n}^2 p &= 1/[2(3\pi^2)^{2/3}n^{8/3}] && \text{(B.42)}\\
\partial_{\nabla n}^3 p &= 0 && \text{(B.43)}
\end{aligned}$$

For $z = \tau^w/\tau$:

$$\begin{aligned}
\partial_n z &= -z/n && \text{(B.44)}\\
\partial_n^2 z &= \frac{z}{2n^2} && \text{(B.45)}\\
\partial_n^3 z &= -3|\nabla n|^2/(\tau 4n^4) && \text{(B.46)}\\
\partial_{\nabla n} z &= \frac{\nabla n}{4n\tau} && \text{(B.47)}\\
\partial_{\nabla n}^2 z &= \frac{1}{4n\tau} && \text{(B.48)}\\
\partial_{\nabla n}^3 z &= 0 && \text{(B.49)}\\
\partial_\tau z &= -\frac{\tau^w}{\tau^2} && \text{(B.50)}\\
\partial_\tau^2 z &= \frac{2z}{\tau^2} && \text{(B.51)}\\
\partial_\tau^3 z &= -\frac{6z}{\tau^3} && \text{(B.52)}
\end{aligned}$$

For $r_s = (4\pi/3)^{-1/3}/n^{1/3}$:

$$\begin{aligned}
\partial_n r_s &= -\frac{(4\pi/3)^{-1/3}}{3n^{4/3}} && \text{(B.53)}\\
\partial_n^2 r_s &= \frac{4(4\pi/3)^{-1/3}}{9n^{7/3}} && \text{(B.54)}\\
\partial_n^3 r_s &= -\frac{28(4\pi/3)^{1/3}}{27n^{10/3}} && \text{(B.55)}
\end{aligned}$$

For $\beta = 0.066725(1 + 0.1r_s)/(1 + 0.1778r_s)$:

$$\partial_{r_s}\beta = -0.0052/(1 + 0.1778r_s)^2 \tag{B.56}$$

$$\partial^2_{r_s}\beta = \frac{0.00185 + 0.00033r_s}{(1 + 0.1778r_s)^4} \tag{B.57}$$

$$\partial^3_{r_s}\beta = \frac{0.00033(1 + 0.1778r_s)^4 - 0.7112(0.00185 + 0.00033r_s)}{(1 + 0.1778r_s)^8} \cdot \frac{1}{(1 + 0.1778r_s)^5} \tag{B.58}$$

$\zeta = \frac{n_\uparrow - n_\downarrow}{n}$ and for $\phi = [(1 + \zeta)^{2/3} + (1 - \zeta)^{2/3}]/2$ we have:

$$\partial_\zeta\phi = 1/3[(1 + \zeta)^{-1/3} - (1 - \zeta)^{-1/3}] \tag{B.59}$$

$$\partial^2_\zeta\phi = -1/9[(1 + \zeta)^{-4/3} - (1 - \zeta)^{-4/3}] \tag{B.60}$$

$$\partial^3_\zeta\phi = 4/27[(1 + \zeta)^{-7/3} - (1 - \zeta)^{-7/3}] \tag{B.61}$$

For $d_s(\zeta) = [(1 + \zeta)^{5/3} + (1 - \zeta)^{5/3}]/2$:

$$\partial_\zeta d_s = 5/6[(1 + \zeta)^{2/3} - (1 - \zeta)^{2/3}] \tag{B.62}$$

$$\partial^2_\zeta d_s = 10/18[(1 + \zeta)^{-1/3} + (1 - \zeta)^{-1/3}] \tag{B.63}$$

$$\partial^3_\zeta d_s = -5/27[(1 + \zeta)^{-4/3} - (1 - \zeta)^{-4/3}] \tag{B.64}$$

For $\alpha = (\tau - \tau^w)/\tau^{unif} = (5p/3)(z^{-1} - 1)$ we have:

$$\partial_n \alpha = 5/3[-p(\partial_n z)/z^2 + \partial_n p \cdot (1/z - 1)] \tag{B.65}$$

$$\partial_n^2 \alpha = 5/3[-\partial_n p \partial_n z/z^2 - p\partial_n^2 z/z^2 + 2p(\partial_n z)^2/z^3 + \partial_n^2 p(1/z - 1) - \partial_n p \partial_n z/z^2] \tag{B.66}$$

$$\begin{aligned}\partial_n^3 \alpha = 5/3[&-\partial_n^2 p \partial_n z/z^2 - \partial_n p \partial_n^2 z/z^2 + 2\partial_n p(\partial_n z)^2/z^3 - \partial_n p \partial_n^2 z/z^2 - p\partial_n^3 z/z^2 \\ &+2p\partial_n^2 z \partial_n z/z^3 + 2\partial_n p(\partial_n z)^2/z^3 + 4p\partial_n z \partial_n^2 z/z^3 - 6p(\partial_n z)^3/z^4) \\ &+\partial_n^3 p(1/z - 1 + \partial_n^2 p \partial_n z/z^2 - \partial_n^2 p \partial_n z/z^2 \\ &-\partial_n p \partial_n^2 z/z^2 + 2\partial_n p(\partial_n z)^2/z^3]\end{aligned} \tag{B.67}$$

$$\partial_{\nabla n} \alpha = \frac{\alpha \partial_{\nabla n} p}{p} - \frac{5p}{3z^2} \partial_{\nabla n} z \tag{B.68}$$

$$\partial_{\nabla n}^2 \alpha = \frac{\partial_{\nabla n} \alpha \partial_{\nabla n} p}{p} - \frac{\alpha(\partial_{\nabla n} p)^2}{p^2} + \frac{\alpha \partial_{\nabla n}^2 p}{p} - \frac{5\partial_{\nabla n} p \partial_{\nabla n} z}{3z^2} + \frac{10p(\partial_{\nabla n} z)^2}{3z^3} - \frac{5p\partial_{\nabla n}^2 z}{3z^2} \tag{B.69}$$

$$\begin{aligned}\partial_{\nabla n}^3 \alpha = &\frac{\partial_{\nabla n}^2 \alpha \partial_{\nabla n} p}{p} - \frac{\partial_{\nabla n} \alpha(\partial_{\nabla n} p)^2}{p^2} + \frac{\partial_{\nabla n} \alpha \partial_{\nabla n}^2 p}{p} - \frac{\partial_{\nabla n} \alpha(\partial_{\nabla n} p)^2}{p^2} - 2\frac{\alpha \partial_{\nabla n} p \partial_{\nabla n}^2 p}{p^2} \\ &+\frac{\partial_{\nabla n} \alpha \partial_{\nabla n}^2 p}{p} - \frac{\alpha \partial_{\nabla n} p \partial_{\nabla n}^2 p}{p^2} - \frac{5\partial_{\nabla n}^2 p \partial_{\nabla n} z}{3z^2} + \frac{10\partial_{\nabla n} p(\partial_{\nabla n} z)^2}{3z^3} - \frac{5\partial_{\nabla n} p \partial_{\nabla n}^2 z}{3z^2} \\ &+\frac{10\partial_{\nabla n} p(\partial_{\nabla n} z)^2}{3z^3} + \frac{20p\partial_{\nabla n} z \partial_{\nabla n}^2 z}{3z^3} - \frac{30p(\partial_{\nabla n} z)^3}{3z^4} - \frac{5\partial_{\nabla n} p \partial_{\nabla n}^2 z}{3z^2} \\ &+\frac{10p\partial_{\nabla n} z \partial_{\nabla n}^2 z}{3z^3}\end{aligned} \tag{B.70}$$

$$\partial_\tau \alpha = 1/\tau^{unif} \tag{B.71}$$

$$\partial_\tau^2 \alpha = 0 \tag{B.72}$$

$$\partial_\tau^3 \alpha = 0 \tag{B.73}$$

For $x = \mu_{ak}p[1 + (b_4p/\mu_{ak})\exp(-|b_4|p/\mu_{ak})] + \{b_1p + b_2(1-\alpha)\exp[-b_3(1-\alpha)^2]\}^2$ we have:

$$\begin{aligned}
\partial_p x &= \mu_{ak} + b_4 p\exp(-b_4p/\mu_{ak})[2 - pb_4/\mu_{ak}] + 2b_1(b_1p + b_2(1-\alpha) \\
&\quad \cdot\exp(-b_3(1-\alpha)^2)) && \text{(B.74)} \\
\partial_p^2 x &= b_4\exp(-b_4p/\mu_{ak})[2 - pb_4/\mu_{ak}] - \frac{b_4^2}{\mu_{ak}}\exp(-b_4p/\mu_{ak}) \\
&\quad \cdot[3 - pb_4/\mu_{ak}] + 2b_1^2 && \text{(B.75)} \\
\partial_p^3 x &= -\frac{2b_4^2}{\mu_{ak}}\exp(-b_4p/\mu_{ak})[3 - pb_4/\mu_{ak}] + \frac{b_4^3p}{\mu_{ak}^2}\exp(-b_4p/\mu_{ak})[5 - pb_4/\mu_{ak}] \\
&\quad -\frac{b_4^2}{\mu_{ak}}\exp(-b_4p/\mu_{ak}) && \text{(B.76)} \\
\partial_\alpha x &= 2b_2\exp(-b_3(1-\alpha)^2)\cdot(b_1p + b_2(1-\alpha)\exp(-b_3(1-\alpha)^2)) \\
&\quad \cdot(2b_3(1-\alpha)^2 - 1) && \text{(B.77)} \\
\partial_\alpha^2 x &= 4b_2b_3\exp(-b_3(1-\alpha)^2)(b_1p + b_2(1-\alpha)\exp(-b_3(1-\alpha)^2)) \\
&\quad \cdot(2b_3(1-\alpha)^3 - 3(1-\alpha)) \\
&\quad +2b_2\exp(-b_3(1-\alpha)^2)(b_2\exp(-b_3(1-\alpha)^2)[2b_3(1-\alpha)^2 - 1]) \\
&\quad \cdot(2b_3(1-\alpha)^2 - 1) && \text{(B.78)} \\
\partial_\alpha^3 x &= 8b_2b_3^2(1-\alpha)\exp(-b_3(1-\alpha)^2)(b_1p + b_2(1-\alpha)\exp(-b_3(1-\alpha)^2)) \\
&\quad \cdot(2b_3(1-\alpha)^3 - 3(1-\alpha)) \\
&\quad +4b_2b_3\exp(-b_3(1-\alpha)^2)(b_2\exp(-b_3(1-\alpha)^2)[2b_3(1-\alpha)^2 - 1]) \\
&\quad \cdot(2b_3(1-\alpha)^3 - 3(1-\alpha)) \\
&\quad +4b_2b_3\exp(-b_3(1-\alpha)^2)(b_1p + b_2(1-\alpha)\exp(-b_3(1-\alpha)^2)) \\
&\quad \cdot(-6b_3(1-\alpha)^2 + 3) \\
&\quad +4b_2b_3(1-\alpha)\exp(-b_3(1-\alpha)^2)(b_2\exp(-b_3(1-\alpha)^2)[2b_3(1-\alpha)^2 - 1]) \\
&\quad \cdot(2b_3(1-\alpha)^2 - 1) \\
&\quad +2b_2\exp(-b_3(1-\alpha)^2)(b_2b_3\exp(-b_3(1-\alpha)^2)[4b_3(1-\alpha)^3 - 6(1-\alpha)]) \\
&\quad \cdot(2b_3(1-\alpha)^2 - 1) \\
&\quad +2b_2\exp(-b_3(1-\alpha)^2)(b_2\exp(-b_3(1-\alpha)^2)[2b_3(1-\alpha)^2 - 1]) \\
&\quad (-4b_3(1-\alpha)) && \text{(B.79)}
\end{aligned}$$

For $h_x^1 = 1 + k_1 - k_1/(1 + x/k_1) = \frac{k_1+x+k_1x}{k_1+x}$:

$$\partial_x h_x^1 = k_1^2/(k_1 + x^2) \tag{B.80}$$
$$\partial_x^2 h_x^1 = -\frac{2k_1^2 x}{(k_1 + x^2)^2} \tag{B.81}$$
$$\partial_x^3 h_x^1 = \frac{6k_1^2x^4 + 4k_1^3x^2 - 2k_1^4}{(k_1 + x^2)^4} \tag{B.82}$$
$$\partial_p h_x^1 = \partial_x h_x^1 \partial_p x \tag{B.83}$$
$$\partial_p^2 h_x^1 = \partial_x^2 h_x^1 (\partial_p x)^2 + \partial_x h_x^1 \partial_p^2 x \tag{B.84}$$
$$\partial_p^3 h_x^1 = \partial_x^3 h_x^1 (\partial_p x)^3 + 3\partial_x^2 h_x^1 \partial_p x \partial_p^2 x + \partial_x h_x^1 \partial_p^3 x \tag{B.85}$$
$$\partial_\alpha h_x^1 = \partial_x h_x^1 \partial_\alpha x \tag{B.86}$$
$$\partial_\alpha^2 h_x^1 = \partial_x^2 h_x^1 (\partial_\alpha x)^2 + \partial_x h_x^1 \partial_\alpha^2 x \tag{B.87}$$
$$\partial_\alpha^3 h_x^1 = \partial_x^3 h_x^1 (\partial_\alpha x)^3 + 3\partial_x^2 h_x^1 \partial_\alpha x \partial_\alpha^2 x + \partial_x h_x^1 \partial_\alpha^3 x \tag{B.88}$$

For $f_x(\alpha) = \exp(-c_{1x}\alpha/(1-\alpha))\Theta(1-\alpha) - d_x \exp[c_{2x}/(1-\alpha))\Theta(\alpha-1)$ we have:

$$\partial_\alpha f_x = \begin{cases} -\frac{c_{1x}\exp(-c_{1x}\alpha/(1-\alpha))}{(1-\alpha)^2} & \text{if } \alpha < 1 \\ -\frac{d_x c_{2x}\exp(c_{2x}/(1-\alpha)}{(1-\alpha)^2} & \text{if } \alpha > 1 \end{cases} \tag{B.89}$$

$$\partial_\alpha^2 f_x = \begin{cases} \frac{c_{1x}\exp(-c_{1x}\alpha/(1-\alpha))(c_{1x}-2(1-\alpha))}{(1-\alpha)^4} & \text{if } \alpha < 1 \\ \frac{d_x c_{2x}\exp(c_{2x}/(1-\alpha))(-c_{2x}-2(1-\alpha))}{(1-\alpha)^4} & \text{if } \alpha > 1 \end{cases} \tag{B.90}$$

$$\partial_\alpha^3 f_x = \begin{cases} \frac{c_{1x}\exp(-c_{1x}\alpha/(1-\alpha))(-c_{1x}^2/(1-\alpha)^2+6c_{1x}/(1-\alpha)-6)}{(1-\alpha)^4} & \text{if } \alpha < 1 \\ \frac{d_x c_{2x}\exp(c_{2x}/(1-\alpha))(-c_{2x}^2/(1-\alpha)^2-6c_{2x}/(1-\alpha)-6)}{(1-\alpha)^4} & \text{if } \alpha > 1 \end{cases} \tag{B.91}$$

For $g_x(p) = 1 - \exp(-a_1/p^{1/4})$:

$$\partial_p g_x = -\frac{a_1 \exp(-a_1/p^{1/4})}{4p^{5/4}} \tag{B.92}$$
$$\partial_p^2 g_x = \frac{a_1 \exp(-a_1/p^{1/4})(-a_1 + 5p^{1/4})}{16p^{10/4}} \tag{B.93}$$
$$\partial_p^3 g_x = \frac{a_1 \exp(-a_1/p^{1/4})(-4a_1^2p^{5/4} + 60a_1p^{3/2} + 20p^{7/4} - 200p^{3/8})}{256p^5} \tag{B.94}$$

For $\epsilon_x^{unif} = -(3/4\pi)(3\pi^2 n)^{1/3}$:

$$\partial_n \epsilon_x^{unif} = -1/4(3/\pi)^{1/3} n^{-2/3} \tag{B.95}$$
$$\partial_n^2 \epsilon_x^{unif} = 1/6(3/\pi)^{1/3} n^{-5/3} \tag{B.96}$$
$$\partial_n^3 \epsilon_x^{unif} = -5/18(3/\pi)^{1/3} n^{-8/3} \tag{B.97}$$

For $F_x = \{h_x^1(p,\alpha) + f_x(\alpha)[h_x^0 - h_x^1(p,\alpha)]\}g_x(p)$:

$$\begin{aligned}
\partial_p F_x &= \partial_p h_x^1(1-f_x)g_x + (h_x^1 + f_x(h_x^0 - h_x^1))\partial_p g_x && \text{(B.98)}\\
\partial_p^2 F_x &= \partial_p^2 h_x^1(1-f_x)g_x + \partial_p g_x[\partial_p h_x^1(2-2f_x)] \\
&\quad +(h_x^1 + f_x(h_x^0 - h_x^1))\partial_p^2 g_x && \text{(B.99)}\\
\partial_p^3 F_x &= \partial_p^3 h_x^1(1-f_x)g_x + \partial_p^2 h_x^1(1-f_x)\partial_p g_x + \partial_p^2 g_x[\partial_p h_x^1(2-f_x) - f_x\partial_p h_x^1] \\
&\quad +\partial_p g_x[\partial_p^2 h_x^1(2-2f_x)] + (\partial_p h_x^1 - f_x\partial_p h_x^1)\partial_p^2 g_x \\
&\quad +(h_x^1 + f_x(h_x^0 - h_x^1))\partial_p^3 g_x && \text{(B.100)}\\
\partial_\alpha F_x &= (\partial_\alpha h_x^1 + \partial_\alpha f_x(h_x^0 - h_x^1) - f_x\partial_\alpha h_x^1)g_x && \text{(B.101)}\\
\partial_\alpha^2 F_x &= [\partial_\alpha^2 h_x^1(1-f_x) + \partial_\alpha^2 f_x(h_x^0 - h_x^1) - 2\partial_\alpha f_x\partial_\alpha h_x^1]g_x && \text{(B.102)}\\
\partial_\alpha^3 F_x &= [\partial_\alpha^3 h_x^1(1-f_x) + \partial_\alpha^3 f_x(h_x^0 - h_x^1) - 3\partial_\alpha^2 f_x\partial_\alpha h_x^1 - 3\partial_\alpha f_x\partial_\alpha^2 h_x^1]g_x && \text{(B.103)}\\
\partial_n F_x &= \partial_\alpha F_x\partial_n\alpha + \partial_p F_x\partial_n p && \text{(B.104)}\\
\partial_n^2 F_x &= \partial_\alpha^2 F_x(\partial_n\alpha)^2 + \partial_\alpha F_x\partial_n^2\alpha + \partial_p^2 F_x(\partial_n p)^2 + \partial_p F_x\partial_n^2 p && \text{(B.105)}\\
\partial_n^3 F_x &= \partial_\alpha^3 F_x(\partial_n\alpha)^3 + \partial_n^2\alpha(2\partial_\alpha^2 F_x\partial_n\alpha + \partial_\alpha^2 F_x) + \partial_\alpha F_x\partial_n^3\alpha \\
&\quad +\partial_p^3 F_x(\partial_n p)^2\partial_n p + \partial_n^2 p(2\partial_p^2 F_x\partial_n p + \partial_p^2 F_x) + \partial_p F_x\partial_n^3 p && \text{(B.106)}\\
\partial_{\nabla n} F_x &= \partial_\alpha F_x\partial_{\nabla n}\alpha + \partial_p F_x\partial_{\nabla n} p && \text{(B.107)}\\
\partial_{\nabla n}^2 F_x &= \partial_\alpha^2 F_x(\partial_{\nabla n}\alpha)^2 + \partial_\alpha F_x\partial_{\nabla n}^2\alpha + \partial_p^2 F_x(\partial_{\nabla n} p)^2 + \partial_p F_x\partial_{\nabla n}^2 p && \text{(B.108)}\\
\partial_{\nabla n}^3 F_x &= \partial_\alpha^3 F_x(\partial_{\nabla n}\alpha)^3 + 3\partial_{\nabla n}^2\alpha\partial_\alpha^2 F_x\partial_{\nabla n}\alpha + \partial_\alpha F_x\partial_{\nabla n}^3\alpha \\
&\quad +\partial_p^3 F_x(\partial_{\nabla n} p)^3 + 3\partial_{\nabla n}^2 p\partial_p^2 F_x\partial_{\nabla n} p + \partial_p F_x\partial_{\nabla n}^3 p && \text{(B.109)}\\
\partial_\tau F_x &= \partial_\alpha F_x\partial_\tau\alpha && \text{(B.110)}\\
\partial_\tau^2 F_x &= \partial_\alpha^2 F_x(\partial_\tau\alpha)^2 && \text{(B.111)}\\
\partial_\tau^3 F_x &= \partial_\alpha^3 F_x(\partial_\tau\alpha)^3 && \text{(B.112)}
\end{aligned}$$

Now, finally, we can deal with the second and third derivatives of A_x:

$$\begin{aligned}
\partial_n A_x &= n\epsilon_x^{unif}\partial_n F_x + 4/3\epsilon_x^{unif} F_x && \text{(B.113)}\\
\partial_n^2 A_x &= \epsilon_x^{unif}(8/3\partial_n F_x + n\partial_n^2 F_x) + 4/3\partial_n\epsilon_x^{unif} F_x && \text{(B.114)}\\
\partial_n^3 A_x &= \partial_n\epsilon_x^{unif}(8/3\partial_n F_x + n\partial_n^2 F_x) + \epsilon_x^{unif}(11/3\partial_n^2 F_x + n\partial_n^3 F_x) \\
&\quad +4/3\partial_n^2\epsilon_x^{unif} F_x + 4/3\partial_n\epsilon_x^{unif}\partial_n F_x && \text{(B.115)}\\
\partial_{\nabla n} A_x &= n\epsilon_x^{unif}\partial_{\nabla n} F_x && \text{(B.116)}\\
\partial_{\nabla n}^2 A_x &= n\epsilon_x^{unif}\partial_{\nabla n}^2 F_x && \text{(B.117)}\\
\partial_{\nabla n}^3 A_x &= n\epsilon_x^{unif}\partial_{\nabla n}^3 F_x && \text{(B.118)}\\
\partial_\tau A_x &= n\epsilon_x^{unif}\partial_\tau F_x && \text{(B.119)}\\
\partial_\tau^2 A_x &= n\epsilon_x^{unif}\partial_\tau^2 F_x && \text{(B.120)}\\
\partial_\tau^3 A_x &= n\epsilon_x^{unif}\partial_\tau^3 F_x && \text{(B.121)}\\
& && \text{(B.122)}
\end{aligned}$$

B.3.2 Derivatives necessary for the correlation and TSPIN=.TRUE. part

For $w_1 = \exp(-\epsilon_c^{LSDA1}/(\gamma\phi^3)) - 1$ we have:

$$\partial_{r_s} w_1 = -\exp(-\epsilon_c^{LSDA1}/(\gamma\phi^3))\frac{\partial_{r_s}\epsilon_c^{LSDA1}}{\gamma\phi^3} \tag{B.123}$$

$$\begin{aligned}\partial_{r_s}^2 w_1 = {} & \exp(-\epsilon_c^{LSDA1}/(\gamma\phi^3))\frac{(\partial_{r_s}\epsilon_c^{LSDA1})^2}{\gamma^2\phi^6} \\ & -\exp(-\epsilon_c^{LSDA1}/(\gamma\phi^3))\frac{\partial_{r_s}^2\epsilon_c^{LSDA1}}{\gamma\phi^3}\end{aligned} \tag{B.124}$$

$$\begin{aligned}\partial_{r_s}^3 w_1 = {} & \exp(-\epsilon_c^{LSDA1}/(\gamma\phi^3))\frac{(\partial_{r_s}\epsilon_c^{LSDA1})^3}{\gamma^3\phi^9} \\ & +3\exp(-\epsilon_c^{LSDA1}/(\gamma\phi^3))\frac{\partial_{r_s}\epsilon_c^{LSDA1}\partial_{r_s}^2\epsilon_c^{LSDA1}}{\gamma^2\phi^6} \\ & -\exp(-\epsilon_c^{LSDA1}/(\gamma\phi^3))\frac{\partial_{r_s}^3\epsilon_c^{LSDA1}}{\gamma\phi^3}\end{aligned} \tag{B.125}$$

$$\partial_\zeta w_1 = (3\epsilon_c^{LSDA1}/(\gamma\phi^4)\partial_\zeta\phi - \frac{\partial_\zeta\epsilon_c^{LSDA1}}{\gamma\phi^3})\exp(-\epsilon_c^{LSDA1}/(\gamma\phi^3)) \tag{B.126}$$

$$\begin{aligned}\partial_\zeta^2 w_1 = {} & (\frac{3\partial_\zeta\epsilon_c^{LSDA1}\partial_\zeta\phi}{\gamma\phi^4} - \frac{12\epsilon_c^{LSDA1}(\partial_\zeta\phi)^2}{\gamma\phi^5} - \frac{3\epsilon_c^{LSDA1}\partial_\zeta^2\phi}{\gamma\phi^4} \\ & +\frac{3\partial_\zeta\phi\partial_\zeta\epsilon_c^{LSDA1}}{\gamma\phi^4} - \frac{\partial_\zeta^2\epsilon_c^{LSDA1}}{\gamma\phi^3})\exp(-\epsilon_c^{LSDA1}/(\gamma\phi^3))\end{aligned} \tag{B.127}$$

$$\begin{aligned}\partial_\zeta^3 w_1 = {} & [\frac{(3\partial_\zeta^2\epsilon_c^{LSDA1}\partial_\zeta\phi + 3\partial_\zeta\epsilon_c^{LSDA1}\partial_\zeta^2\phi)\gamma\phi^4 - 12\partial_\zeta\epsilon_c^{LSDA1}(\partial_\zeta\phi)^2\phi^3\gamma}{\gamma^2\phi^8} \\ & -\frac{(12\partial_\zeta\epsilon_c^{LSDA1}(\partial_\zeta\phi)^2 + 24\epsilon_c^{LSDA1}\partial_\zeta\phi\partial_\zeta^2\phi)\gamma\phi^5 - 60\epsilon_c^{LSDA1}(\partial_\zeta\phi)^2\partial_\zeta\phi\gamma\phi^4}{\gamma^2\phi^{10}} \\ & -\frac{(3\partial_\zeta\epsilon_c^{LSDA1}\partial_\zeta^2\phi + 3\epsilon_c^{LSDA1}\partial_\zeta^3\phi)\gamma\phi^4 - 12\epsilon_c^{LSDA1}\partial_\zeta^2\phi\partial_\zeta\phi\gamma\phi^3}{\gamma^2\phi^8} \\ & +\frac{(3\partial_\zeta^2\phi\partial_\zeta\epsilon_c^{LSDA1} + 3\partial_\zeta\phi\partial_\zeta^2\epsilon_c^{LSDA1})\gamma\phi^4 - 12(\partial_\zeta\phi)^2\partial_\zeta\epsilon_c^{LSDA1}\gamma\phi^3}{\gamma^2\phi^8} \\ & -\frac{\gamma\phi^3\partial_\zeta^3\epsilon_c^{LSDA1} - 3\partial_\zeta^2\epsilon_c^{LSDA1}\gamma\phi^2\partial_\zeta\phi}{\gamma^2\phi^6}]\exp(-\epsilon_c^{LSDA1}/(\gamma\phi^3)) \\ & +[\frac{3\partial_\zeta\epsilon_c^{LSDA1}\partial_\zeta\phi - 3\epsilon_c^{LSDA1}\partial_\zeta^2\phi + 3\partial_\zeta\phi\partial_\zeta\epsilon_c^{LSDA1}}{\gamma\phi^4} \\ & -\frac{12\epsilon_c^{LSDA1}(\partial_\zeta\phi)^2}{\gamma\phi^5} - \frac{\partial_\zeta^2\epsilon_c^{LSDA1}}{\gamma\phi^3}]\partial_\zeta w_1 \\ & +[\frac{(3\partial_\zeta\epsilon_c^{LSDA1}\partial_\zeta\phi + 3\epsilon_c^{LSDA1}\partial_\zeta^2\phi)\gamma\phi^4 - 12\epsilon_c^{LSDA1}(\partial_\zeta\phi)^2\gamma\phi^3}{\gamma^2\phi^8} \\ & -\frac{\partial_\zeta^2\epsilon_c^{LSDA1}\gamma\phi^3 - 3\partial_\zeta\epsilon_c^{LSDA1}\partial_\zeta\phi\gamma\phi^2}{\gamma^2\phi^6}]\partial_\zeta w_1 \\ & +[\frac{3\epsilon_c^{LSDA1}\partial_\zeta\phi}{\gamma\phi^4} - \frac{\partial_\zeta\epsilon_c^{LSDA1}}{\gamma\phi^3}]\partial_\zeta^2 w_1\end{aligned} \tag{B.128}$$

For $A = \beta(r_s)/(\gamma w_1)$ we have:

$$\partial_{r_s} A = \frac{\partial_{r_s}\beta}{\gamma w_1} - \frac{A\partial_{r_s} w_1}{w_1} \tag{B.129}$$

$$\partial^2_{r_s} A = \frac{\partial^2_{r_s}\beta}{\gamma w_1} - \frac{\partial_{r_s}\beta\partial_{r_s} w_1}{\gamma w_1^2} - \frac{\partial_{r_s} A\partial_{r_s} w_1}{w_1} - \frac{A\partial^2_{r_s} w_1}{w_1} + \frac{A(\partial_{r_s} w_1)^2}{w_1^2} \tag{B.130}$$

$$\begin{aligned}\partial^3_{r_s} A = {} & \frac{\partial^3_{r_s}\beta}{\gamma w_1} - 2\frac{\partial^2_{r_s}\beta\partial_{r_s} w_1}{\gamma w_1^2} - \frac{\partial_{r_s}\beta\partial^2_{r_s} w_1\gamma w_1^2 - 2\partial_{r_s}\beta(\partial_{r_s} w_1)^2\gamma w_1}{\gamma^2 w_1^4} \\ & - \frac{(\partial^2_{r_s} A\partial_{r_s} w_1 + 2\partial_{r_s} A\partial^2_{r_s} w_1)w_1 - \partial_{r_s} A(\partial_{r_s} w_1)^2 - A\partial^2_{r_s} w_1\partial_{r_s} w_1}{w_1^2} \\ & + \frac{(\partial_{r_s} A(\partial_{r_s} w_1)^2 + 2A\partial_{r_s} w_1\partial^2_{r_s} w_1)w_1^2 - 2A(\partial_{r_s} w_1)^2 w_1\partial_{r_s} w_1}{w_1^4}\end{aligned} \tag{B.131}$$

$$\partial_\zeta A = -\frac{A\partial_\zeta w_1}{w_1} \tag{B.132}$$

$$\partial^2_\zeta A = -\frac{\partial_\zeta A\partial_\zeta w_1 + A\partial^2_\zeta w_1}{w_1} + \frac{A(\partial_\zeta w_1)^2}{w_1^2} \tag{B.133}$$

$$\begin{aligned}\partial^3_\zeta A = {} & -\frac{(\partial^2_\zeta A\partial_\zeta w_1 + 2\partial_\zeta A\partial^2_\zeta w_1 + A\partial^3_\zeta w_1)w_1 - (\partial_\zeta A\partial_\zeta w_1 + A\partial^2_\zeta w_1)\partial_\zeta w_1}{w_1^2} \\ & + \frac{w_1(\partial_\zeta A(\partial_\zeta w_1)^2 + 2A\partial_\zeta w_1\partial^2_\zeta w_1 - 2A(\partial_\zeta w_1)^3 w_1)}{w_1^4}\end{aligned} \tag{B.134}$$

For $t^2 = (3\pi^2/16)^{2/3} p/(\phi^2 r_s)$ we have:

$$\partial_{r_s} t^2 = -\frac{t^2}{r_s} \tag{B.135}$$

$$\partial^2_{r_s} t^2 = -\frac{\partial_{r_s} t^2 r_s - t^2}{r_s^2} \tag{B.136}$$

$$\partial^3_{r_s} t^2 = -\frac{\partial^2_{r_s} t^2 r_s^2 - 2\partial_{r_s} t^2 r_s^2 + t^2 r_s}{r_s^4} \tag{B.137}$$

$$\partial_p t^2 = (3\pi^2/16)^{2/3}/(\phi^2 r_s) \tag{B.138}$$

$$\partial^2_p t^2 = 0 \tag{B.139}$$

$$\partial^2_p t^2 = 0 \tag{B.140}$$

$$\partial_\zeta t^2 = -\frac{2t^2\partial_\zeta\phi}{\phi} \tag{B.141}$$

$$\partial^2_\zeta t^2 = -\frac{2\partial_\zeta t^2\partial_\zeta\phi + 2t^2\partial^2_\zeta\phi}{\phi} + \frac{2t^2(\partial_\zeta\phi)^2}{\phi^2} \tag{B.142}$$

$$\begin{aligned}\partial^3_\zeta t^2 = {} & -\frac{(2\partial^2_\zeta t^2\partial_\zeta\phi + 4\partial_\zeta t^2\partial^2_\zeta\phi + 2t^2\partial^3_\zeta\phi)\phi - (2\partial_\zeta t^2\partial_\zeta\phi + 2t^2\partial^2_\zeta\phi)\partial_\zeta\phi}{\phi^2} \\ & + \frac{(2\partial_\zeta t^2(\partial_\zeta\phi)^2 + 4t^2\partial_\zeta\phi\partial^2_\zeta\phi)\phi^2 - 4t^2(\partial_\zeta\phi)^3}{\phi^4}\end{aligned} \tag{B.143}$$

For $g(At^2) = (1+4At^2)^{-1/4}$ we have:

$$\partial_{r_s} g = -(1+4At^2)^{-5/4}(\partial_{r_s} At^2 + A\partial_{r_s} t^2) \tag{B.144}$$

$$\begin{aligned}\partial^2_{r_s} g = {} & 5(1+4At^2)^{-9/4}(\partial_{r_s} At^2 + A\partial_{r_s} t^2)^2 - (1+4At^2)^{-5/4} \\ & \cdot(\partial^2_{r_s} At^2 + 2\partial_{r_s} A\partial_{r_s} t^2 + A\partial^2_{r_s} t^2)\end{aligned} \tag{B.145}$$

$$\begin{aligned}\partial^3_{r_s} g = {} & -45(1+4At^2)^{-13/4}(\partial_{r_s} At^2 + A\partial_{r_s} t^2)^3 \\ & +10(1+4At^2)^{-9/4}(\partial_{r_s} At^2 + A\partial_{r_s} t^2)(\partial^2_{r_s} At^2 + 2\partial_{r_s} A\partial_{r_s} t^2 + A\partial^2_{r_s} t^2) \\ & +5(1+4At^2)^{-9/4}(\partial_{r_s} At^2 + A\partial_{r_s} t^2)(\partial^2_{r_s} At^2 + 2\partial_{r_s} A\partial_{r_s} t^2 + A\partial^2_{r_s} t^2) \\ & -(1+4At^2)^{-5/4}(\partial^3_{r_s} At^2 + 3\partial^2_{r_s} A\partial_{r_s} t^2 + 3\partial_{r_s} A\partial^2_{r_s} t^2 + A\partial^3_{r_s} t^2)\end{aligned} \tag{B.146}$$

$$\partial_\zeta g = -(1+4At^2)^{-5/4}(\partial_\zeta At^2 + A\partial_\zeta t^2) \tag{B.147}$$

$$\begin{aligned}\partial^2_\zeta g = {} & 5(1+4At^2)^{-9/4}(\partial_\zeta At^2 + A\partial_\zeta t^2)^2 - (1+4At^2)^{-5/4} \\ & \cdot(\partial^2_\zeta At^2 + 2\partial_\zeta A\partial_\zeta t^2 + A\partial^2_\zeta t^2)\end{aligned} \tag{B.148}$$

$$\begin{aligned}\partial^3_\zeta g = {} & -45(1+4At^2)^{-13/4}(\partial_\zeta At^2 + A\partial_\zeta t^2)^3 \\ & +10(1+4At^2)^{-9/4}(\partial_\zeta At^2 + A\partial_\zeta t^2)(\partial^2_\zeta At^2 + 2\partial_\zeta A\partial_\zeta t^2 + A\partial^2_\zeta t^2) \\ & +5(1+4At^2)^{-9/4}(\partial_\zeta At^2 + A\partial_\zeta t^2)(\partial^2_\zeta At^2 + 2\partial_\zeta A\partial_\zeta t^2 + A\partial^2_\zeta t^2) \\ & -(1+4At^2)^{-5/4}(\partial^3_\zeta At^2 + 3\partial^2_\zeta A\partial_\zeta t^2 + 3\partial_\zeta A\partial^2_\zeta t^2 + A\partial^3_\zeta t^2)\end{aligned} \tag{B.149}$$

$$\partial_p g = -(1+4At^2)^{-5/4} A\partial_p t^2 \tag{B.150}$$

$$\partial^2_p g = 5(1+4At^2)^{-9/4}(A\partial_p t^2)^2 \tag{B.151}$$

$$\partial^3_p g = -45(1+4At^2)^{-13/4}(A\partial_p t^2)^3 \tag{B.152}$$

For $H_1 = \gamma\phi^3 \ln[1 + w_1(1-g)]$ we have:

$$\partial_{r_s} H_1 = \frac{\gamma\phi^3(\partial_{r_s} w_1(1-g) - w_1\partial_{r_s} g)}{1 + w_1(1-g)} \tag{B.153}$$

$$\begin{aligned}\partial^2_{r_s} H_1 = {} & \gamma\phi^3[\frac{\partial^2_{r_s} w_1(1-g) - 2\partial_{r_s} w_1\partial_{r_s} g - w_1\partial^2_{r_s} g}{1 + w_1(1-g)} \\ & - \frac{(\partial_{r_s} w_1(1-g) - w_1\partial_{r_s} g)^2}{(1 + w_1(1-g))^2}]\end{aligned} \tag{B.154}$$

$$\begin{aligned}\partial^3_{r_s} H_1 = {} & \gamma\phi^3[\frac{\partial^3_{r_s} w_1(1-g) - 3\partial^2_{r_s} w_1\partial_{r_s} g - 3\partial_{r_s} w_1\partial^2_{r_s} g - w_1\partial^3_{r_s} g}{1 + w_1(1-g)} \\ & - \frac{(3\partial^2_{r_s} w_1(1-g) - 6\partial_{r_s} w_1\partial_{r_s} g - 3w_1\partial^2_{r_s} g)(\partial_{r_s} w_1(1-g) - w_1\partial_{r_s} g)}{(1 + w_1(1-g))^2} \\ & - \frac{2(\partial_{r_s} w_1(1-g) - w_1\partial_{r_s} g)^3}{(1 + w_1(1-g))^4}]\end{aligned} \tag{B.155}$$

$$\partial_\zeta H_1 = \gamma\phi^3 \frac{\partial_\zeta w_1(1-g) - w_1\partial_\zeta g}{1 + w_1(1-g)} + 3\gamma\phi^2\partial_\zeta\phi \ln(1 + w_1(1-g)) \tag{B.156}$$

$$\begin{aligned}\partial^2_\zeta H_1 = {} & 3\gamma\phi^2\partial_\zeta\phi \frac{\partial_\zeta w_1(1-g) - w_1\partial_\zeta g}{1 + w_1(1-g)} \\ & + \gamma\phi^3[\frac{\partial^2_\zeta w_1(1-g) - 2\partial_\zeta w_1\partial_\zeta g - w_1\partial^2_\zeta g}{1 + w_1(1-g)} - \frac{(\partial_\zeta w_1(1-g) - w_1\partial_\zeta g)^2}{(1 + w_1(1-g))^2}] \\ & + 3\gamma\phi[2(\partial_\zeta\phi)^2 \ln(1 + w_1(1-g)) + \phi\partial^2_\zeta\phi \ln(1 + w_1(1-g)) \\ & + \phi\partial_\zeta\phi \frac{\partial_\zeta w_1(1-g) - w_1\partial_\zeta g}{1 + w_1(1-g)}]\end{aligned} \tag{B.157}$$

$$\begin{aligned}\partial^3_\zeta H_1 = {} & 3\gamma\phi^2\partial^2_\zeta\phi \frac{\partial_\zeta w_1(1-g) - w_1\partial_\zeta g}{1 + w_1(1-g)} + 6\gamma\phi(\partial_\zeta g)^2 \frac{\partial_\zeta w_1(1-g) - w_1\partial_\zeta g}{1 + w_1(1-g)} \\ & + [\frac{\partial^2_\zeta w_1(1-g) - 2\partial_\zeta w_1\partial_\zeta g - w_1\partial^2_\zeta g}{1 + w_1(1-g)} - \frac{(\partial_\zeta w_1(1-g) - w_1\partial_\zeta g)^2}{(1 + w_1(1-g))^2}] \\ & \cdot 6\gamma\phi^2\partial_\zeta\phi \\ & + \gamma\phi^3[\frac{\partial^3_\zeta w_1(1-g) - 3\partial^2_\zeta w_1\partial_\zeta g - 3\partial_\zeta w_1\partial^2_\zeta g - w_1\partial^3_\zeta g}{1 + w_1(1-g)} \\ & - \frac{(3\partial^2_\zeta w_1(1-g) - 6\partial_\zeta w_1\partial_\zeta g - 3w_1\partial^2_\zeta g)(\partial_\zeta w_1(1-g) - w_1\partial_\zeta g)}{(1 + w_1(1-g))^2} \\ & - 2\frac{(\partial_\zeta w_1(1-g) - w_1\partial_\zeta g)^3}{(1 + w_1(1-g))^4}] + 3\gamma\partial_\zeta\phi[2(\partial_\zeta\phi)^2 \ln(1 + w_1(1-g)) \\ & + \phi\partial^2_\zeta\phi \ln(1 + w_1(1-g)) + \phi\partial_\zeta\phi \frac{\partial_\zeta w_1(1-g) - w_1\partial_\zeta g}{1 + w_1(1-g)}] \\ & + 3\gamma\phi[5\partial_\zeta\phi\partial^2_\zeta\phi \ln(1 + w_1(1-g)) + 3(\partial_\zeta\phi)^2 \frac{\partial_\zeta w_1(1-g) - w_1\partial_\zeta g}{1 + w_1(1-g)} \\ & + \phi\partial^3_\zeta\phi \ln(1 + w_1(1-g)) + 2\phi\partial^2_\zeta\phi \frac{\partial_\zeta w_1(1-g) - w_1\partial_\zeta g}{1 + w_1(1-g)} \\ & + \phi\partial_\zeta\phi\{\frac{\partial^2_\zeta w_1(1-g) - 2\partial_\zeta w_1\partial_\zeta g - w_1\partial^2_\zeta g}{1 + w_1(1-g)} \\ & - \frac{(\partial_\zeta w_1(1-g) - w_1\partial_\zeta g)^2}{(1 + w_1(1-g))^2}\}]\end{aligned} \tag{B.158}$$

$$\partial_p H_1 = -\gamma\phi^3 \frac{w_1 \partial_p g}{1 + w_1(1-g)} \tag{B.159}$$

$$\partial_p^2 H_1 = -\gamma\phi^3 w_1 \frac{\partial_p^2 g(1 + w_1(1-g)) + w_1(\partial_p g)^2}{(1 + w_1(1-g))^2} \tag{B.160}$$

$$\partial_p^3 H_1 = -\gamma\phi^3 w_1 [\frac{\partial_p^3 g(1 + w_1(1-g)) + \partial_p^2 g \partial_p g w_1}{(1 + w_1(1-g))^2} + \frac{2w_1 \partial_p g(\partial_p^2 g(1 + w_1(1-g)) + w_1(\partial_p g)^2)}{(1 + w_1(1-g))^3}] \tag{B.161}$$

For $\epsilon_c^1 = \epsilon_c^{LSDA1} + H_1$ we have:

$$\partial_{r_s} \epsilon_c^1 = \partial_{r_s} \epsilon_c^{LSDA1} + \partial_{r_s} H_1 \tag{B.162}$$

$$\partial_{r_s}^2 \epsilon_c^1 = \partial_{r_s}^2 \epsilon_c^{LSDA1} + \partial_{r_s}^2 H_1 \tag{B.163}$$

$$\partial_{r_s}^3 \epsilon_c^1 = \partial_{r_s}^3 \epsilon_c^{LSDA1} + \partial_{r_s} 32 H_1 \tag{B.164}$$

$$\partial_p \epsilon_c^1 = \partial_p H_1 \tag{B.165}$$

$$\partial_p^2 \epsilon_c^1 = \partial_p^2 H_1 \tag{B.166}$$

$$\partial_p^3 \epsilon_c^1 = \partial_p^3 H_1 \tag{B.167}$$

$$\partial_\zeta \epsilon_c^1 = \partial_\zeta \epsilon_c^{LSDA1} + \partial_\zeta H_1 \tag{B.168}$$

$$\partial_\zeta^2 \epsilon_c^1 = \partial_\zeta^2 \epsilon_c^{LSDA1} + \partial_\zeta^2 H_1 \tag{B.169}$$

$$\partial_\zeta^3 \epsilon_c^1 = \partial_\zeta^3 \epsilon_c^{LSDA1} + \partial_\zeta^3 H_1 \tag{B.170}$$

For $\epsilon_c^{LDA0} = -b_{1c}/(1 + b_{2c} r_s^{1/2} + b_{3c} r_s)$ we have:

$$\partial_{r_s} \epsilon_c^{LDA0} = -\frac{b_{1c}(\frac{1}{2} b_{2c} r_s^{-1/2} + b_{3c})}{(1 + b_{2c} r_s^{1/2} + b_{3c} r_s)^2} \tag{B.171}$$

$$\partial_{r_s}^2 \epsilon_c^{LDA0} = \frac{b_{1c} r_s^{-3/2}}{4(1 + b_{2c} r_s^{1/2} + b_{3c} r_s)^2} + 2\frac{b_{1c}(\frac{1}{2} b_{2c} r_s^{-1/2} + b_{3c})}{(1 + b_{2c} r_s^{1/2} + b_{3c} r_s)^3} \tag{B.172}$$

$$\partial_{r_s}^3 \epsilon_c^{LDA0} = -\frac{b_{1c}(1 + b_{2c} r_s^{1/2} + b_{3c} r_s)(3/2 r_s^{-5/2} + 2 r_s^{-3/2}(\frac{1}{2} b_{2c} r_s^{-1/2} + b_{3c}))}{4(1 + b_{2c} r_s^{1/2} + b_{3c} r_s)^4} + 2\frac{b_{1c}(1 + b_{2c} r_s^{1/2} + b_{3c} r_s)^2(-\frac{1}{2} b_{2c} r_s^{-3/2}(1 + b_{2c} r_s^{1/2} + b_{3c} r_s) - 3(\frac{1}{2} b_{2c} r_s^{-1/2} + b_{3c})^3)}{(1 + b_{2c} r_s^{1/2} + b_{3c} r_s)^6} \tag{B.173}$$

For $d_x(\zeta) = [(1+\zeta)^{4/3} + (1-\zeta)^{4/3}]/2$ we have:

$$\partial_\zeta d_x = \frac{2}{3}[(1+\zeta)^{1/3} - (1-\zeta)^{1/3}] \tag{B.174}$$

$$\partial_\zeta^2 d_x = \frac{2}{9}[(1+\zeta)^{-2/3} + (1-\zeta)^{-2/3}] \tag{B.175}$$

$$\partial_\zeta^3 d_x = -\frac{4}{27}[(1+\zeta)^{-5/3} - (1-\zeta)^{-5/3}] \tag{B.176}$$

For $G_c(\zeta) = \{1 - 2.3631[d_x(\zeta) - 1]\}(1 - \zeta^{12})$ we have:

$$\begin{aligned}
\partial_\zeta G_c &= -2.3631\partial_\zeta d_x(1-\zeta^{12}) - 12\zeta^{11}\{1 - 2.3631[d_x - 1]\} && \text{(B.177)}\\
\partial^2_\zeta G_c &= -2.3631\partial^2_\zeta d_x(1-\zeta^{12}) + 56.7144\partial_\zeta d_x\zeta^{11} \\
&\quad -132\zeta^{10}\{1 - 2.3631[d_x - 1]\} && \text{(B.178)}\\
\partial^3_\zeta G_c &= -2.3631\partial^3_\zeta d_x(1-\zeta^{12}) + 85.0716\partial^2_\zeta d_x\zeta^{11} + 935.7876\partial_\zeta d_x\zeta^{10} \\
&\quad -1320\zeta^{9}\{1 - 2.3631[d_x - 1]\} && \text{(B.179)}
\end{aligned}$$

For $\zeta = \frac{n_\uparrow - n_\downarrow}{n_\uparrow + n_\downarrow} = \frac{n_\uparrow - n_\downarrow}{n}$ we have:

$$\begin{aligned}
\partial_{n_\uparrow}\zeta &= \frac{2n_\downarrow}{n^2} && \text{(B.180)}\\
\partial^2_{n_\uparrow}\zeta &= -\frac{4n_\downarrow}{n^3} && \text{(B.181)}\\
\partial^3_{n_\uparrow}\zeta &= \frac{12n_\downarrow}{n^4} && \text{(B.182)}\\
\partial_{n_\downarrow}\zeta &= -\frac{2n_\uparrow}{n^2} && \text{(B.183)}\\
\partial^2_{n_\downarrow}\zeta &= \frac{4n_\uparrow}{n^3} && \text{(B.184)}\\
\partial^3_{n_\downarrow}\zeta &= -\frac{12n_\uparrow}{n^4} && \text{(B.185)}
\end{aligned}$$

For $g_\infty = (1 + 4\chi_\infty p)^{-1/4}$ we have:

$$\begin{aligned}
\partial_p g_\infty &= -\chi_\infty(1 + 4\chi_\infty p)^{-5/4} && \text{(B.186)}\\
\partial^2_p g_\infty &= 5\chi^2_\infty(1 + 4\chi_\infty p)^{-9/4} && \text{(B.187)}\\
\partial^3_p g_\infty &= -45\chi^3_\infty(1 + 4\chi_\infty p)^{-13/4} && \text{(B.188)}
\end{aligned}$$

For $w_0 = \exp(-\epsilon_c^{LDA0}/b_{1c}) - 1$ we have:

$$\begin{aligned}
\partial_{r_s} w_0 &= -\exp(-\epsilon_c^{LDA0}/b_{1c})\frac{\partial_{r_s}\epsilon_c^{LDA0}}{b_{1c}} && \text{(B.189)}\\
\partial^2_{r_s} w_0 &= \exp(-\epsilon_c^{LDA0}/b_{1c})\frac{(\partial_{r_s}\epsilon_c^{LDA0})^2}{b_{1c^2}} - \exp(-\epsilon_c^{LDA0}/b_{1c})\frac{\partial^2_{r_s}\epsilon_c^{LDA0}}{b_{1c}} && \text{(B.190)}\\
\partial^3_{r_s} w_0 &= \exp(-\epsilon_c^{LDA0}/b_{1c})\frac{(\partial_{r_s}\epsilon_c^{LDA0})^3}{b^3_{1c}} + 3\exp(-\epsilon_c^{LDA0}/b_{1c})\frac{\partial_{r_s}\epsilon_c^{LDA0}\partial^2_{r_s}\epsilon_c^{LDA0}}{b^2_{1c}} \\
&\quad -\exp(-\epsilon_c^{LDA0}/b_{1c})\frac{\partial^3_{r_s}\epsilon_c^{LDA0}}{b_{1c}} && \text{(B.191)}\\
& && \text{(B.192)}
\end{aligned}$$

For $H_0 = b_{1c}\ln(1 + w_0(1 - g_\infty))$ we have:

$$\partial_{r_s} H_0 = \frac{b_{1c}\partial_{r_s} w_0(1-g_\infty)}{1 + w_0(1-g_\infty)} \tag{B.193}$$

$$\partial^2_{r_s} H_0 = \frac{b_{1c}\partial^2_{r_s} w_0(1-g_\infty)(1 + w_0(1-g_\infty)) - b_{1c}(\partial_{r_s} w_0(1-g_\infty))^2}{(1 + w_0(1-g_\infty))^2} \tag{B.194}$$

$$\begin{aligned}\partial^3_{r_s} H_0 = {} & \frac{b_{1c}\partial^3_{r_s} w_0(1-g_\infty)(1 + w_0(1-g_\infty)) - b_{1c}\partial^2_{r_s} w_0 \partial_{r_s} w_0(1-g_\infty)^2}{(1 + w_0(1-g_\infty))^2} \\ & - \frac{[b_{1c}\partial^2_{r_s} w_0(1-g_\infty)(1 + w_0(1-g_\infty)) - b_{1c}(\partial_{r_s} w_0(1-g_\infty))^2]}{(1 + w_0(1-g_\infty))^3} \\ & \cdot \frac{2\partial_{r_s} w_0(1-g_\infty)}{(1 + w_0(1-g_\infty))^3}\end{aligned} \tag{B.195}$$

$$\partial_p H_0 = -\frac{b_{1c} w_0 \partial_p g_\infty}{1 + w_0(1-g_\infty)} \tag{B.196}$$

$$\partial^2_p H_0 = -\frac{b_{1c} w_0 \partial^2_p g_\infty}{1 + w_0(1-g_\infty)} - \frac{b_{1c}(w_0\partial_p g_\infty)^2}{(1 + w_0(1-g_\infty))^2} \tag{B.197}$$

$$\begin{aligned}\partial^3_p H_0 = {} & -\frac{b_{1c} w_0 \partial^3_p g_\infty (1 + w_0(1-g_\infty)) + b_{1c} w_0^2 \partial^2_p g_\infty \partial_p g_\infty}{(1 + w_0(1-g_\infty))^2} \\ & - \frac{2b_{1c} w_0^2 \partial_p g_\infty \partial^2_p g_\infty (1 + w_0(1-g_\infty))^2 + 2b_{1c}(w_0\partial_p g_\infty)^3}{(1 + w_0(1-g_\infty))^4} \\ & \cdot \frac{1}{(1 + w_0(1-g_\infty))^3}\end{aligned} \tag{B.198}$$

For $\alpha = \frac{5}{3}p(z^{-1} - 1)\frac{1}{d_s(\zeta)}$ we have:

$$\partial_{n_\uparrow}\alpha = \frac{5}{3}(-pz^{-2}\partial_n z + \partial_n p(z^{-1} - 1))/d_s - \frac{\alpha}{d_s}\partial_\zeta d_s \partial_{n_\uparrow}\zeta \tag{B.199}$$

$$\begin{aligned}\partial^2_{n_\uparrow}\alpha = {} & \frac{-10\partial_n p z^{-2}\partial_n z + 10pz^{-3}(\partial_n z)^2 - 5pz^{-2}\partial^2_n z + 5\partial^2_n p(z^{-1}-1) - 3\partial_{n_\uparrow}\alpha\partial_\zeta d_s \partial_{n_\uparrow}\zeta}{3d_s} \\ & - \frac{3\alpha\partial^2_\zeta d_s(\partial_{n_\uparrow}\zeta)^2 - 3\alpha\partial_\zeta d_s \partial^2_{n_\uparrow}\zeta}{3d_s} \\ & + \frac{(5pz^{-2}\partial_n z + 5\partial_n p(z^{-1}-1))\partial_\zeta d_s \partial_{n_\uparrow}\zeta + 3\alpha(\partial_\zeta d_s \partial_{n_\uparrow}\zeta)^2}{3d_s^2}\end{aligned} \tag{B.200}$$

Let

$$\begin{aligned}a_\uparrow = {} & -10\partial_n p z^{-2}\partial_n z + 10pz^{-3}(\partial_n z)^2 - 5pz^{-2}\partial^2_n z + 5\partial^2_n p(z^{-1}-1) - 3\partial_{n_\uparrow}\alpha\partial_\zeta d_s\partial_{n_\uparrow}\zeta \\ & -3\alpha\partial^2_\zeta d_s(\partial_{n_\uparrow}\zeta)^2 - 3\alpha\partial_\zeta d_s\partial^2_{n_\uparrow}\zeta\end{aligned} \tag{B.201}$$

$$b_\uparrow = (5pz^{-2}\partial_n z + 5\partial_n p(z^{-1}-1))\partial_\zeta d_s\partial_{n_\uparrow}\zeta + 3\alpha(\partial_\zeta d_s\partial_{n_\uparrow}\zeta)^2 \tag{B.202}$$

then we have for $\partial^3_{n_\uparrow}\alpha$:

$$\begin{aligned}
\partial^3_{n_\uparrow}\alpha \;=\; & \frac{-15\partial_n^2 p z^{-2}\partial_n z + 30\partial_n p z^{-3}(\partial_n z)^2 - 15\partial_n p z^{-2}\partial_n^2 z - 30 p z^{-4}(\partial_n z)^3}{3d_s} \\
& + \frac{30 p z^{-3}\partial_n z\partial_n^2 z - 5 p z^{-2}\partial_n^3 z + 5\partial_n^3 p(z^{-1}-1)}{3d_s} \\
& + \frac{-3\partial^2_{n_\uparrow}\alpha\partial_\zeta d_s\partial_{n_\uparrow}\zeta - 6\partial_{n_\uparrow}\alpha\partial_\zeta^2 d_s(\partial_{n_\uparrow}\zeta)^2 - 3\alpha\partial_\zeta^3 d_s(\partial_{n_\uparrow}\zeta)^3}{3d_s} \\
& - \frac{9\alpha\partial_\zeta^2 d_s\partial_{n_\uparrow}\zeta\partial^2_{n_\uparrow}\zeta - 3\alpha\partial_\zeta d_s\partial^3_{n_\uparrow}\zeta}{3d_s} \\
& - \frac{(a_\uparrow)\cdot 3\partial_\zeta d_s\partial_{n_\uparrow}\zeta}{9d_s^2} \\
& + \frac{(-10 p z^{-2}(\partial_n z)^2 + 5 p z^{-2}\partial_n^2 z + 5\partial_n^2 p(z^{-1}-1))\partial_\zeta d_s\partial_{n_\uparrow}\zeta}{3d_s^2} \\
& + \frac{(5 p z^{-2}\partial_n z + 5\partial_n p(z^{-1}-1))(\partial_\zeta^2 d_s(\partial_{n_\uparrow}\zeta)^2 + \partial_\zeta d_s\partial^2_{n_\uparrow}\zeta)}{3d_s^2} \\
& + \frac{3\partial_{n_\uparrow}\alpha(\partial_\zeta d_s\partial_{n_\uparrow}\zeta)^2 + 6\alpha\partial_\zeta d_s\partial_{n_\uparrow}\zeta(\partial_\zeta^2 d_s(\partial_{n_\uparrow}\zeta)^2 + \partial_\zeta d_s\partial^2_{n_\uparrow}\zeta)}{3d_s^2} \\
& - \frac{(b_\uparrow)\cdot 2\partial_\zeta d_s\partial_{n_\uparrow}\zeta}{3d_s^3}
\end{aligned} \tag{B.203}$$

This is done analogously for $n_\downarrow$ and will not be shown here. The derivatives of α with respect to $\nabla n_{\uparrow,\downarrow}$ and $\tau_{\uparrow,\downarrow}$ are the same as for ∇n and τ, respectively. See above.

For

$$\begin{aligned}
f_c(\alpha) \;=\; & \exp[-c_{1c}\alpha/(1-\alpha)]\theta(1-\alpha) \\
& -d_c\exp[c_{2c}/(1-\alpha)]\theta(\alpha-1)]
\end{aligned} \tag{B.204}$$

the derivatives with respect to α are the same as for f_x (see above) by substituting $c_{1x}\to c_{1c}$ and $d_x\to d_c$. With respect to the other variables we have:

$$
\begin{aligned}
\partial_{n_\uparrow} f_c &= \partial_\alpha f_c \partial_{n_\uparrow}\alpha && \text{(B.205)}\\
\partial^2_{n_\uparrow} f_c &= \partial^2_\alpha f_c (\partial_{n_\uparrow}\alpha)^2 + \partial_\alpha f_c \partial^2_{n_\uparrow}\alpha && \text{(B.206)}\\
\partial^3_{n_\uparrow} f_c &= \partial^3_\alpha f_c (\partial_{n_\uparrow}\alpha)^3 + 3\partial^2_\alpha f_c \partial_{n_\uparrow}\alpha \partial^2_{n_\uparrow}\alpha + \partial_\alpha f_c \partial^3_{n_\uparrow}\alpha && \text{(B.207)}\\
\partial_{n_\downarrow} f_c &= \partial_\alpha f_c \partial_{n_\downarrow}\alpha && \text{(B.208)}\\
\partial^2_{n_\downarrow} f_c &= \partial^2_\alpha f_c (\partial_{n_\downarrow}\alpha)^2 + \partial_\alpha f_c \partial^2_{n_\downarrow}\alpha && \text{(B.209)}\\
\partial^3_{n_\downarrow} f_c &= \partial^3_\alpha f_c (\partial_{n_\downarrow}\alpha)^3 + 3\partial^2_\alpha f_c \partial_{n_\downarrow}\alpha \partial^2_{n_\downarrow}\alpha + \partial_\alpha f_c \partial^3_{n_\downarrow}\alpha && \text{(B.210)}\\
\partial_{\nabla n} f_c &= \partial_\alpha f_c \partial_{\nabla n}\alpha && \text{(B.211)}\\
\partial^2_{\nabla n} f_c &= \partial^2_\alpha f_c (\partial_{\nabla n}\alpha)^2 + \partial_\alpha f_c \partial^2_{\nabla n}\alpha && \text{(B.212)}\\
\partial^3_{\nabla n} f_c &= \partial^3_\alpha f_c (\partial_{\nabla n}\alpha)^3 + 3\partial^2_\alpha f_c \partial_{\nabla n}\alpha \partial^2_{\nabla n}\alpha + \partial_\alpha f_c \partial^3_{\nabla n}\alpha && \text{(B.213)}\\
\partial_{\tau_\uparrow} f_c &= \partial_\alpha f_c \partial_{\tau_\uparrow}\alpha && \text{(B.214)}\\
\partial^2_{\tau_\uparrow} f_c &= \partial^2_\alpha f_c (\partial_{\tau_\uparrow}\alpha)^2 + \partial_\alpha f_c \partial^2_{\tau_\uparrow}\alpha && \text{(B.215)}\\
\partial^3_{\tau_\uparrow} f_c &= \partial^3_\alpha f_c (\partial_{\tau_\uparrow}\alpha)^3 + 3\partial^2_\alpha f_c \partial_{\tau_\uparrow}\alpha \partial^2_{\tau_\uparrow}\alpha + \partial_\alpha f_c \partial^3_{\tau_\uparrow}\alpha && \text{(B.216)}\\
\partial_{\tau_\downarrow} f_c &= \partial_\alpha f_c \partial_{\tau_\downarrow}\alpha && \text{(B.217)}\\
\partial^2_{\tau_\downarrow} f_c &= \partial^2_\alpha f_c (\partial_{\tau_\downarrow}\alpha)^2 + \partial_\alpha f_c \partial^2_{\tau_\downarrow}\alpha && \text{(B.218)}\\
\partial^3_{\tau_\downarrow} f_c &= \partial^3_\alpha f_c (\partial_{\tau_\downarrow}\alpha)^3 + 3\partial^2_\alpha f_c \partial_{\tau_\downarrow}\alpha \partial^2_{\tau_\downarrow}\alpha + \partial_\alpha f_c \partial^3_{\tau_\downarrow}\alpha && \text{(B.219)}\\
& && \text{(B.220)}
\end{aligned}
$$

For $\epsilon_c^1 = \epsilon_c^{LSDA1} + H_1$ we have:

$$
\begin{aligned}
\partial_{n_\uparrow}\epsilon_c^1 &= \partial_{r_s}\epsilon_c^1 \partial_n r_s + \partial_\zeta \epsilon_c^1 \partial_{n_\uparrow}\zeta + \partial_p \epsilon_c^1 \partial_n p && \text{(B.221)}\\
\partial^2_{n_\uparrow}\epsilon_c^1 &= \partial^2_{r_s}\epsilon_c^1 (\partial_n r_s)^2 + \partial_{r_s}\epsilon_c^1 \partial^2_n r_s + \partial^2_\zeta \epsilon_c^1 (\partial_{n_\uparrow}\zeta)^2 + \partial_\zeta \epsilon_c^1 \partial^2_{n_\uparrow}\zeta \\
&\quad + \partial^2_p \epsilon_c^1 (\partial_n p)^2 + \partial_p \epsilon_c^1 \partial^2_n p && \text{(B.222)}\\
\partial^3_{n_\uparrow}\epsilon_c^1 &= \partial^3_{r_s}\epsilon_c^1 (\partial_n r_s)^3 + 3\partial^2_{r_s}\epsilon_c^1 \partial_n r_s \partial^2_n r_s + \partial_{r_s}\epsilon_c^1 \partial^3_n r_s + \partial^3_\zeta \epsilon_c^1 (\partial_{n_\uparrow}\zeta)^3 + 3\partial^2_\zeta \epsilon_c^1 \partial^2_{n_\uparrow}\zeta \partial_{n_\uparrow}\zeta \\
&\quad + \partial_\zeta \epsilon_c^1 \partial^3_{n_\uparrow}\zeta + \partial^3_p \epsilon_c^1 (\partial_n p)^3 + 3\partial^2_p \epsilon_c^1 \partial^2_n p \partial_n p + \partial_p \epsilon_c^1 \partial^3_n p && \text{(B.223)}\\
\partial_{n_\downarrow}\epsilon_c^1 &= \partial_{r_s}\epsilon_c^1 \partial_n r_s + \partial_\zeta \epsilon_c^1 \partial_{n_\downarrow}\zeta + \partial_p \epsilon_c^1 \partial_n p && \text{(B.224)}\\
\partial^2_{n_\downarrow}\epsilon_c^1 &= \partial^2_{r_s}\epsilon_c^1 (\partial_n r_s)^2 + \partial_{r_s}\epsilon_c^1 \partial^2_n r_s + \partial^2_\zeta \epsilon_c^1 (\partial_{n_\downarrow}\zeta)^2 + \partial_\zeta \epsilon_c^1 \partial^2_{n_\downarrow}\zeta \\
&\quad + \partial^2_p \epsilon_c^1 (\partial_n p)^2 + \partial_p \epsilon_c^1 \partial^2_n p && \text{(B.225)}\\
\partial^3_{n_\downarrow}\epsilon_c^1 &= \partial^3_{r_s}\epsilon_c^1 (\partial_n r_s)^3 + 3\partial^2_{r_s}\epsilon_c^1 \partial_n r_s \partial^2_n r_s + \partial_{r_s}\epsilon_c^1 \partial^3_n r_s + \partial^3_\zeta \epsilon_c^1 (\partial_{n_\downarrow}\zeta)^3 + 3\partial^2_\zeta \epsilon_c^1 \partial^2_{n_\downarrow}\zeta \partial_{n_\downarrow}\zeta \\
&\quad + \partial_\zeta \epsilon_c^1 \partial^3_{n_\downarrow}\zeta + \partial^3_p \epsilon_c^1 (\partial_n p)^3 + 3\partial^2_p \epsilon_c^1 \partial^2_n p \partial_n p + \partial_p \epsilon_c^1 \partial^3_n p && \text{(B.226)}\\
\partial_{\nabla n}\epsilon_c^1 &= \partial_p \epsilon_c^1 \partial_{\nabla n} p && \text{(B.227)}\\
\partial^2_{\nabla n}\epsilon_c^1 &= \partial^2_p \epsilon_c^1 (\partial_{\nabla n} p)^2 + \partial_p \epsilon_c^1 \partial^2_{\nabla n} p && \text{(B.228)}\\
\partial^3_{\nabla n}\epsilon_c^1 &= \partial^3_p \epsilon_c^1 (\partial_{\nabla n} p)^3 + 3\partial^2_p \epsilon_c^1 \partial_{\nabla n} p \partial^2_{\nabla n} p + \partial_p \epsilon_c^1 \partial^3_{\nabla n} p && \text{(B.229)}
\end{aligned}
$$

For $\epsilon_c^0 = (\epsilon_c^{LDA0} + H_0)G_c(\zeta)$ we have:

$$\begin{aligned}
\partial_{r_s}\epsilon_c^0 &= (\partial_{r_s}\epsilon_c^{LDA0} + \partial_{r_s}H_0)G_c && \text{(B.230)}\\
\partial_{r_s}^2\epsilon_c^0 &= (\partial_{r_s}^2\epsilon_c^{LDA0} + \partial_{r_s}^2H_0)G_c && \text{(B.231)}\\
\partial_{r_s}^3\epsilon_c^0 &= (\partial_{r_s}^3\epsilon_c^{LDA0} + \partial_{r_s}^3H_0)G_c && \text{(B.232)}\\
\partial_p\epsilon_c^0 &= \partial_pH_0G_c && \text{(B.233)}\\
\partial_p^2\epsilon_c^0 &= \partial_p^2H_0G_c && \text{(B.234)}\\
\partial_p^3\epsilon_c^0 &= \partial_p^3H_0G_c && \text{(B.235)}\\
\partial_\zeta\epsilon_c^0 &= (\epsilon_c^{LDA0} + H_0)\partial_\zeta G_c && \text{(B.236)}\\
\partial_\zeta^2\epsilon_c^0 &= (\epsilon_c^{LDA0} + H_0)\partial_\zeta^2 G_c && \text{(B.237)}\\
\partial_\zeta^3\epsilon_c^0 &= (\epsilon_c^{LDA0} + H_0)\partial_\zeta^3 G_c && \text{(B.238)}\\
& && \text{(B.239)}
\end{aligned}$$

The derivatives of ϵ_c^0 with respect to $n_{\uparrow,\downarrow}$ and ∇n are analogous to the derivatives of ϵ_c^1 and will thus not be shown.

For $\epsilon_c = \epsilon_c^1 + f_c(\alpha)(\epsilon_c^0 - \epsilon_c^1)$ we have:

$$\begin{aligned}
\partial_{n_\uparrow}\epsilon_c &= \partial_{n_\uparrow}\epsilon_c^1 + \partial_{n_\uparrow}f_c(\epsilon_c^0 - \epsilon_c^1) + f_c(\partial_{n_\uparrow}\epsilon_c^0 - \partial_{n_\uparrow}\epsilon_c^1) && \text{(B.240)}\\
\partial_{n_\uparrow}^2\epsilon_c &= \partial_{n_\uparrow}^2\epsilon_c^1 + \partial_{n_\uparrow}^2 f_c(\epsilon_c^0 - \epsilon_c^1) + 2\partial_{n_\uparrow}f_c(\partial_{n_\uparrow}\epsilon_c^0 - \partial_{n_\uparrow}\epsilon_c^1)\\
&\quad + f_c(\partial_{n_\uparrow}^2\epsilon_c^0 - \partial_{n_\uparrow}^2\epsilon_c^1) && \text{(B.241)}\\
\partial_{n_\uparrow}^3\epsilon_c &= \partial_{n_\uparrow}^3\epsilon_c^1 + \partial_{n_\uparrow}^3 f_c(\epsilon_c^0 - \epsilon_c^1) + 3\partial_{n_\uparrow}^2 f_c(\partial_{n_\uparrow}\epsilon_c^0 - \partial_{n_\uparrow}\epsilon_c^1)\\
&\quad + 3\partial_{n_\uparrow}f_c(\partial_{n_\uparrow}^2\epsilon_c^0 - \partial_{n_\uparrow}^2\epsilon_c^1) + f_c(\partial_{n_\uparrow}^3\epsilon_c^0 - \partial_{n_\uparrow}^3\epsilon_c^1) && \text{(B.242)}\\
\partial_{n_\downarrow}\epsilon_c &= \partial_{n_\downarrow}\epsilon_c^1 + \partial_{n_\downarrow}f_c(\epsilon_c^0 - \epsilon_c^1) + f_c(\partial_{n_\downarrow}\epsilon_c^0 - \partial_{n_\downarrow}\epsilon_c^1) && \text{(B.243)}\\
\partial_{n_\downarrow}^2\epsilon_c &= \partial_{n_\downarrow}^2\epsilon_c^1 + \partial_{n_\downarrow}^2 f_c(\epsilon_c^0 - \epsilon_c^1) + 2\partial_{n_\downarrow}f_c(\partial_{n_\downarrow}\epsilon_c^0 - \partial_{n_\downarrow}\epsilon_c^1)\\
&\quad + f_c(\partial_{n_\downarrow}^2\epsilon_c^0 - \partial_{n_\downarrow}^2\epsilon_c^1) && \text{(B.244)}\\
\partial_{n_\downarrow}^3\epsilon_c &= \partial_{n_\downarrow}^3\epsilon_c^1 + \partial_{n_\downarrow}^3 f_c(\epsilon_c^0 - \epsilon_c^1) + 3\partial_{n_\downarrow}^2 f_c(\partial_{n_\downarrow}\epsilon_c^0 - \partial_{n_\downarrow}\epsilon_c^1)\\
&\quad + 3\partial_{n_\downarrow}f_c(\partial_{n_\downarrow}^2\epsilon_c^0 - \partial_{n_\downarrow}^2\epsilon_c^1) + f_c(\partial_{n_\downarrow}^3\epsilon_c^0 - \partial_{n_\downarrow}^3\epsilon_c^1) && \text{(B.245)}\\
\partial_{\nabla n}\epsilon_c &= \partial_{\nabla n}\epsilon_c^1 + \partial_{\nabla n}f_c(\epsilon_c^0 - \epsilon_c^1) + f_c(\partial_{\nabla n}\epsilon_c^0 - \partial_{\nabla n}\epsilon_c^1) && \text{(B.246)}\\
\partial_{\nabla n}^2\epsilon_c &= \partial_{\nabla n}^2\epsilon_c^1 + \partial_{\nabla n}^2 f_c(\epsilon_c^0 - \epsilon_c^1) + 2\partial_{\nabla n}f_c(\partial_{\nabla n}\epsilon_c^0 - \partial_{\nabla n}\epsilon_c^1)\\
&\quad + f_c(\partial_{\nabla n}^2\epsilon_c^0 - \partial_{\nabla n}^2\epsilon_c^1) && \text{(B.247)}\\
\partial_{\nabla n}^3\epsilon_c &= \partial_{\nabla n}^3\epsilon_c^1 + \partial_{\nabla n}^3 f_c(\epsilon_c^0 - \epsilon_c^1) + 3\partial_{\nabla n}^2 f_c(\partial_{\nabla n}\epsilon_c^0 - \partial_{\nabla n}\epsilon_c^1)\\
&\quad + 3\partial_{\nabla n}f_c(\partial_{\nabla n}^2\epsilon_c^0 - \partial_{\nabla n}^2\epsilon_c^1) + f_c(\partial_{\nabla n}^3\epsilon_c^0 - \partial_{\nabla n}^3\epsilon_c^1) && \text{(B.248)}
\end{aligned}$$

We have

$$E_c[n_\uparrow, n_\downarrow] = \int d^3r n\epsilon_c(r_s, \zeta, p, \alpha) \qquad \text{(B.249)}$$

Let $A_c = n\epsilon_c(r_s, \beta, p, \alpha)$. Then we have:

$$\partial_{n_\uparrow} A_c = n\partial_{n_\uparrow}\epsilon_c + \epsilon_c \tag{B.250}$$
$$\partial^2_{n_\uparrow} A_c = 2\partial_{n_\uparrow}\epsilon_c + n\partial^2_{n_\uparrow}\epsilon_c \tag{B.251}$$
$$\partial^3_{n_\uparrow} A_c = 3\partial^2_{n_\uparrow}\epsilon_c + n\partial^3_{n_\uparrow}\epsilon_c \tag{B.252}$$
$$\partial_{n_\downarrow} A_c = n\partial_{n_\downarrow}\epsilon_c + \epsilon_c \tag{B.253}$$
$$\partial^2_{n_\downarrow} A_c = 2\partial_{n_\downarrow}\epsilon_c + n\partial^2_{n_\downarrow}\epsilon_c \tag{B.254}$$
$$\partial^3_{n_\downarrow} A_c = 3\partial^2_{n_\downarrow}\epsilon_c + n\partial^3_{n_\downarrow}\epsilon_c \tag{B.255}$$
$$\partial_{\nabla n} A_c = n\partial_{\nabla n}\epsilon_c \tag{B.256}$$
$$\partial^2_{\nabla n} A_c = n\partial^2_{\nabla n}\epsilon_c \tag{B.257}$$
$$\partial^3_{\nabla n} A_c = n\partial^3_{\nabla n}\epsilon_c \tag{B.258}$$
$$\partial_{\tau_\uparrow} A_c = n\partial_{\tau_\uparrow} f_c(\epsilon_c^0 - \epsilon_c^1) \tag{B.259}$$
$$\partial^2_{\tau_\uparrow} A_c = n\partial^2_{\tau_\uparrow} f_c(\epsilon_c^0 - \epsilon_c^1) \tag{B.260}$$
$$\partial^3_{\tau_\uparrow} A_c = n\partial^3_{\tau_\uparrow} f_c(\epsilon_c^0 - \epsilon_c^1) \tag{B.261}$$
$$\partial_{\tau_\downarrow} A_c = n\partial_{\tau_\downarrow} f_c(\epsilon_c^0 - \epsilon_c^1) \tag{B.262}$$
$$\partial^2_{\tau_\downarrow} A_c = n\partial^2_{\tau_\downarrow} f_c(\epsilon_c^0 - \epsilon_c^1) \tag{B.263}$$
$$\partial^3_{\tau_\downarrow} A_c = n\partial^3_{\tau_\downarrow} f_c(\epsilon_c^0 - \epsilon_c^1) \tag{B.264}$$
$$\tag{B.265}$$

B.4 Transformations

General Chain Rule in case of first, second and third derivative for two variables: So, for $g(t) = f(x(t), y(t))$ we have:

$$g'(t) = \frac{\partial f}{\partial x}\cdot\frac{\partial x}{\partial t} + \frac{\partial f}{\partial y}\cdot\frac{\partial y}{\partial t} \tag{B.266}$$

$$\begin{aligned} g''(t) &= \frac{\partial f}{\partial x}\cdot\frac{\partial^2 x}{\partial t^2} + \frac{\partial f}{\partial y}\cdot\frac{\partial^2 y}{\partial t^2} + \left(\frac{dx}{dt}\right)^2\frac{\partial^2 f}{\partial x^2} \\ &+ \frac{dx}{dt}\frac{dy}{dt}\left(\frac{\partial^2 f}{\partial y\partial x} + \frac{\partial^2 f}{\partial x\partial y}\right) + \left(\frac{dy}{dt}\right)^2\frac{\partial^2 f}{\partial y^2} \end{aligned} \tag{B.267}$$

$$\begin{aligned} g'''(t) &= \frac{\partial f}{\partial x}\frac{d^3x}{dt^3} + 3\frac{\partial^2 f}{\partial x^2}\frac{d^2x}{dt^2}\frac{dx}{dt} + 2\frac{\partial^2 f}{\partial y\partial x}\frac{d^2x}{dt^2}\frac{dy}{dt} + \left(\frac{dx}{dt}\right)^2\left(\frac{dx}{dt}\frac{\partial^3 f}{\partial x^3} + \frac{dy}{dt}\frac{\partial^3 f}{\partial y\partial x^2}\right) \\ &+ \frac{dx}{dt}\frac{d^2y}{dt^2}\frac{\partial^2 f}{\partial y\partial x} + \frac{dx}{dt}\frac{dy}{dt}\left(\frac{dx}{dt}\frac{\partial^3 f}{\partial y\partial x^2} + \frac{dy}{dt}\frac{\partial^3 f}{\partial y^2\partial x}\right) \\ &+ \frac{\partial f}{\partial y}\frac{d^3y}{dt^3} + 3\frac{\partial^2 f}{\partial y^2}\frac{d^2y}{dt^2}\frac{dy}{dt} + 2\frac{\partial^2 f}{\partial x\partial y}\frac{d^2y}{dt^2}\frac{dx}{dt} + \left(\frac{dy}{dt}\right)^2\left(\frac{dy}{dt}\frac{\partial^3 f}{\partial y^3} + \frac{dx}{dt}\frac{\partial^3 f}{\partial x\partial y^2}\right) \\ &+ \frac{dy}{dt}\frac{d^2x}{dt^2}\frac{\partial^2 f}{\partial x\partial y} + \frac{dy}{dt}\frac{dx}{dt}\left(\frac{dy}{dt}\frac{\partial^3 f}{\partial x\partial y^2} + \frac{dx}{dt}\frac{\partial^3 f}{\partial x^2\partial y}\right) \end{aligned} \tag{B.268}$$

With the above three equations we can transform all the derivatives w.r.t. $n_\uparrow, n_\downarrow, \tau_\uparrow, \tau_\downarrow, \nabla n_t$ to derivatives w.r.t. n_t, n_s, τ_t, τ_s and $(\nabla n_t)^2$.

First of all, we can use n_t, n_s, τ_t, τ_s and $(\nabla n_t)^2$ to express the other variables as:

$$n_\uparrow = \frac{1}{2}(n_t + n_s) \tag{B.269}$$

$$n_\downarrow = \frac{1}{2}(n_t - n_s) \tag{B.270}$$

$$\tau_\uparrow = \frac{1}{2}(\tau_t + \tau_s) \tag{B.271}$$

$$\tau_\downarrow = \frac{1}{2}(\tau_t - \tau_s) \tag{B.272}$$

$$\nabla n_t = \sqrt{(\nabla n_t)^2} \tag{B.273}$$

Since we already have the first three derivatives of A_{xc} w.r.t. $n_\uparrow, n_\downarrow, \tau_\uparrow, \tau_\downarrow, \nabla n_t$, we get the transformed derivatives of the first order as:

$$\frac{\partial A_{xc}}{\partial n_t} = \frac{1}{2}\frac{\partial A_{xc}}{\partial n_\uparrow} + \frac{1}{2}\frac{\partial A_{xc}}{\partial n_\downarrow} \tag{B.274}$$

$$\frac{\partial A_{xc}}{\partial n_s} = \frac{1}{2}\frac{\partial A_{xc}}{\partial n_\uparrow} - \frac{1}{2}\frac{\partial A_{xc}}{\partial n_\downarrow} \tag{B.275}$$

$$\frac{\partial A_{xc}}{\partial \tau_t} = \frac{1}{2}\frac{\partial A_{xc}}{\partial \tau_\uparrow} + \frac{1}{2}\frac{\partial A_{xc}}{\partial \tau_\downarrow} \tag{B.276}$$

$$\frac{\partial A_{xc}}{\partial \tau_s} = \frac{1}{2}\frac{\partial A_{xc}}{\partial \tau_\uparrow} - \frac{1}{2}\frac{\partial A_{xc}}{\partial \tau_\downarrow} \tag{B.277}$$

$$\frac{\partial A_{xc}}{\partial (\nabla n_t)^2} = \frac{\partial A_{xc}}{\partial \nabla n_t}\frac{1}{2\nabla n_t} \tag{B.278}$$

Since A_{xc} doesn't depend on $(\nabla n_s)^2$ and $(\nabla n_t)(\nabla n_s)$ the derivatives with respect to these are zero and are thus not necessary here.[2]

For the transformations of the second order (excluding the offsite-terms) we have:

$$\frac{\partial^2 A_{xc}}{\partial n_t^2} = \frac{1}{4}\frac{\partial^2 A_{xc}}{\partial n_\uparrow^2} + \frac{1}{4}\frac{\partial^2 A_{xc}}{\partial n_\downarrow^2} \tag{B.279}$$

$$\frac{\partial^2 A_{xc}}{\partial n_s^2} = \frac{1}{4}\frac{\partial^2 A_{xc}}{\partial n_\uparrow^2} + \frac{1}{4}\frac{\partial^2 A_{xc}}{\partial n_\downarrow^2} \tag{B.280}$$

$$\frac{\partial^2 A_{xc}}{\partial \tau_t^2} = \frac{1}{4}\frac{\partial^2 A_{xc}}{\partial \tau_\uparrow^2} + \frac{1}{4}\frac{\partial^2 A_{xc}}{\partial \tau_\downarrow^2} \tag{B.281}$$

$$\frac{\partial^2 A_{xc}}{\partial \tau_s^2} = \frac{1}{4}\frac{\partial^2 A_{xc}}{\partial \tau_\uparrow^2} + \frac{1}{4}\frac{\partial^2 A_{xc}}{\partial \tau_\downarrow^2} \tag{B.282}$$

$$\frac{\partial^2 A_{xc}}{\partial (\nabla n_t)^{2\,2}} = \frac{1}{4(\nabla n_t)^2}\frac{\partial^2 A_{xc}}{\partial \nabla n_t^2} - \frac{1}{4(\nabla n_t)^3}\frac{\partial A_{xc}}{\partial \nabla n_t} \tag{B.283}$$

Finally, the transformations of the third order (excluding the offsite-terms):

$$\frac{\partial^3 A_{xc}}{\partial n_t^3} = \frac{1}{8}\frac{\partial^3 A_{xc}}{\partial n_\uparrow^3} + \frac{1}{8}\frac{\partial^3 A_{xc}}{\partial n_\downarrow^3} \tag{B.284}$$

$$\frac{\partial^3 A_{xc}}{\partial n_s^3} = \frac{1}{8}\frac{\partial^3 A_{xc}}{\partial n_\uparrow^3} - \frac{1}{8}\frac{\partial^3 A_{xc}}{\partial n_\downarrow^3} \tag{B.285}$$

$$\frac{\partial^3 A_{xc}}{\partial \tau_t^3} = \frac{1}{8}\frac{\partial^3 A_{xc}}{\partial \tau_\uparrow^3} + \frac{1}{8}\frac{\partial^3 A_{xc}}{\partial \tau_\downarrow^3} \tag{B.286}$$

$$\frac{\partial^3 A_{xc}}{\partial \tau_s^3} = \frac{1}{8}\frac{\partial^3 A_{xc}}{\partial \tau_\uparrow^3} - \frac{1}{8}\frac{\partial^3 A_{xc}}{\partial \tau_\downarrow^3} \tag{B.287}$$

$$\frac{\partial^3 A_{xc}}{\partial (\nabla n_t)^{2\,3}} = \frac{\partial A_{xc}}{\partial \nabla n_t}\frac{3}{8(\nabla n_t)^5} - \frac{\partial^2 A_{xc}}{\partial \nabla n_t^2}\frac{3}{8(\nabla n_t)^4} + \frac{1}{8(\nabla n_t)^3}\frac{\partial^3 A_{xc}}{\partial \nabla n_t^3} \tag{B.288}$$

[2] I'm saying A_{xc} does not depend on these because I couldn't find any instance of either $(\nabla n_s)^2$ (or even ∇n_s) and $(\nabla n_t)(\nabla n_s)$ appearing in any of the equations of the paper or the supplementary material.

B.4.1 Mixed Terms for the transformations

The first derivative of each transformation doesn't contain any mixed terms. For the derivatives of the second and third derivatives I need the following mixed terms:

$$\begin{aligned}
\frac{\partial^2 A_{xc}}{\partial n_t^2} &: \rightarrow \frac{\partial^2 A_{xc}}{\partial n_\uparrow \partial n_\downarrow}, \frac{\partial^2 A_{xc}}{\partial n_\downarrow \partial n_\uparrow} \\
\frac{\partial^2 A_{xc}}{\partial n_s^2} &: \rightarrow \frac{\partial^2 A_{xc}}{\partial n_\uparrow \partial n_\downarrow}, \frac{\partial^2 A_{xc}}{\partial n_\downarrow \partial n_\uparrow} \text{same as above, but sign diff. for mixed terms} \\
\frac{\partial^2 A_{xc}}{\partial \tau_t^2} &: \rightarrow \frac{\partial^2 A_{xc}}{\partial \tau_\uparrow \partial \tau_\downarrow}, \frac{\partial^2 A_{xc}}{\partial \tau_\downarrow \partial \tau_\uparrow} \\
\frac{\partial^2 A_{xc}}{\partial \tau_s^2} &: \rightarrow \frac{\partial^2 A_{xc}}{\partial \tau_\uparrow \partial \tau_\downarrow}, \frac{\partial^2 A_{xc}}{\partial \tau_\downarrow \partial \tau_\uparrow} \text{same as above, but sign diff. for mixed terms} \\
\frac{\partial^2 A_{xc}}{\partial (\nabla n_t)^{2 2}} &: \text{doesn't have any mixed terms to be calculated}
\end{aligned}$$

The main ingredient of the mixed terms seems to be ζ. Thus, we have

$$\partial_{n_\uparrow} \zeta = \frac{2n_\downarrow}{n_t^2} \tag{B.289}$$

$$\partial_{n_\downarrow} \zeta = -\frac{2n_\uparrow}{n_t^2} \tag{B.290}$$

$$\partial_{n_\downarrow} \partial_{n_\uparrow} \zeta = \frac{2n_s}{n_t^3} \tag{B.291}$$

$$\partial_{n_\uparrow} \partial_{n_\downarrow} \zeta = -\frac{2n_s}{n_t^3} \tag{B.292}$$

$$\partial_{n_\uparrow} \partial_{n_\downarrow}^2 \zeta = \frac{-8n_\uparrow + 4n_\downarrow}{n_t^4} \tag{B.293}$$

$$\partial_{n_\downarrow} \partial_{n_\uparrow}^2 \zeta = \frac{4n_\uparrow - 8n_\downarrow}{n_t^4} \tag{B.294}$$

According to the recipe of switching in the correct ζ derivatives into the existing derivatives, we have the following derivatives being affected by the changes: α(including $a_\uparrow, b_\uparrow$)), $f_c, \epsilon_c^1, \epsilon_c^0, \epsilon_c, A_c$.

Thus, we have now:

$$\begin{aligned}
\partial_{n_\downarrow} \partial_{n_\uparrow} \alpha = & \frac{-10 \partial_n p z^{-2} \partial_n z + 10 p z^{-3} (\partial_n z)^2 - 5 p z^{-2} \partial_n^2 z + 5 \partial_n^2 p (z^{-1} - 1)}{3 d_s} \\
& - \frac{3 \partial_{n_\downarrow} \alpha \partial_\zeta d_s \partial_{n_\uparrow} \zeta - 3 \alpha \partial_\zeta^2 d_s \partial_{n_\downarrow} \zeta \partial_{n_\uparrow} \zeta - 3 \alpha \partial_\zeta d_s \partial_{n_\downarrow} \partial_{n_\uparrow} \zeta}{3 d_s} \\
& + \frac{(5 p z^{-2} \partial_n z + 5 \partial_n p (z^{-1} - 1)) \partial_\zeta d_s \partial_{n_\downarrow} \zeta + 3 \alpha (\partial_\zeta d_s)^2 \partial_{n_\uparrow} \zeta \partial_{n_\downarrow} \zeta}{3 d_s^2}
\end{aligned}$$

$$
\begin{aligned}
\partial_{n_\uparrow}\partial_{n_\downarrow}\alpha &= \frac{-10\partial_n p z^{-2}\partial_n z + 10pz^{-3}(\partial_n z)^2 - 5pz^{-2}\partial_n^2 z + 5\partial_n^2 p(z^{-1}-1)}{3d_s} \\
&\quad - \frac{3\partial_{n_\uparrow}\alpha\partial_\zeta d_s\partial_{n_\downarrow}\zeta - 3\alpha\partial_\zeta^2 d_s\partial_{n_\uparrow}\zeta\partial_{n_\downarrow}\zeta - 3\alpha\partial_\zeta d_s\partial_{n_\uparrow}\partial_{n_\downarrow}\zeta}{3d_s} \\
&\quad + \frac{(5pz^{-2}\partial_n z + 5\partial_n p(z^{-1}-1))\partial_\zeta d_s\partial_{n_\uparrow}\zeta + 3\alpha(\partial_\zeta d_s)^2\partial_{n_\downarrow}\zeta\partial_{n_\uparrow}\zeta}{3d_s^2}
\end{aligned}
$$

Let

$$
\begin{aligned}
a_\uparrow &= -10\partial_n p z^{-2}\partial_n z + 10pz^{-3}(\partial_n z)^2 - 5pz^{-2}\partial_n^2 z + 5\partial_n^2 p(z^{-1}-1) \\
&\quad -3\partial_{n_\uparrow}\alpha\partial_\zeta d_s\partial_{n_\uparrow}\zeta - 3\alpha\partial_\zeta^2 d_s(\partial_{n_\uparrow}\zeta)^2 - 3\alpha\partial_\zeta d_s\partial_{n_\uparrow}^2\zeta \qquad \text{(B.295)} \\
b_\uparrow &= (5pz^{-2}\partial_n z + 5\partial_n p(z^{-1}-1))\partial_\zeta d_s\partial_{n_\uparrow}\zeta + 3\alpha(\partial_\zeta d_s\partial_{n_\uparrow}\zeta)^2 \qquad \text{(B.296)}
\end{aligned}
$$

and

$$
\begin{aligned}
a_\downarrow &= -10\partial_n p z^{-2}\partial_n z + 10pz^{-3}(\partial_n z)^2 - 5pz^{-2}\partial_n^2 z + 5\partial_n^2 p(z^{-1}-1) \\
&\quad -3\partial_{n_\downarrow}\alpha\partial_\zeta d_s\partial_{n_\downarrow}\zeta - 3\alpha\partial_\zeta^2 d_s(\partial_{n_\downarrow}\zeta)^2 - 3\alpha\partial_\zeta d_s\partial_{n_\downarrow}^2\zeta \qquad \text{(B.297)} \\
b_\downarrow &= (5pz^{-2}\partial_n z + 5\partial_n p(z^{-1}-1))\partial_\zeta d_s\partial_{n_\downarrow}\zeta + 3\alpha(\partial_\zeta d_s\partial_{n_\downarrow}\zeta)^2 \qquad \text{(B.298)}
\end{aligned}
$$

$$
\begin{aligned}
\partial_{n_\downarrow}\partial_{n_\uparrow}^2\alpha &= \frac{-15\partial_n^2 p z^{-2}\partial_n z + 30\partial_n p z^{-3}(\partial_n z)^2 - 15\partial_n p z^{-2}\partial_n^2 z - 30pz^{-4}(\partial_n z)^3}{3d_s} \\
&\quad + \frac{30pz^{-3}\partial_n z\partial_n^2 z - 5pz^{-2}\partial_n^3 z + 5\partial_n^3 p(z^{-1}-1)}{3d_s} \\
&\quad + \frac{-3\partial_{n_\downarrow}\partial_{n_\uparrow}\alpha\partial_\zeta d_s\partial_{n_\uparrow}\zeta - 3\partial_{n_\uparrow}\alpha\partial_\zeta^2 d_s\partial_{n_\downarrow}\zeta\partial_{n_\uparrow}\zeta - 3\partial_{n_\uparrow}\alpha\partial_\zeta d_s\partial_{n_\downarrow}\partial_{n_\uparrow}\zeta}{3ds} \\
&\quad + \frac{-3\partial_{n_\downarrow}\alpha\partial_\zeta^2 d_s(\partial_{n_\uparrow}\zeta)^2 - 3\alpha\partial_\zeta^3 d_s(\partial_{n_\uparrow}\zeta)^2\partial_{n_\downarrow}\zeta - 6\alpha\partial_\zeta^2 d_s\partial_{n_\uparrow}\zeta\partial_{n_\downarrow}\partial_{n_\uparrow}\zeta}{3ds} \\
&\quad + \frac{-3\partial_{n_\downarrow}\alpha\partial_\zeta d_s\partial_{n_\uparrow}^2\zeta - 3\alpha\partial_\zeta^2 d_s\partial_{n_\downarrow}\zeta\partial_{n_\uparrow}^2\zeta - 3\alpha\partial_\zeta d_s\partial_{n_\downarrow}\partial_{n_\uparrow}^2\zeta}{3ds} \\
&\quad - \frac{(a_\uparrow)\cdot 3\partial_\zeta d_s\partial_{n_\downarrow}\zeta}{9d_s^2} \\
&\quad + \frac{(-10pz^{-2}(\partial_n z)^2 + 5pz^{-2}\partial_n^2 z + 5\partial_n^2 p(z^{-1}-1))\partial_\zeta d_s\partial_{n_\uparrow}\zeta}{3d_s^2} \\
&\quad + \frac{(5pz^{-2}\partial_n z + 5\partial_n p(z^{-1}-1))(\partial_\zeta^2 d_s\partial_{n_\downarrow}\zeta\partial_{n_\uparrow}\zeta + \partial_\zeta d_s\partial_{n_\downarrow}\partial_{n_\uparrow}\zeta)}{3d_s^2} \\
&\quad + \frac{3\partial_{n_\downarrow}\alpha(\partial_\zeta d_s\partial_{n_\uparrow}\zeta)^2 + 6\alpha\partial_\zeta d_s\partial_{n_\uparrow}\zeta\cdot(\partial_\zeta^2 d_s\partial_{n_\downarrow}\zeta\partial_{n_\uparrow}\zeta + \partial_\zeta d_s\partial_{n_\downarrow}\partial_{n_\uparrow}\zeta)}{3d_s^2} \\
&\quad - \frac{(b_\uparrow)\cdot 2\partial_\zeta d_s\partial_{n_\downarrow}\zeta}{3d_s^3} \qquad \text{(B.299)}
\end{aligned}
$$

$$
\begin{aligned}
\partial_{n_\uparrow}\partial^2_{n_\downarrow}\alpha \;=\;& \frac{-15\partial_n^2 p z^{-2}\partial_n z + 30\partial_n p z^{-3}(\partial_n z)^2 - 15\partial_n p z^{-2}\partial_n^2 z - 30 p z^{-4}(\partial_n z)^3}{3d_s} \\
&+\frac{30 p z^{-3}\partial_n z\partial_n^2 z - 5 p z^{-2}\partial_n^3 z + 5\partial_n^3 p(z^{-1}-1)}{3d_s} \\
&+\frac{-3\partial_{n_\uparrow}\partial_{n_\downarrow}\alpha\partial_\zeta d_s\partial_{n_\downarrow}\zeta - 3\partial_{n_\downarrow}\alpha\partial_\zeta^2 d_s\partial_{n_\uparrow}\zeta\partial_{n_\downarrow}\zeta - 3\partial_{n_\downarrow}\alpha\partial_\zeta d_s\partial_{n_\uparrow}\partial_{n_\downarrow}\zeta}{3ds} \\
&+\frac{-3\partial_{n_\uparrow}\alpha\partial_\zeta^2 d_s(\partial_{n_\downarrow}\zeta)^2 - 3\alpha\partial_\zeta^3 d_s(\partial_{n_\downarrow}\zeta)^2\partial_{n_\uparrow}\zeta - 6\alpha\partial_\zeta^2 d_s\partial_{n_\downarrow}\zeta\partial_{n_\uparrow}\partial_{n_\downarrow}\zeta}{3ds} \\
&+\frac{-3\partial_{n_\uparrow}\alpha\partial_\zeta d_s\partial^2_{n_\downarrow}\zeta - 3\alpha\partial_\zeta^2 d_s\partial_{n_\uparrow}\zeta\partial^2_{n_\downarrow}\zeta - 3\alpha\partial_\zeta d_s\partial_{n_\uparrow}\partial^2_{n_\downarrow}\zeta}{3ds} \\
&-\frac{(a_\downarrow)\cdot 3\partial_\zeta d_s\partial_{n_\uparrow}\zeta}{9d_s^2} \\
&+\frac{(-10 p z^{-2}(\partial_n z)^2 + 5 p z^{-2}\partial_n^2 z + 5\partial_n^2 p(z^{-1}-1))\partial_\zeta d_s\partial_{n_\downarrow}\zeta}{3d_s^2} \\
&+\frac{(5 p z^{-2}\partial_n z + 5\partial_n p(z^{-1}-1))(\partial_\zeta^2 d_s\partial_{n_\uparrow}\zeta\partial_{n_\downarrow}\zeta + \partial_\zeta d_s\partial_{n_\uparrow}\partial_{n_\downarrow}\zeta)}{3d_s^2} \\
&+\frac{3\partial_{n_\uparrow}\alpha(\partial_\zeta d_s\partial_{n_\downarrow}\zeta)^2 + 6\alpha\partial_\zeta d_s\partial_{n_\downarrow}\zeta\cdot(\partial_\zeta^2 d_s\partial_{n_\uparrow}\zeta\partial_{n_\downarrow}\zeta + \partial_\zeta d_s\partial_{n_\uparrow}\partial_{n_\downarrow}\zeta)}{3d_s^2} \\
&-\frac{(b_\downarrow)\cdot 2\partial_\zeta d_s\partial_{n_\uparrow}\zeta}{3d_s^3}
\end{aligned}
\tag{B.300}
$$

In case of $\tau_\uparrow$ and $\tau_\downarrow$ it is done analogously. **(They are mostly zero.)**

For f_c we have:

$$
\begin{aligned}
\partial_{n_\downarrow}\partial_{n_\uparrow} f_c &= \partial_\alpha^2 f_c\partial_{n_\downarrow}\alpha\partial_{n_\uparrow}\alpha + \partial_\alpha f_c\partial_{n_\downarrow}\partial_{n_\uparrow}\alpha && \text{(B.301)}\\
\partial_{n_\uparrow}\partial_{n_\downarrow} f_c &= \partial_\alpha^2 f_c\partial_{n_\uparrow}\alpha\partial_{n_\downarrow}\alpha + \partial_\alpha f_c\partial_{n_\uparrow}\partial_{n_\downarrow}\alpha && \text{(B.302)}\\
\partial_{n_\downarrow}\partial^2_{n_\uparrow} f_c &= \partial_\alpha^3 f_c\partial_{n_\downarrow}\alpha(\partial_{n_\uparrow}\alpha)^2 + 2\partial_\alpha^2 f_c\partial_{n_\uparrow}\alpha\partial_{n_\downarrow}\partial_{n_\uparrow}\alpha \\
&\quad +\partial_\alpha^2 f_c\partial_{n_\downarrow}\alpha\partial^2_{n_\uparrow}\alpha + \partial_\alpha f_c\partial_{n_\downarrow}\partial^2_{n_\uparrow}\alpha && \text{(B.303)}\\
\partial_{n_\uparrow}\partial^2_{n_\downarrow} f_c &= \partial_\alpha^3 f_c\partial_{n_\uparrow}\alpha(\partial_{n_\downarrow}\alpha)^2 + 2\partial_\alpha^2 f_c\partial_{n_\downarrow}\alpha\partial_{n_\uparrow}\partial_{n_\downarrow}\alpha \\
&\quad +\partial_\alpha^2 f_c\partial_{n_\uparrow}\alpha\partial^2_{n_\downarrow}\alpha + \partial_\alpha f_c\partial_{n_\uparrow}\partial^2_{n_\downarrow}\alpha && \text{(B.304)}
\end{aligned}
$$

In case of $\tau_\uparrow$ and $\tau_\downarrow$ it is done analogously.
For ϵ_c^1 we have:

$$\begin{aligned}
\partial_{n_\downarrow}\partial_{n_\uparrow}\epsilon_c^1 &= \partial_{r_s}^2\epsilon_c^1(\partial_n r_s)^2 + \partial_{r_s}\epsilon_c^1\partial_n^2 r_s + \partial_\zeta^2\epsilon_c^1\partial_{n_\downarrow}\zeta\partial_{n_\uparrow}\zeta + \partial_\zeta\epsilon_c^1\partial_{n_\downarrow}\partial_{n_\uparrow}\zeta \\
&\quad +\partial_p^2\epsilon_c^1(\partial_n p)^2 + \partial_p\epsilon_c^1\partial_n^2 p && \text{(B.305)} \\
\partial_{n_\uparrow}\partial_{n_\downarrow}\epsilon_c^1 &= \partial_{r_s}^2\epsilon_c^1(\partial_n r_s)^2 + \partial_{r_s}\epsilon_c^1\partial_n^2 r_s + \partial_\zeta^2\epsilon_c^1\partial_{n_\uparrow}\zeta\partial_{n_\downarrow}\zeta + \partial_\zeta\epsilon_c^1\partial_{n_\uparrow}\partial_{n_\downarrow}\zeta \\
&\quad +\partial_p^2\epsilon_c^1(\partial_n p)^2 + \partial_p\epsilon_c^1\partial_n^2 p && \text{(B.306)} \\
\partial_{n_\downarrow}\partial_{n_\uparrow}^2\epsilon_c^1 &= \partial_{r_s}^3\epsilon_c^1(\partial_n r_s)^3 + 3\partial_{r_s}^2\epsilon_c^1\partial_n r_s\partial_n^2 r_s + \partial_{r_s}\epsilon_c^1\partial_n^3 r_s \\
&\quad +\partial_\zeta^3\epsilon_c^1\partial_{n_\downarrow}\zeta(\partial_{n_\uparrow}\zeta)^2 + 2\partial_\zeta^2\epsilon_c^1\partial_{n_\uparrow}\zeta\partial_{n_\downarrow}\partial_{n_\uparrow}\zeta \\
&\quad +\partial_\zeta^2\epsilon_c^1\partial_{n_\downarrow}\zeta\partial_{n_\uparrow}^2\zeta + \partial_\zeta\epsilon_c^1\partial_{n_\downarrow}\partial_{n_\uparrow}^2\zeta \\
&\quad +\partial_p^3\epsilon_c^1(\partial_n p)^3 + 3\partial_p^2\epsilon_c^1\partial_n^2 p\partial_n p + \partial_p\epsilon_c^1\partial_n^3 p && \text{(B.307)} \\
\partial_{n_\uparrow}\partial_{n_\downarrow}^2\epsilon_c^1 &= \partial_{r_s}^3\epsilon_c^1(\partial_n r_s)^3 + 3\partial_{r_s}^2\epsilon_c^1\partial_n r_s\partial_n^2 r_s + \partial_{r_s}\epsilon_c^1\partial_n^3 r_s \\
&\quad +\partial_\zeta^3\epsilon_c^1\partial_{n_\uparrow}\zeta(\partial_{n_\downarrow}\zeta)^2 + 2\partial_\zeta^2\epsilon_c^1\partial_{n_\downarrow}\zeta\partial_{n_\uparrow}\partial_{n_\downarrow}\zeta \\
&\quad +\partial_\zeta^2\epsilon_c^1\partial_{n_\uparrow}\zeta\partial_{n_\downarrow}^2\zeta + \partial_\zeta\epsilon_c^1\partial_{n_\uparrow}\partial_{n_\downarrow}^2\zeta \\
&\quad +\partial_p^3\epsilon_c^1(\partial_n p)^3 + 3\partial_p^2\epsilon_c^1\partial_n^2 p\partial_n p + \partial_p\epsilon_c^1\partial_n^3 p && \text{(B.308)}
\end{aligned}$$

For ϵ_c^0 we have:

$$\begin{aligned}
\partial_{n_\downarrow}\partial_{n_\uparrow}\epsilon_c^0 &= \partial_{r_s}^2\epsilon_c^0(\partial_n r_s)^2 + \partial_{r_s}\epsilon_c^0\partial_n^2 r_s + \partial_\zeta^2\epsilon_c^0\partial_{n_\downarrow}\zeta\partial_{n_\uparrow}\zeta + \partial_\zeta\epsilon_c^0\partial_{n_\downarrow}\partial_{n_\uparrow}\zeta \\
&\quad +\partial_p^2\epsilon_c^0(\partial_n p)^2 + \partial_p\epsilon_c^0\partial_n^2 p && \text{(B.309)} \\
\partial_{n_\uparrow}\partial_{n_\downarrow}\epsilon_c^0 &= \partial_{r_s}^2\epsilon_c^0(\partial_n r_s)^2 + \partial_{r_s}\epsilon_c^0\partial_n^2 r_s + \partial_\zeta^2\epsilon_c^0\partial_{n_\uparrow}\zeta\partial_{n_\downarrow}\zeta + \partial_\zeta\epsilon_c^0\partial_{n_\uparrow}\partial_{n_\downarrow}\zeta \\
&\quad +\partial_p^2\epsilon_c^0(\partial_n p)^2 + \partial_p\epsilon_c^0\partial_n^2 p && \text{(B.310)} \\
\partial_{n_\downarrow}\partial_{n_\uparrow}^2\epsilon_c^0 &= \partial_{r_s}^3\epsilon_c^0(\partial_n r_s)^3 + 3\partial_{r_s}^2\epsilon_c^0\partial_n r_s\partial_n^2 r_s + \partial_{r_s}\epsilon_c^0\partial_n^3 r_s \\
&\quad +\partial_\zeta^3\epsilon_c^0\partial_{n_\downarrow}\zeta(\partial_{n_\uparrow}\zeta)^2 + 2\partial_\zeta^2\epsilon_c^0\partial_{n_\uparrow}\zeta\partial_{n_\downarrow}\partial_{n_\uparrow}\zeta \\
&\quad +\partial_\zeta^2\epsilon_c^0\partial_{n_\downarrow}\zeta\partial_{n_\uparrow}^2\zeta + \partial_\zeta\epsilon_c^0\partial_{n_\downarrow}\partial_{n_\uparrow}^2\zeta \\
&\quad +\partial_p^3\epsilon_c^0(\partial_n p)^3 + 3\partial_p^2\epsilon_c^0\partial_n^2 p\partial_n p + \partial_p\epsilon_c^0\partial_n^3 p && \text{(B.311)} \\
\partial_{n_\uparrow}\partial_{n_\downarrow}^2\epsilon_c^0 &= \partial_{r_s}^3\epsilon_c^0(\partial_n r_s)^3 + 3\partial_{r_s}^2\epsilon_c^0\partial_n r_s\partial_n^2 r_s + \partial_{r_s}\epsilon_c^0\partial_n^3 r_s \\
&\quad +\partial_\zeta^3\epsilon_c^0\partial_{n_\uparrow}\zeta(\partial_{n_\downarrow}\zeta)^2 + 2\partial_\zeta^2\epsilon_c^0\partial_{n_\downarrow}\zeta\partial_{n_\uparrow}\partial_{n_\downarrow}\zeta \\
&\quad +\partial_\zeta^2\epsilon_c^0\partial_{n_\uparrow}\zeta\partial_{n_\downarrow}^2\zeta + \partial_\zeta\epsilon_c^0\partial_{n_\uparrow}\partial_{n_\downarrow}^2\zeta \\
&\quad +\partial_p^3\epsilon_c^0(\partial_n p)^3 + 3\partial_p^2\epsilon_c^0\partial_n^2 p\partial_n p + \partial_p\epsilon_c^0\partial_n^3 p && \text{(B.312)}
\end{aligned}$$

ϵ_c^1 and ϵ_c^0 **don't** have a $\tau_{\uparrow,\downarrow}$ dependence.

For ϵ_c we have:

$$\begin{aligned}
\partial_{n_\downarrow}\partial_{n_\uparrow}\epsilon_c &= \partial_{n_\downarrow}\partial_{n_\uparrow}\epsilon_c^1 + \partial_{n_\downarrow}\partial_{n_\uparrow}f_c(\epsilon_c^0-\epsilon_c^1) + \partial_{n_\uparrow}f_c(\partial_{n_\downarrow}\epsilon_c^0 - \partial_{n_\downarrow}\epsilon_c^1) \\
&\quad +\partial_{n_\downarrow}f_c(\partial_{n_\uparrow}\epsilon_c^0 - \partial_{n_\uparrow}\epsilon_c^1) + f_c(\partial_{n_\downarrow}\partial_{n_\uparrow}\epsilon_c^0 - \partial_{n_\downarrow}\partial_{n_\uparrow}\epsilon_c^1) \qquad \text{(B.313)} \\
\partial_{n_\uparrow}\partial_{n_\downarrow}\epsilon_c &= \partial_{n_\uparrow}\partial_{n_\downarrow}\epsilon_c^1 + \partial_{n_\uparrow}\partial_{n_\downarrow}f_c(\epsilon_c^0-\epsilon_c^1) + \partial_{n_\downarrow}f_c(\partial_{n_\uparrow}\epsilon_c^0 - \partial_{n_\uparrow}\epsilon_c^1) \\
&\quad +\partial_{n_\uparrow}f_c(\partial_{n_\downarrow}\epsilon_c^0 - \partial_{n_\downarrow}\epsilon_c^1) + f_c(\partial_{n_\uparrow}\partial_{n_\downarrow}\epsilon_c^0 - \partial_{n_\uparrow}\partial_{n_\downarrow}\epsilon_c^1) \qquad \text{(B.314)} \\
\partial_{n_\downarrow}\partial_{n_\uparrow}^2\epsilon_c &= \partial_{n_\downarrow}\partial_{n_\uparrow}^2\epsilon_c^1 + \partial_{n_\downarrow}\partial_{n_\uparrow}^2f_c(\epsilon_c^0-\epsilon_c^1) + \partial_{n_\uparrow}^2f_c(\partial_{n_\downarrow}\epsilon_c^0 - \partial_{n_\downarrow}\epsilon_c^1) \\
&\quad +2\partial_{n_\downarrow}\partial_{n_\uparrow}f_c(\partial_{n_\uparrow}\epsilon_c^0 - \partial_{n_\uparrow}\epsilon_c^1) + 2\partial_{n_\uparrow}f_c(\partial_{n_\downarrow}\partial_{n_\uparrow}\epsilon_c^0 - \partial_{n_\downarrow}\partial_{n_\uparrow}\epsilon_c^1) \\
&\quad +\partial_{n_\downarrow}f_c(\partial_{n_\uparrow}^2\epsilon_c^0 - \partial_{n_\uparrow}^2\epsilon_c^1) + f_c(\partial_{n_\downarrow}\partial_{n_\uparrow}^2\epsilon_c^0 - \partial_{n_\downarrow}\partial_{n_\uparrow}^2\epsilon_c^1) \qquad \text{(B.315)} \\
\partial_{n_\uparrow}\partial_{n_\downarrow}^2\epsilon_c &= \partial_{n_\uparrow}\partial_{n_\downarrow}^2\epsilon_c^1 + \partial_{n_\uparrow}\partial_{n_\downarrow}^2f_c(\epsilon_c^0-\epsilon_c^1) + \partial_{n_\downarrow}^2f_c(\partial_{n_\uparrow}\epsilon_c^0 - \partial_{n_\uparrow}\epsilon_c^1) \\
&\quad +2\partial_{n_\uparrow}\partial_{n_\downarrow}f_c(\partial_{n_\downarrow}\epsilon_c^0 - \partial_{n_\downarrow}\epsilon_c^1) + 2\partial_{n_\downarrow}f_c(\partial_{n_\uparrow}\partial_{n_\downarrow}\epsilon_c^0 - \partial_{n_\uparrow}\partial_{n_\downarrow}\epsilon_c^1) \\
&\quad +\partial_{n_\uparrow}f_c(\partial_{n_\downarrow}^2\epsilon_c^0 - \partial_{n_\downarrow}^2\epsilon_c^1) + f_c(\partial_{n_\uparrow}\partial_{n_\downarrow}^2\epsilon_c^0 - \partial_{n_\uparrow}\partial_{n_\downarrow}^2\epsilon_c^1) \qquad \text{(B.316)}
\end{aligned}$$

For A_c we have:

$$\begin{aligned}
\partial_{n_\downarrow}\partial_{n_\uparrow}A_c &= \partial_{n_\uparrow}\epsilon_c + n\partial_{n_\downarrow}\partial_{n_\uparrow}\epsilon_c + \partial_{n_\downarrow}\epsilon_c \qquad \text{(B.317)} \\
\partial_{n_\uparrow}\partial_{n_\downarrow}A_c &= \partial_{n_\downarrow}\epsilon_c + n\partial_{n_\uparrow}\partial_{n_\downarrow}\epsilon_c + \partial_{n_\uparrow}\epsilon_c \qquad \text{(B.318)} \\
\partial_{n_\downarrow}\partial_{n_\uparrow}^2A_c &= 2\partial_{n_\downarrow}\partial_{n_\uparrow}\epsilon_c + \partial_{n_\uparrow}^2\epsilon_c + n\partial_{n_\downarrow}\partial_{n_\uparrow}^2\epsilon_c \qquad \text{(B.319)} \\
\partial_{n_\uparrow}\partial_{n_\downarrow}^2A_c &= 2\partial_{n_\uparrow}\partial_{n_\downarrow}\epsilon_c + \partial_{n_\downarrow}^2\epsilon_c + n\partial_{n_\uparrow}\partial_{n_\downarrow}^2\epsilon_c \qquad \text{(B.320)} \\
\partial_{\tau_\downarrow}\partial_{\tau_\uparrow}A_c &= n\partial_{\tau_\downarrow}\partial_{\tau_\uparrow}f_c(\epsilon_c^0-\epsilon_c^1) \qquad \text{(B.321)} \\
\partial_{\tau_\uparrow}\partial_{\tau_\downarrow}A_c &= n\partial_{\tau_\uparrow}\partial_{\tau_\downarrow}f_c(\epsilon_c^0-\epsilon_c^1) \qquad \text{(B.322)} \\
\partial_{\tau_\downarrow}\partial_{\tau_\uparrow}^2A_c &= n\partial_{\tau_\downarrow}\partial_{\tau_\uparrow}^2f_c(\epsilon_c^0-\epsilon_c^1) \qquad \text{(B.323)} \\
\partial_{\tau_\uparrow}\partial_{\tau_\downarrow}^2A_c &= n\partial_{\tau_\uparrow}\partial_{\tau_\downarrow}^2f_c(\epsilon_c^0-\epsilon_c^1) \qquad \text{(B.324)}
\end{aligned}$$

B.5 Notes

ϵ_c^{lsda1} I defined wrongly in the Code. In the code I used E_C of PW92 instead of the actual correlation energy of the uniform electron gas. Additionally, I didn't have the derivatives with respect to r_s, in which case I set them randomly. Here I want to

derive those terms using the simple correlation energy of the uniform gas given by Chachiyo in 2016[Cha16]:

$$\epsilon_c^{lsda1} = a\ln(1+\frac{b}{r_s}+\frac{c}{r_s^2}) \tag{B.325}$$

$$\partial r_s \epsilon_c^{lsda1} = -\frac{ab(r_s+2)}{r_s(r_s^2+br_s+b)} \tag{B.326}$$

$$\partial_{r_s}^2 \epsilon_c^{lsda1} = \frac{ab(2r_s^3+(b+6)r_s^2+4br_s+2b)}{r_s^2(r_s^2+br_s+b)^2} \tag{B.327}$$

$$\partial_{r_s}^3 \epsilon_c^{lsda1} = -\frac{2ab(3r_s^2+(3b+12)r_s^4+(b^2+15b)r_s^3)}{r_s^3(r_s^2+br_s+b)^3} + \frac{(6b^2+6b)r_s^2+6b^2r_s+2b^2}{r_s^3(r_s^2+br_s+b)^3} \tag{B.328}$$

where we have:

$$a = \frac{\ln 2 - 1}{4\pi^2} \tag{B.329}$$

and

$$b = 27.4203609$$

If the tipping point between the low-density and high-density limits in (B.325) appears at r_s=1, exactly at the Bohr Radius, then b=c.

Bibliography

[AB99] Carlo Adamo and Vincenzo Barone. „Toward reliable density functional methods without adjustable parameters: The PBE0 model“. In: *The Journal of Chemical Physics* 110.13 (1999), pp. 6158–6170 (cit. on p. 26).

[ABD06] H. Amara, C. Bichara, and F. Ducastelle. „Formation of carbon nanostructures on nickel surfaces: A tight-binding grand canonical Monte Carlo study“. In: *Phys. Rev. B* 73 (11 Mar. 2006), p. 113404 (cit. on p. 2).

[AE10] Grazyna Antczak and Gert Ehrlich. *Surface diffusion: metals, metal atoms, and clusters*. Cambridge University Press, 2010 (cit. on p. 54).

[AF11] Peter W Atkins and Ronald S Friedman. *Molecular quantum mechanics*. Oxford university press, 2011 (cit. on pp. 5–7, 9).

[AH17] Hamda A. Al-Thani and Falah S. Hasoon. „Role of Pre-Layer Mo Films in Microstructural and Morphological Properties of Over-Layer CIGS Films“. In: *MRS Advances* 2.53 (June 2017), pp. 3215–3224 (cit. on p. 2).

[Ban+21] Tanmay Banerjee, Filip Podjaski, Julia Kröger, Bishnu P Biswal, and Bettina V Lotsch. „Polymer photocatalysts for solar-to-chemical energy conversion“. In: *Nature Reviews Materials* 6.2 (2021), pp. 168–190 (cit. on p. 1).

[BCG15] Tim Baldsiefen, Attila Cangi, and E. K. U. Gross. „Reduced-density-matrix-functional theory at finite temperature: Theoretical foundations“. In: *Phys. Rev. A* 92 (5 Nov. 2015), p. 052514 (cit. on p. 38).

[BEG19] Christoph Bannwarth, Sebastian Ehlert, and Stefan Grimme. „GFN2-xTB—An accurate and broadly parametrized self-consistent tight-binding quantum chemical method with multipole electrostatics and density-dependent dispersion contributions“. In: *Journal of chemical theory and computation* 15.3 (2019), pp. 1652–1671 (cit. on p. 49).

[BF12] Peter E. Blöchl and Clemens Först. *Node-less atomic wave functions, Pauli repulsion and systematic projector augmentation*. 2012 (cit. on p. 31).

[Blö20] Peter E. Blöchl. „Manual for the Projector Augmented Wave Method“. English. In: (2020) (cit. on p. 26).

[Blö94a] P. E. Blöchl. „Projector augmented-wave method“. In: *Phys. Rev. B* 50 (24 Dec. 1994), pp. 17953–17979 (cit. on p. 15).

[Blö94b] P. E. Blöchl. „Projector augmented-wave method“. In: *Phys. Rev. B* 50 (24 Dec. 1994), pp. 17953–17979 (cit. on pp. 26, 29, 65).

[BPP13a] Peter E. Blöchl, Thomas Pruschke, and Michael Potthoff. „Density-matrix functionals from Green's functions“. In: *Phys. Rev. B* 88 (20 Nov. 2013), p. 205139 (cit. on p. 27).

[BPP13b] Peter E. Blöchl, Thomas Pruschke, and Michael Potthoff. „Density-matrix functionals from Green's functions“. In: *Phys. Rev. B* 88 (20 Nov. 2013), p. 205139 (cit. on p. 38).

[Bro74] Benjamin Collins Brodie. „IV. On the action of electricity on gases.—II. On the electric decomposition of carbonic-acid gas“. In: *Philosophical Transactions of the Royal Society of London* 164 (1874), pp. 83–103. eprint: `https://royalsocietypublishing.org/doi/pdf/10.1098/rstl.1874.0004` (cit. on p. 1).

[Bun80] P.R. Bunker. „Carbon suboxide as a semirigid bender“. In: *Journal of Molecular Spectroscopy* 80.2 (Apr. 1980), pp. 422–437 (cit. on p. 33).

[BWP11a] P. E. Blöchl, C. F. J. Walther, and Th. Pruschke. „Method to include explicit correlations into density-functional calculations based on density-matrix functional theory“. In: *Phys. Rev. B* 84 (2011), p. 205101 (cit. on p. 27).

[BWP11b] Peter E. Blöchl, Christian F. J. Walther, and Thomas Pruschke. „Method to include explicit correlations into density-functional calculations based on density-matrix functional theory“. In: *Phys. Rev. B* 84 (20 Nov. 2011), p. 205101 (cit. on p. 39).

[BWP11c] Peter E. Blöchl, Christian F. J. Walther, and Thomas Pruschke. „Method to include explicit correlations into density-functional calculations based on density-matrix functional theory“. In: *Physical Review B* 84.20 (Nov. 2011) (cit. on pp. 39, 40).

[Car+21] Marco Carroli, Alex G Dixon, Martin Herder, et al. „Multiresponsive nonvolatile memories based on optically switchable ferroelectric organic field-effect transistors“. In: *Advanced Materials* 33.14 (2021), p. 2007965 (cit. on p. 1).

[Cha16] Teepanis Chachiyo. „Communication: Simple and accurate uniform electron gas correlation energy for the full range of densities“. In: *The Journal of Chemical Physics* 145.2 (July 2016), p. 021101 (cit. on p. 100).

[CP85a] R. Car and M. Parrinello. „Unified Approach for Molecular Dynamics and Density-Functional Theory“. In: *Phys. Rev. Lett.* 55 (22 Nov. 1985), pp. 2471–2474 (cit. on p. 15).

[CP85b] R. Car and M. Parrinello. „Unified Approach for Molecular Dynamics and Density-Functional Theory“. In: *Phys. Rev. Lett.* 55 (22 Nov. 1985), pp. 2471–2474 (cit. on pp. 23, 24).

[CPP86] T Carofiglio, L Pandolfo, and G Paiaro. „Carbon suboxide polymers“. In: *European polymer journal* 22.6 (1986), pp. 491–497 (cit. on p. 1).

[CR93] S. Cincotti and J. P. Rabe. „Self-assembled alkane monolayers on MoSe2 and MoS2“. In: *Applied Physics Letters* 62.26 (1993), pp. 3531–3533. eprint: `https://doi.org/10.1063/1.109017` (cit. on p. 56).

[DB93] Richard Dronskowski and Peter E Bloechl. „Crystal orbital Hamilton populations (COHP): energy-resolved visualization of chemical bonding in solids based on density-functional calculations“. In: *The Journal of Physical Chemistry* 97.33 (1993), pp. 8617–8624 (cit. on p. 30).

[DMR76] J.A. Duckett, I.M. Mills, and A.G. Robiette. „The two-dimensional anharmonic oscillator“. In: *Journal of Molecular Spectroscopy* 63.2 (Nov. 1976), pp. 249–264 (cit. on p. 33).

[DW06] Otto Diels and Bertram Wolf. „Ueber das Kohlensuboxyd. I“. In: *Berichte der deutschen chemischen Gesellschaft* 39.1 (1906), pp. 689–697 (cit. on p. 1).

[EBB20] Marco Eckhoff, Peter E Blöchl, and Jörg Behler. „Hybrid density functional theory benchmark study on lithium manganese oxides“. In: *Physical Review B* 101.20 (2020), p. 205113 (cit. on pp. 26, 28).

[Fen49] Werner Fenchel. „On conjugate convex functions“. In: *Canadian Journal of Mathematics* 1.1 (1949), pp. 73–77 (cit. on p. 36).

[GAE03] Alexei Grechnev, Rajeev Ahuja, and Olle Eriksson. „Balanced crystal orbital overlap population—a tool for analysing chemical bonds in solids“. In: *Journal of Physics: Condensed Matter* 15.45 (Oct. 2003), pp. 7751–7761 (cit. on p. 26).

[Gag17] Paul A Gagniuc. *Markov chains: from theory to implementation and experimentation*. John Wiley & Sons, 2017 (cit. on p. 54).

[Gao+20] Yuan-Fei Gao, Si-Ming Pang, Hai-Hong Bao, et al. „Growth mechanism for vertically oriented layered In_2Se_3 nanoplates“. In: *Phys. Rev. Materials* 4 (3 Mar. 2020), p. 034002 (cit. on pp. 50, 56).

[GBS17] Stefan Grimme, Christoph Bannwarth, and Philip Shushkov. „A Robust and Accurate Tight-Binding Quantum Chemical Method for Structures, Vibrational Frequencies, and Noncovalent Interactions of Large Molecular Systems Parametrized for All spd-Block Elements (Z = 1–86)“. In: *Journal of Chemical Theory and Computation* 13.5 (2017). PMID: 28418654, pp. 1989–2009. eprint: `https://doi.org/10.1021/acs.jctc.7b00118` (cit. on pp. 2, 49).

[Ger+20] Victor Gervilla, Mohammad Zarshenas, Davide G. Sangiovanni, and Kostas Sarakinos. „Anomalous versus Normal Room-Temperature Diffusion of Metal Adatoms on Graphene“. In: *The Journal of Physical Chemistry Letters* 11.21 (2020). PMID: 32986445, pp. 8930–8936. eprint: `https://doi.org/10.1021/acs.jpclett.0c02375` (cit. on p. 54).

[Gil75] T. L. Gilbert. „Hohenberg-Kohn theorem for nonlocal external potentials“. In: *Physical Review B* 12.6 (Sept. 1975), pp. 2111–2120 (cit. on p. 35).

[Gio] GiorgioP-DoomsdayClockIsAt-90. *How can the fictitious mass in the Car-Parrinello method reproduce the quot;realquot; dynamics?* Physics Stack Exchange. eprint: `https://physics.stackexchange.com/q/455162` (cit. on p. 24).

[Gio19] Toni Giorgino. „Computing diffusion coefficients in macromolecular simulations: the Diffusion Coefficient Tool for VMD“. In: *Journal of Open Source Software* 4.41 (2019), p. 1698 (cit. on p. 54).

[GN57] R. J. Gillespie and R. S. Nyholm. „Inorganic stereochemistry“. In: *Q. Rev. Chem. Soc.* 11 (4 1957), pp. 339–380 (cit. on p. 32).

[Hel06] N Helbig. *Orbital functionals in density-matrix- and current-density-functional theory*. May 2006 (cit. on p. 38).

[HG11] Joshua W. Hollett and Peter M. W. Gill. „The two faces of static correlation“. In: *The Journal of Chemical Physics* 134.11 (Mar. 2011) (cit. on p. 10).

[HH83] Timothy Hughbanks and Roald Hoffmann. „Chains of trans-edge-sharing molybdenum octahedra: metal-metal bonding in extended systems“. In: *Journal of the American Chemical Society* 105.11 (1983), pp. 3528–3537 (cit. on p. 29).

[HK64] P. Hohenberg and W. Kohn. „Inhomogeneous Electron Gas“. In: *Phys. Rev.* 136 (3B Nov. 1964), B864–B871 (cit. on pp. 5, 6).

[HKS14] Daniel Himmel, Ingo Krossing, and Andreas Schnepf. „Dative Bonds in Main-Group Compounds: A Case for Fewer Arrows!“ In: *Angewandte Chemie International Edition* 53.2 (2014), pp. 370–374. eprint: `https://onlinelibrary.wiley.com/doi/pdf/10.1002/anie.201300461` (cit. on p. 33).

[HSE03] Jochen Heyd, Gustavo E. Scuseria, and Matthias Ernzerhof. „Hybrid functionals based on a screened Coulomb potential“. In: *The Journal of Chemical Physics* 118.18 (May 2003), pp. 8207–8215 (cit. on p. 26).

[HSE06] Jochen Heyd, Gustavo E. Scuseria, and Matthias Ernzerhof. „Erratum: “Hybrid functionals based on a screened Coulomb potential” [J. Chem. Phys. 118, 8207 (2003)]“. In: *The Journal of Chemical Physics* 124.21 (June 2006) (cit. on p. 26).

[htta] Wildcat (https://chemistry.stackexchange.com/users/186/wildcat). *What is the difference between dynamic and static electronic correlation*. Chemistry Stack Exchange. URL:https://chemistry.stackexchange.com/q/59555 (version: 2016-09-23). eprint: `https://chemistry.stackexchange.com/q/59555` (cit. on p. 10).

[httb] Andrew (https://physics.stackexchange.com/users/27732/andrew). *What is the “exchange energy of electrons”?* Physics Stack Exchange. eprint: `https://physics.stackexchange.com/q/678138` (cit. on p. 10).

[HUJ00] Graeme Henkelman, Blas P. Uberuaga, and Hannes Jónsson. „A climbing image nudged elastic band method for finding saddle points and minimum energy paths“. In: *The Journal of Chemical Physics* 113.22 (2000), pp. 9901–9904. eprint: `https://doi.org/10.1063/1.1329672` (cit. on p. 49).

[JJ86] Per Jensen and J.W.C. Johns. „The infrared spectrum of carbon suboxide in the 6 fundamental region: Experimental observation and semirigid bender analysis“. In: *Journal of Molecular Spectroscopy* 118.1 (1986), pp. 248–266 (cit. on p. 33).

[KBM09] Jiří Klimeš, David R Bowler, and Angelos Michaelides. „Chemical accuracy for the van der Waals density functional“. In: *Journal of Physics: Condensed Matter* 22.2 (Dec. 2009), p. 022201 (cit. on p. 49).

[KH93] G. Kresse and J. Hafner. „Ab initio molecular dynamics for liquid metals“. In: *Phys. Rev. B* 47 (1 Jan. 1993), pp. 558–561 (cit. on p. 49).

[KH94a] G Kresse and J Hafner. „Norm-conserving and ultrasoft pseudopotentials for first-row and transition elements“. In: *Journal of Physics: Condensed Matter* 6.40 (Oct. 1994), pp. 8245–8257 (cit. on p. 49).

[KH94b] G. Kresse and J. Hafner. „Ab initio molecular-dynamics simulation of the liquid-metal–amorphous-semiconductor transition in germanium“. In: *Phys. Rev. B* 49 (20 May 1994), pp. 14251–14269 (cit. on p. 49).

[KJ99] Georg Kresse and Daniel Joubert. „From ultrasoft pseudopotentials to the projector augmented-wave method“. In: *Physical review b* 59.3 (1999), p. 1758 (cit. on p. 49).

[KK04] K. Kohary and S. Kugler. „Growth of Amorphous Silicon: Low Energy Molecular Dynamics Simulation of Atomic Bombardment“. In: *Molecular Simulation* 30.1 (2004), pp. 17–22. eprint: https://doi.org/10.1080/08927020310001624690 (cit. on p. 2).

[Kop00] Jacek Koput. „An ab initio study on the equilibrium structure and CCC bending energy levels of carbon suboxide“. In: *Chemical Physics Letters* 320.3 (2000), pp. 237–244 (cit. on p. 33).

[Kre+96] G Kresse et al. „Software vasp, vienna, 1999; g. kresse, j. furthmüller“. In: *Phys. Rev. B* 54.11 (1996), p. 169 (cit. on p. 49).

[Kre96] G Kresse. „Comput. matter sci. 6, 15 (1996);(d) kresse, g., and furthmuller“. In: *Phys. Rev. B* 54 (1996), pp. 11–169 (cit. on p. 49).

[Kru+06] Aliaksandr V. Krukau, Oleg A. Vydrov, Artur F. Izmaylov, and Gustavo E. Scuseria. „Influence of the exchange screening parameter on the performance of screened hybrid functionals“. In: *The Journal of Chemical Physics* 125.22 (Dec. 2006) (cit. on pp. 26, 27).

[KS65] W. Kohn and L. J. Sham. „Self-Consistent Equations Including Exchange and Correlation Effects“. In: *Phys. Rev.* 140 (4A Nov. 1965), A1133–A1138 (cit. on p. 8).

[Küh+20] Thomas D. Kühne, Marcella Iannuzzi, Mauro Del Ben, et al. „CP2K: An electronic structure and molecular dynamics software package - Quickstep: Efficient and accurate electronic structure calculations“. In: *The Journal of Chemical Physics* 152.19 (2020), p. 194103. eprint: https://doi.org/10.1063/5.0007045 (cit. on p. 50).

[Kuo+17] C -Y Kuo, T Haupricht, J Weinen, et al. „Challenges from experiment: electronic structure of NiO“. In: *The European Physical Journal Special Topics* 226 (2017), pp. 2445–2456 (cit. on p. 26).

[Küp+18] Michael Küpers, Philipp M. Konze, Alexander Meledin, et al. „Controlled Crystal Growth of Indium Selenide, In2Se3, and the Crystal Structures of α-In2Se3“. In: *Inorganic Chemistry* 57.18 (2018). PMID: 30153016, pp. 11775–11781. eprint: https://doi.org/10.1021/acs.inorgchem.8b01950 (cit. on p. 55).

[Leg87] Adrien Marie Legendre. *Mémoire sur l'intégration de quelques équations aux différences partielles*. Imprimerie royale, 1787 (cit. on p. 36).

[Lev79a] Mel Levy. „Universal variational functionals of electron densities, first-order density matrices, and natural spin-orbitals and solution of the v -representability problem“. In: *Proceedings of the National Academy of Sciences* 76.12 (Dec. 1979), pp. 6062–6065 (cit. on pp. 12, 13).

[Lev79b] Mel Levy. „Universal variational functionals of electron densities, first-order density matrices, and natural spin-orbitals and solution of the v-representability problem“. In: *Proceedings of the National Academy of Sciences* 76.12 (1979), pp. 6062–6065 (cit. on pp. 5, 37).

[Lev82] Mel Levy. „Electron densities in search of Hamiltonians“. In: *Phys. Rev. A* 26 (3 Sept. 1982), pp. 1200–1208 (cit. on p. 12).

[Liu+20] Le Liu, Yuanyuan Kan, Ke Gao, et al. „Graphdiyne derivative as multifunctional solid additive in binary organic solar cells with 17.3% efficiency and high reproductivity“. In: *Advanced Materials* 32.11 (2020), p. 1907604 (cit. on p. 1).

[Liu+22] Wu Liu, Haotian Li, Bo Qiao, et al. „Highly efficient CIGS solar cells based on a new CIGS bandgap gradient design characterized by numerical simulation“. In: *Solar Energy* 233 (Feb. 2022), pp. 337–344 (cit. on p. 2).

[Mar04] Richard M. Martin. *Electronic Structure: Basic Theory and Practical Methods*. Cambridge University Press, Apr. 2004 (cit. on pp. 6–8, 12, 24).

[Mer65] N David Mermin. „Thermal properties of the inhomogeneous electron gas“. In: *Physical Review* 137.5A (1965), A1441 (cit. on p. 7).

[Mir+16] Hossein Mirhosseini, Janos Kiss, Guido Roma, and Claudia Felser. „Reducing the Schottky barrier height at the MoSe2/Mo(110) interface in thin-film solar cells: Insights from first-principles calculations“. In: *Thin Solid Films* 606 (May 2016), pp. 143–147 (cit. on p. 50).

[Mir21] Hossein Mirhosseini. *Untitled Manuscript*. unpublished. 2021 (cit. on p. 54).

[MP76] Hendrik J. Monkhorst and James D. Pack. „Special points for Brillouin-zone integrations“. In: *Phys. Rev. B* 13 (12 June 1976), pp. 5188–5192 (cit. on p. 49).

[MPM12] S K Mahatha, K D Patel, and Krishnakumar S R Menon. „Electronic structure investigation of MoS2and MoSe2using angle-resolved photoemission spectroscopy andab initioband structure studies“. In: *Journal of Physics: Condensed Matter* 24.47 (Oct. 2012), p. 475504 (cit. on p. 56).

[MS20] Stefano Mazzanti and Aleksandr Savateev. „Emerging Concepts in Carbon Nitride Organic Photocatalysis“. In: *ChemPlusChem* 85.11 (2020), pp. 2499–2517 (cit. on p. 1).

[MS99] Eisaku Miyoshi and Norihiro Shida. „An ab initio study on the structure of the ground state of the C3O2 molecule“. In: *Chemical Physics Letters* 303.1–2 (Apr. 1999), pp. 50–56 (cit. on p. 33).

[Odz+22] Mateusz Odziomek, Paolo Giusto, Janina Kossmann, et al. „“Red Carbon”: A Rediscovered Covalent Crystalline Semiconductor“. In: *Advanced Materials* 34.40 (2022), p. 2206405 (cit. on p. 1).

[Pau94] Wolfgang Pauli. „Exclusion Principle and Quantum Mechanics“. In: *Writings on Physics and Philosophy*. Springer Berlin Heidelberg, 1994, pp. 165–181 (cit. on pp. 9, 10).

[PBE96] John P. Perdew, Kieron Burke, and Matthias Ernzerhof. „Generalized Gradient Approximation Made Simple“. In: *Phys. Rev. Lett.* 77 (18 Oct. 1996), pp. 3865–3868 (cit. on p. 11).

[PEB96] John P. Perdew, Matthias Ernzerhof, and Kieron Burke. „Rationale for mixing exact exchange with density functional approximations“. In: *The Journal of Chemical Physics* 105.22 (1996), pp. 9982–9985 (cit. on p. 28).

[Pet18] Michael ten Brink Peter E. Blöchl Robert Schade. „CP-PAW Hands-On Course on First-Principles Calculations“. English. In: (2018) (cit. on p. 29).

[PG15] Katarzyna Pernal and Klaas J. H. Giesbertz. „Reduced Density Matrix Functional Theory (RDMFT) and Linear Response Time-Dependent RDMFT (TD-RDMFT)“. In: *Density-Functional Methods for Excited States*. Springer International Publishing, 2015, pp. 125–183 (cit. on p. 35).

[PW94] R.G. Parr and Y. Weitao. *Density-Functional Theory of Atoms and Molecules*. International Series of Monographs on Chemistry. Oxford University Press, 1994 (cit. on pp. 5–7, 9, 10, 12, 13, 36).

[SB08] H Staudinger and St Bereza. „Über Ketene. 11. Mitteilung: Neue Bildungsweisen des Kohlensuboxyds“. In: *Berichte der deutschen chemischen Gesellschaft* 41.3 (1908), pp. 4461–4465 (cit. on p. 1).

[Sch19] Robert Schade. „New methods for the ab-initio simulation of correlated systems“. PhD thesis. Gottingen U., 2019 (cit. on pp. 35, 37–39, 41–44).

[SHY78] AW Snow, H Haubenstock, and N-L Yang. „Poly (carbon suboxide). Characterization, polymerization, and radical structure“. In: *Macromolecules* 11.1 (1978), pp. 77–86 (cit. on p. 1).

[SKB17] Robert Schade, Ebad Kamil, and Peter Blöchl. „Reduced density-matrix functionals from many-particle theory“. In: *The European Physical Journal Special Topics* 226.11 (2017), pp. 2677–2692 (cit. on pp. 36, 38, 39).

[Smi+63] R Nelson Smith, David A Young, Eric N Smith, and Charles C Carter. „The structure and properties of carbon suboxide polymer“. In: *Inorganic Chemistry* 2.4 (1963), pp. 829–838 (cit. on p. 1).

[Sot+17] Mohsen Sotoudeh, Sangeeta Rajpurohit, Peter Blöchl, et al. „Electronic structure of $\mathrm{Pr}_{1-x}\mathrm{Ca}_x\mathrm{MnO}_3$“. In: *Phys. Rev. B* 95 (23 June 2017), p. 235150 (cit. on pp. 26, 28).

[SRP15a] Jianwei Sun, Adrienn Ruzsinszky, and John P. Perdew. „Strongly Constrained and Appropriately Normed Semilocal Density Functional“. In: *Phys. Rev. Lett.* 115 (3 July 2015), p. 036402 (cit. on pp. 1, 71, 74).

[SRP15b] Jianwei Sun, Adrienn Ruzsinszky, and John P. Perdew. „Strongly Constrained and Appropriately Normed Semilocal Density Functional“. In: *Phys. Rev. Lett.* 115 (3 July 2015), p. 036402 (cit. on pp. 11, 22).

[Tao+03] Jianmin Tao, John P. Perdew, Viktor N. Staroverov, and Gustavo E. Scuseria. „Climbing the Density Functional Ladder: Nonempirical Meta–Generalized Gradient Approximation Designed for Molecules and Solids“. In: *Phys. Rev. Lett.* 91 (14 Sept. 2003), p. 146401 (cit. on p. 71).

[Tor+95] J. Tortajada, G. Provot, J.-P. Morizur, et al. „Experimental and theoretical study of carbon suboxide C3O2, protonated carbon suboxide C3HO2+ and C3HO2· radical in the gas phase“. In: *International Journal of Mass Spectrometry and Ion Processes* 141.3 (1995), pp. 241–255 (cit. on p. 33).

[TP11] W. Töws and G. M. Pastor. „Lattice density functional theory of the single-impurity Anderson model: Development and applications“. In: *Phys. Rev. B* 83 (23 June 2011), p. 235101 (cit. on p. 42).

[TP12] W. Töws and G. M. Pastor. „Spin-polarized density-matrix functional theory of the single-impurity Anderson model“. In: *Phys. Rev. B* 86 (24 Dec. 2012), p. 245123 (cit. on p. 42).

[Val80] Steven M. Valone. „Consequences of extending 1-matrix energy functionals from pure–state representable to all ensemble representable 1 matrices“. In: *The Journal of Chemical Physics* 73.3 (Aug. 1980), pp. 1344–1349 (cit. on p. 37).

[Ver67] Loup Verlet. „Computer "Experiments" on Classical Fluids. I. Thermodynamical Properties of Lennard-Jones Molecules“. In: *Phys. Rev.* 159 (1 July 1967), pp. 98–103 (cit. on p. 25).

[VJP91] J. Vander Auwera, J. W. C. Johns, and O. L. Polyansky. „The far infrared spectrum of C3O2“. In: *The Journal of Chemical Physics* 95.4 (1991), pp. 2299–2316 (cit. on p. 33).

[Wan+09] Xinchen Wang, Kazuhiko Maeda, Arne Thomas, et al. „A metal-free polymeric photocatalyst for hydrogen production from water under visible light“. In: *Nature materials* 8.1 (2009), pp. 76–80 (cit. on p. 1).

[Xu+21] Ye Xu, Yong Cui, Huifeng Yao, et al. „A new conjugated polymer that enables the integration of photovoltaic and light-emitting functions in one device“. In: *Advanced Materials* 33.22 (2021), p. 2101090 (cit. on p. 1).

[YCD90] Luping Yu, Mai Chen, and Larry R Dalton. „Ladder polymers: recent developments in syntheses, characterization, and potential applications as electronic and optical materials“. In: *Chemistry of Materials* 2.6 (1990), pp. 649–659 (cit. on p. 1).

[YKR07] Handan Yildirim, Abdelkader Kara, and Talat S. Rahman. „Origin of quasi-constant pre-exponential factors for adatom diffusion on Cu and Ag surfaces“. In: *Phys. Rev. B* 76 (16 Oct. 2007), p. 165421 (cit. on p. 54).

[Yos+17] Kunta Yoshikawa, Hayato Kawasaki, Wataru Yoshida, et al. „Silicon heterojunction solar cell with interdigitated back contacts for a photoconversion efficiency over 26%“. In: *Nature Energy* 2.5 (Mar. 2017) (cit. on p. 2).

[Zhe+08] Hao Zheng, M. H. Xie, H. S. Wu, and Q. K. Xue. „Kinetic energy barriers on the GaN(0001) surface: A nucleation study by scanning tunneling microscopy“. In: *Phys. Rev. B* 77 (4 Jan. 2008), p. 045303 (cit. on p. 56).

Colophon

This thesis was typeset with LaTeX 2$_\varepsilon$. It uses the *Clean Thesis* style developed by Ricardo Langner. The design of the *Clean Thesis* style is inspired by user guide documents from Apple Inc.

Download the *Clean Thesis* style at `http://cleanthesis.der-ric.de/`.

Declaration

I, **Konstantin Tamoev**, hereby declare that I have written my PhD thesis independtly myself, using only the sources cited therein.

Paderborn, June 04, 2024

Konstantin Tamoev